Delft University of Technology

Master thesis

# Imaging peat using neutron and X-ray CT

*Author:*
Sjors Dicker

June 4, 2019

# Imaging peat using neutron and X-ray tomography

by

Sjors Dicker

to obtain the degree of Master of Science
at the Delft University of Technology.



| | | |
|---|---|---|
| Student number: | 4213114 | |
| Thesis committee: | Dr. Ir. D.J.M. Ngan-Tillard, | TU Delft Geo-Engineering, Daily Supervisor |
| | Prof. Dr. C. Jommi, | TU Delft Geo-Engineering |
| | Dr. L. van Eijck, | TU Delft faculty of Applied Physics |
| | Z. Zhou, | TU Delft faculty of Applied Physics |


An electronic version of this thesis is available at `http://repository.tudelft.nl/`.

# 1 Acknowledgements

I would like to thank Dominique Ngan-Tillard, Lambert van Eijck, Zhou Zhou, Cristina Jommi for their supervision and feedback during my master thesis project. Especially Zhou Zhou for his support and helpful thoughts while using the thermal neutron imaging station.
I have to thank Iván Josipovic and Matthieu Boone from the university of Ghent. They made it possible to use their X-ray phase contrast imaging station. Next to this, they supported me while analyzing the images.
Furthermore, I would like to acknowledge Ellen Meijvogel-de Koning and Wim Verwaal for imaging peat using X-ray micro-CT.
Also, I would like to thank Joost van Meel for making it possible to use his Dell station.
Finally, I would like to thank my parents for their support throughout the years.

# 2 Abstract

Peat is formed by biochemical processes and the accumulation of the soil depends on the aerobic and anaerobic conditions. The soil covers five to eight percent of the land surface of the earth. For this thesis a peat coming from a site called Markermeeer, which is a lake between the provinces Noord-Holland and Flevoland in the Netherlands, is used. The fabric of peat consists of a fine dark peat material and fibres. The peat material is made of water and decomposed plant tissue whereas the fibres consist of fragments of (semi-)degraded wood, stems, branches and grass. Furthermore the cell walls of the fibres consists of a primary and a secondary wall which are mostly made of cellulose and lignin. Knowing the fabric of wet peat is of importance to better understand the role of fibres in the unusual behavior of the soil. Previous studies on imaging wet peat with X-ray micro CT has proven to be difficult due to the indistinguishable linear attenuation coefficient of the peat organic matter and water. This coefficient is a function of the interactions of X-rays with the materials present in peat. Flushing a peat sample with lead(II)nitrate have shown to be the most successful approach to show the stems and branches in a peat sample using X-ray micro CT. However, according to Kettridge and Binley (2008) this flushing approach showed that the focus was limited on the larger fibres present in the sample because the different materials in peat have almost the same linear attenuation coefficient and therefore this thesis also focuses on two other techniques to image the fabric of wet peat.

Neutron CT was performed on cylindrical peat samples. This technique uses a thermal neutron beam to image a sample and was available at the Reactor Institute Delft. The resolution of this imaging station is 150 $\mu$m. Since the cell walls and the peat material between the fibres in peat have both a large attenuation coefficient for neutrons, it was not possible to distinguish the fibres from the peat material between the fibres, using this technique. To gain a contrast heavy water was used to replace the water because it has a low attenuation coefficient. Flushing a peat sample with heavy water showed the most effective way to do so. The aim of this procedure was to get a contrast difference between the peat material between the fibres and the fibres itself. A triaxial setup was used to flush the sample with heavy water. Heavy water diffused in the water present in the peat inducing a decrease in attenuation of the peat material between the fibres. The reconstructed tomographic images were filtered using a 3D visualization program Avizo version 9.4. Only the air-filled fibres could be observed on the tomographic images whereas the water-filled fibres could not be observed.

Samples of the same peat were scanned in a dry and wet state using a X-ray micro CT scanner present at the geoscience section of TU Delft. On the tomographic images of the wet sample, white halo were observed representing the cell walls of the fibres. X-ray phase CT present at the Ghent University Centre for X-ray CT was performed on a peat sample coming from the same site. This method results in an image contrast using a large fixed distance for low absorbing materials like peat. The aim of this scan was to reveal more fibres than observed with the X-ray micro CT scan at TU Delft. However, edge enhancement did not occur because of the filtering needed during reconstruction of the raw data to visualize different structures in peat.
The white halo could be thresholded and filtered in avizo resulting in a 3D image of the rod-like fibres. These fibres were randomly orientated. On the micro CT scan of the sample in a dry state other fibrous structures than the rod-like fibres were observed. These fibres were not shown as white halo on the tomographic images of the wet samples.

# Contents

# List of Figures

# List of Tables

# 3 Definitions

1. Fibre: All plant and wood tissue present in peat which have a rod-like shape.

2. Small fibre: Fibre which has a diameter smaller than 60 $\mu$m on the tomographic image(Mikucioniene et al. (2019)).

3. Big fibre: Fibre which has a diameter greater than 60 $\mu$m on the image section(Mikucioniene et al. (2019)).

4. Peat material between the fibres: Fine dark organic matter with a high water content made of (semi-)decomposed plant and wood tissue

5. Radiography: Use of radiation to produce a picture of the inside of an object.

6. CT: Computer tomography involving the production of three-dimensional images by the detection of the absorbance of neutrons or X-rays produced by a source.

7. Avizo: Imaging analysis software to filter CT images.

8. Tomographic image: Slice of the CT images used to show the present fibres.

# 4 Introduction

Before introducing the aim of this research, the formation of the soil and the conditions which have led to their accumulation will be discussed.

Kurbatov (1968) briefly explains 35 years of research into the formation of peat as follows: “The formation of peat is a relatively short biochemical process carried on under the influence of aerobic micro-organisms in the surface layers of the deposits during periods of low subsoil water. As the peat which is formed in the peat-producing layer becomes subjected to anaerobic conditions in the deeper layers of the deposit, it is preserved and shows comparatively little change with time." According to this theory the presence of either aerobic or anaerobic conditions decides whether any organic matter will accumulate and in what form.

Next to the formation and accumulation processes described in section 4.1, the decomposition and chemical composition of the plant tissue in peat are discussed in section 4.2 and 4.3. Furthermore the impact of those tissues on the behavior of peats is described in section 4.4. The difficulties of previous research aiming at imaging the peat fabric are explained in section 4.5. Sections 4.6 and 4.7 are focused on the peat which will be used for this thesis before giving the thesis objectives and problem definition in sections 4.8, 4.9 and 4.10.

## 4.1 Peat cover and formation

Peat is found throughout the world. It covers five to eight percent of the land surface of the earth. Ten percent of this amount are peat deposits which are deposited in a tropical or subtropical climate. Figure 1 displays the total peatland cover per country in percentage of national land area. The peat cover in the world's peatlands has been forming for 360 million years and contains 550 Gt of carbon.

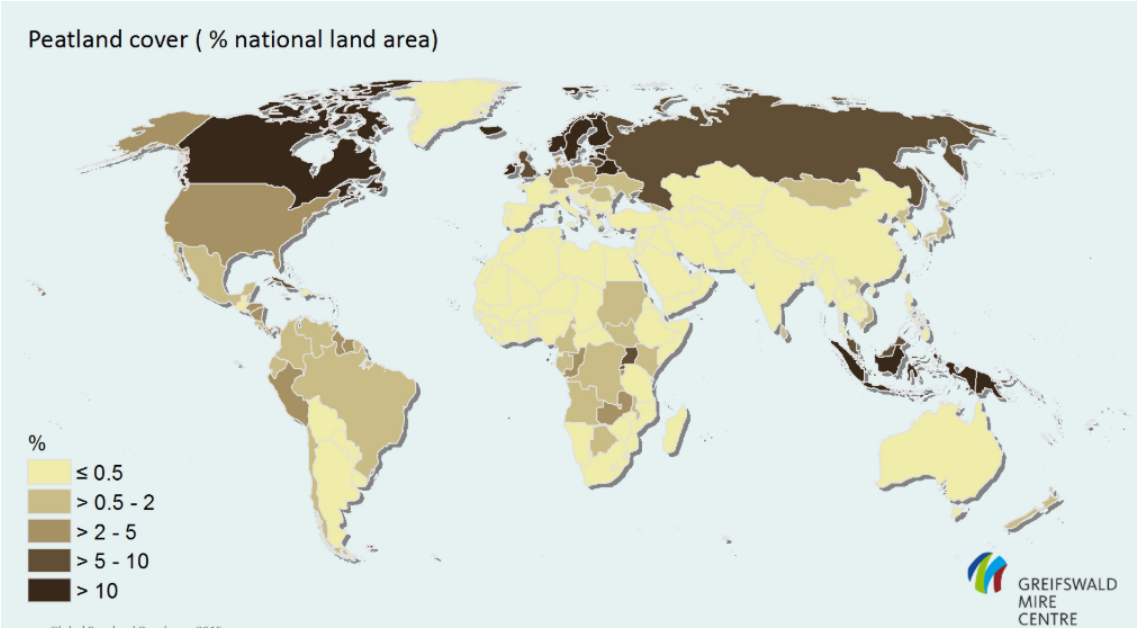


**Figure 1:** *Total peat cover in the world per country.*
*Source: Global peatland database*

Based on Van Breemen (1995), peat occurs in different type of deposits like bogs and fens. Bogs are mossy wetlands. As shown in fig. 2d there is hardly no water circulation and all the water comes from rain and snow in a peat bog. Therefore, bogs have a low level of oxygen because water does not flow in or out of it. Sphagnum peat is common in bogs. This is a moss type of peat which has cells that absorbs water.
Fens are like bogs, however unlike bogs water comes from small streams and groundwater. Grasses and sedges are common plants in fens. The main difference between a fen and a bog is that the soil and water of a fen are richer in nutrients because of their greater water exchange and they are less acidic. As shown in fig.2 most fens become over time bogs and sometimes raised bogs. A raised bog (fig. 2e) is formed when precipitation exceeds evapotranspiration (Gore (1983)).

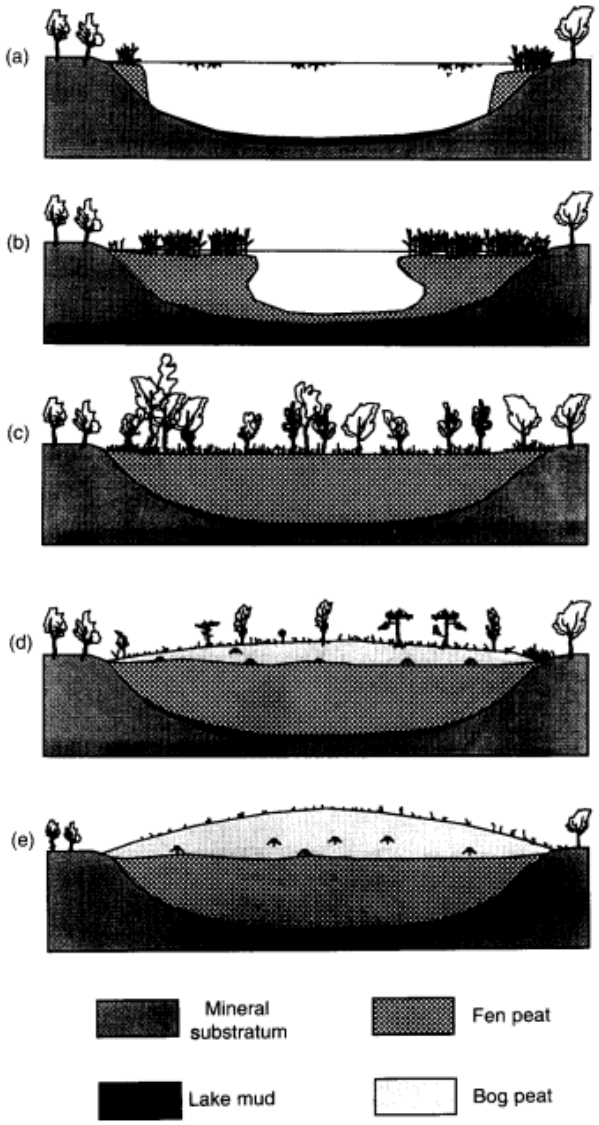


**Figure 2:** *Development of a raised bog by: (a) lake mud; (b)-(c) fen; (d)-(e) bog Source: Van Breemen (1995)*

## 4.2 Decomposition of plant tissue of peat

Where peat starts to degrade, most of their plant tissue is decomposed. Drzymulska (2016) described decomposition as the amount of dark amorphous matter existing in peat. The dark amorphous matter consists of humic compounds and other products of plant decomposition. A peat layer can be divided into an acrotelm layer and a catotelm layer (fig.3). Decomposition is fast in the acrotelm layer and most of the plant mass is mineralised here (Grosse-Brauckmann (1996)). The catotelm peat layer stores the sediments formed in the acrotelm peat layer and is known as the dead part of the peat layer.

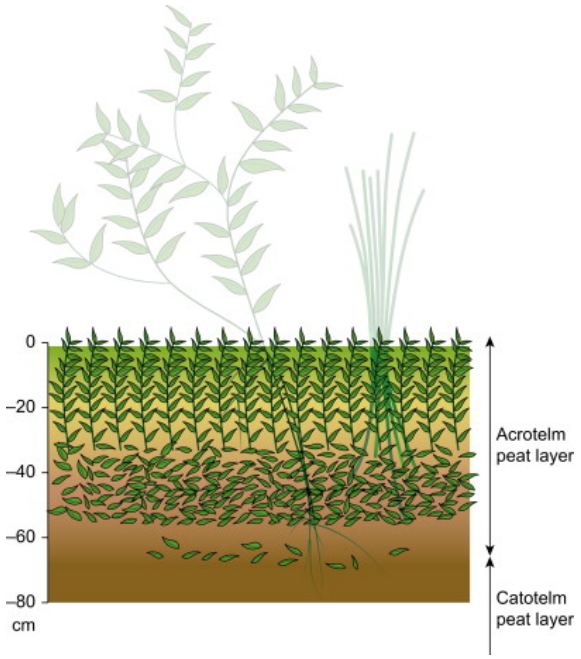


**Figure 3:** *Acrotelm and Catotelm peat layer*
*Source: Frandsen (1997)*

Next to mineralisation another type of transformation related to the decomposition of peat is humification. According to Klavins et al. (2008) the process relates to the production of humic acids. Humification is controlled by both the activity of soil micro-organisms and influence of wind and rain. Another factor that plays a role in peat decomposition is the pH. The rate of decomposition depends on the value of the pH, i.e. the higher the pH the faster decomposition will be. The pH of raised bogs is generally lower than the pH of fen plants, therefore fen plants decompose faster than bog peats. In a partially decomposed peat water is present both inside the fibres and in the peat material between the fibres. This distinction of water is relevant for the scope of the work.

An example of the mode of decomposition of a bog peat is shown in table 1.

| **Condition** | **pH** | **Mode of decay** | **Composition of main product** |
|---|---|---|---|
| Shallow water | 4.5-6.0 | In the top layers of peat bog.<br>Partial loss of cellulose. Hydrolysis and partial oxidation of lignin, and proteins. | C =50 %<br>H= 4.5 %<br>O= 44.7 %<br>N= 0.5 %<br>S= 0.3 % |
| Stagnant shallow water | 3.0-4.5 | Moderately deep in peat-bog.<br>Little aeration, less destruction of cellulose. | C =55 %<br>H= 5.5 %<br>O= 37.5 %<br>N= 1.5 %<br>S= 0.5 % |
| Lowest layer of peat deposit | 3.0 | Maximum depth of peat bog.<br>No aeration, maximum preservation of plant tissues. | C =60 %<br>H= 6.0 %<br>O= 29.0 %<br>N= 2.5 %<br>S= 2.0 % |

**Table 1:** *Example of decay of plant debris in a peat bog*
*Source: Francis and Peters (2013)*

### 4.3 Chemical composition plant tissue of peat

Mesri et al. (1997) used scanning electron micro photographs to illustrate the fibres of a peat from James Bay, northern Canada (fig.4). This study showed that the perforated particles present in the peat had a hollow structure. The fibres are assumed to have also a hollow structure which is either air-filled or water-filled.

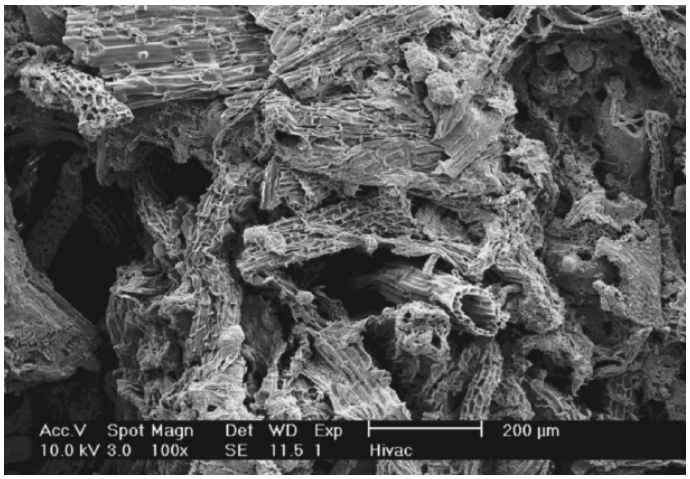


**Figure 4:** *Scanning electron micro photograph of a vertical section of James Bay peat showing network of fibres and perforated hollow particles*
*Source : Mesri et al. (1997)*

The above described peat particles are (decomposed) plant remains. These particles consist of various compounds, which are chains of organic molecules as shown in table 2.

| **Compounds present** | **Percentage of tissue in peat material** | **Average analysis %** | | | | | **Chemical formula** |
|---|---|---|---|---|---|---|---|
| | | C | H | O | N | S | |
| Cellulose | 45-65 | 44.4 | 6.2 | 49.4 | 0 | 0 | $(C_6H_{10}O_5)_n$ |
| Lignin | 20-40 | 63.2 | 6.1 | 30.7 | 0 | 0 | $C_{30}H_{33}O_{11}$ |
| Proteins | 12-25 | 53.5 | 7.0 | 22.0 | 15.5 | 2.0 | $C_{72}H_{112}N_{18}O_{22}S$ |
| Resins | 0.5-15.0 | 80.0 | 10.0 | 10.0 | 0 | 0 | $C_{20}H_{30}O_2$ |
| Waxes | 0.2-4.0 | 82.0 | 14.2 | 3.8 | 0 | 0 | $C_{29}H_{60}O$ |

**Table 2:** *The principal chemical components of plant tissue present in the material between the fibres of peat, their analyses and chemical formulae*
*Source: Francis and Peters (2013)*

These compounds are generally found in the decomposed matter present in the peat material between the fibres of peat. The decomposed matter is a product of wood and plant remains. The preserved fibres in peat consist of almost the same material: cellulose. The cell walls of the fibres can be divided into a primary wall and a secondary wall. Primary walls provide mechanical strength and expand allowing the cell to grow and divide. Pectin allows for primary cell wall extension and plant growth. In the primary wall hemi-cellulose is the most abundant compound, as shown in table 3. The secondary wall is thicker than the primary wall and consists of more lignin as shown in table 4. This compound fills the space between hemi-cellulose, cellulose, and protein (Chen (2014) and Kalluri et al. (2014)). A sketch of both the primary and the secondary cell wall with its compounds is shown in figure 5.

| Compounds present | Percentage of tissue | Chemical formula |
|---|---|---|
| Hemi-cellulose | 40 | $C_6H_{10}O_5$ |
| Cellulose | 30 | $(C_6H_{10}O_5)_n$ |
| Pectin | 30 | $C_6H_{10}O_7$ |

**Table 3:** *The representative compounds of the primary cell with their percentages and chemical formula present in the primary walls of the cells of a fibre*
*Source: Chen (2014) and Kalluri et al. (2014)*

| Compounds present | Percentage of tissue | Chemical formula |
|---|---|---|
| Hemi-cellulose | 25 | $C_6H_{10}O_5$ |
| Cellulose | 25 | $(C_6H_{10}O_5)_n$ |
| Lignin | 25 | $C_{30}H_{33}O_{11}$ |
| Protein | 25 | $C_{72}H_{112}N_{18}O_{22}S$ |

**Table 4:** *The representative compounds of the secondary cell with their percentages and chemical formula present in the secondary walls of the cells of a fibre*
*Source: Chen (2014) and Kalluri et al. (2014)*

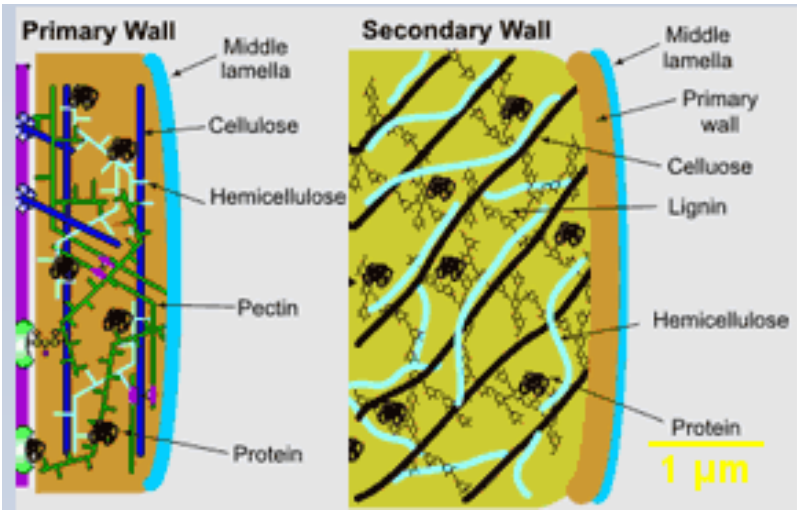


**Figure 5:** *Schematic representation of a plant cell divided into a primary wall and a secondary wall; The abundant compounds in both walls are given*
*Source: University of Georgia*

The fibres present in peat are (partly-decomposed) plant tissue such as roots, stems, grass, wood remains, and leaves. According to Davison et al. (2013) and Kramer (1955), cells of young roots and leaves can have a water content of up to 800 %. Mature stems and leaves of plants contain in general less water than the younger ones. Furthermore grass, seeds, and wood fragments contain less water. To quantify the water content of the cells walls of the fibres, the fibres shown in section 4.7 are dried. They had an average water content of 300%. Therefore, the cell walls of the fibres are assumed to have more or less the same water content.

## 4.4 Consequences of tissues on the behavior of peats compared to other geotechnical materials

Although the behavior and properties of both fibrous peats and inorganic soils are driven by the same mechanisms and factors, the engineering properties of fibrous peats are different from those of inorganic soils.
The high initial permeability of fibrous peats is the first difference between fibrous peats and inorganic soils. Permeability depends on the void ratio, pores and flow channels. The large permeabilities in fibrous peats are related to large void ratios, large pores and straight flow channels. Peats exist at high void ratios due to the porous peat particles and the little effect of overburden pressures on peat deposits. Only the permeability of clean sand is higher than those of fibrous peats due to their large mean pore sizes. The permeability of fibrous peats in vertical direction is typically 1,000 times the initial permeability of soft clay and clayey silts, which can be $10^{-9}$ m/s according to Mesri et al. (1997). However, the permeability of fibrous peats decreases as they compress under loads due to their compressibility. Mesri et al. (1997) proposed an empirical relation between $C_k$ and $e_0$. $C_k$ is the ratio of the gradient of void ratio e over the gradient of logarithm of the permeability in vertical direction $k_v$. This relation is shown below.

$$C_k = \frac{\Delta e}{\Delta log k_v} \tag{1}$$

To compare the behavior of fibrous peats within a general framework, Mesri et al. (1997) constructed a figure which displays the comparison of $C_k$ versus void ratio for five geotechnical materials (fig. 6). Higher values of the ratio of $C_k$ over $e_0$ correspond to more uniform pore sizes.

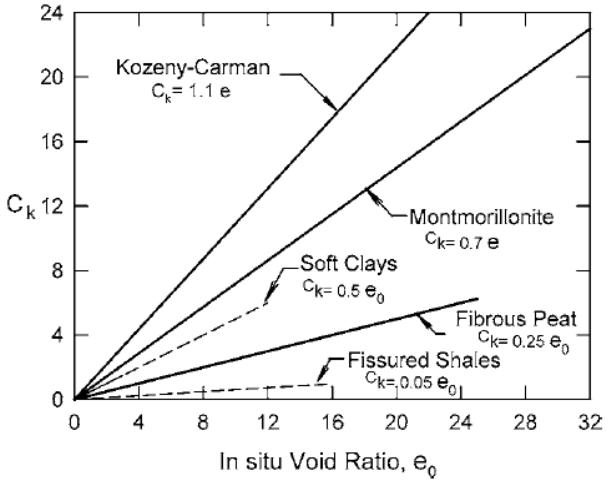


**Figure 6:** *$C_k$ plotted versus $e_0$ in terms of five geotechnical materials; The low values of the ratio of $C_k$ over $e_0$ for fibrous peat means non-uniform pore sizes in the soil. Source Mesri et al. (1997)*

The void ratio decreases because of closing of the macro pores which leads to a decrease in permeability.
Fibrous peats are extremely compressible due to present hollow cellular fibres and the large pores between plant remains. Compression of soils is divided into primary compression and

secondary compression. Primary compression relates to the increase of effective vertical stress whereas secondary compression occurs at constant effective stress. During primary and secondary compression water is expelled from both the peat fibres and the matrix (Mesri et al. (1997)).

Another distinctive characteristic of fibrous peats is the high friction angle compared to inorganic deposits. The values of the friction angle $\phi'$ for fibrous peats extracted from triaxial tests are found to be between 40 and 60°, whereas the values of $\phi'$ for clays and silts are around 35°. Sliding resistance and interlocking are causes of this high friction angle. Interlocking is a function of strength, size, shape and arrangement of soil particles. In the case of peats, tensile strength of the fibres increases significantly particle interlocking (Terzaghi et al. (1996)).

Due to the fibrous fabric, peats are frequently anisotropic. Zwanenburg and Barends (2005) focused on the anisotropy of the stiffness of peat. In the referred paper it is assumed that peat behaves cross anisotropic. This means that there is an axis of symmetry regarding the stiffness parameters, and the stiffness in both horizontal directions is different from the stiffness in the vertical direction. The anisotropic behavior of peat has three main reasons.
The first reason is anisotropy as a function of the geometry of the fibres of peat. The stiffness in main fibre direction is not the same as the stiffness in the direction perpendicular to the fibres. Since Zwanenburg and Barends (2005) assumed that the fibres are orientated in the horizontal direction, the stiffness in the horizontal direction differs from the stiffness in vertical direction.
Another cause for peat to behave anisotropic is the load-induced anisotropy because its stiffness is related to its stress level and rate of compression.
The third cause originates from the irreversible response upon loading and unloading. Upon unloading, the stresses in different directions will change in different ways.

## 4.5 Imaging peat fabric of fibrous peat

Several studies are done on imaging the fabric of dry and wet peat using X-ray micro CT. This technique is a 3D high resolution non-destructive visualization technique which will be described in chapter 5. The technique is based on a difference of the linear attenuation coefficient of the materials present in the peat. The coefficient is dependent on the density of the material, its atomic number and energy of X-rays. It works perfectly on dry peat because the density difference between pores and plant tissue together with peat material between the fibres is big, and therefore those can be distinguished easily.
According to Kettridge and Binley (2008) this technique does not work perfectly on wet peat because the linear attenuation coefficient of peat and water have shown to be indistinguishable within a CT-scan. Therefore, Kettridge and Binley (2008) recommended to prepare the peat samples prior to scanning. Flushing a peat sample with lead(II)nitrate have shown to be the most successful approach. Figure 7 shows that stems and branches are clearly identifiable in the resulting CT-images. In this figure, three threshold attenuation coefficients are shown for each peat slice. Kettridge and Binley (2008) identified the most appropriate threshold linear attenuation by doing so.

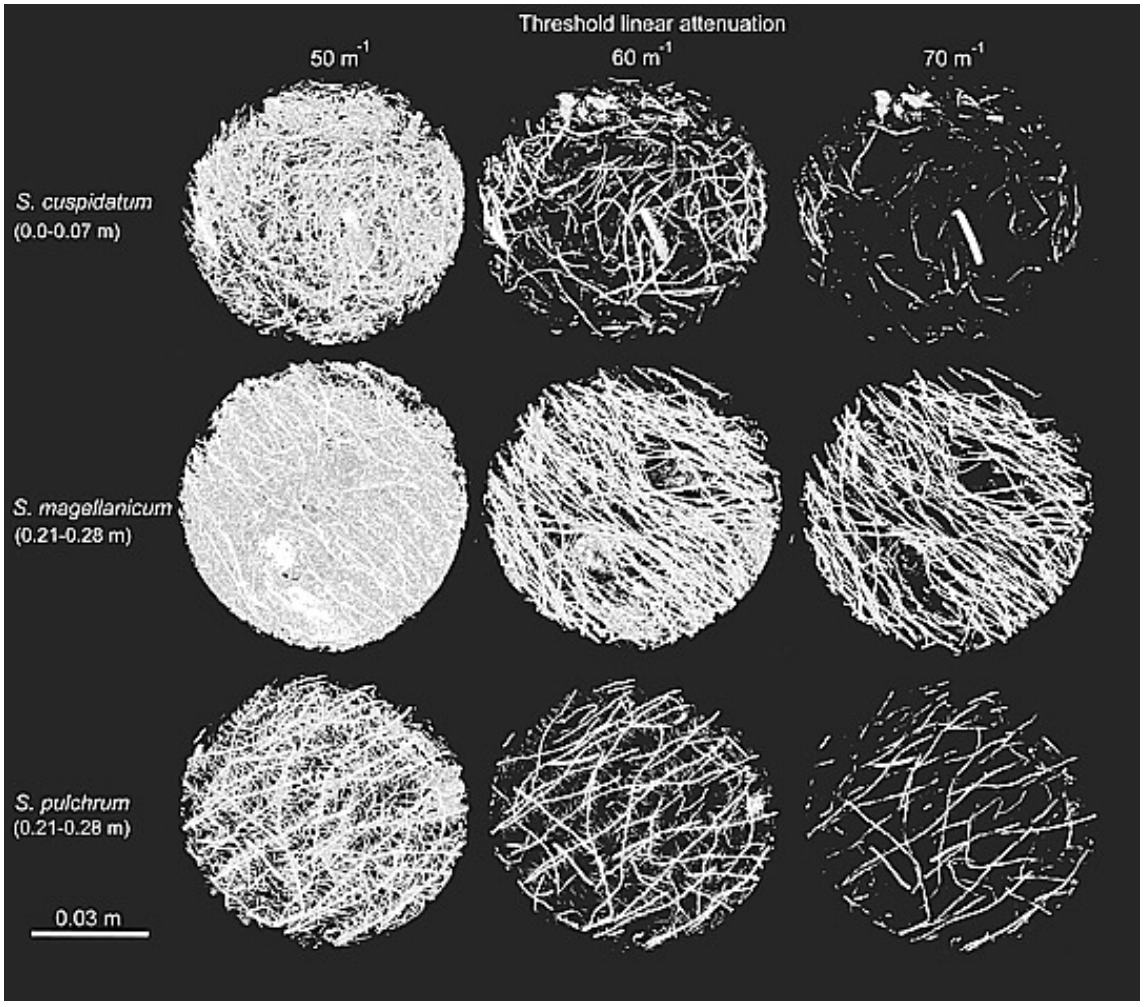


**Figure 7:** *Thin horizontal slices of three different peat cores;*
*Rows represent different threshold attenuations;*
*Vertical columns represent different peat types at different depths,*
*i.e. Sphagnum cuspidatum, Sphagnum mapeat material lanicum, and sphagnum pulchrum;*
*S. magellanicum sample is poorly decomposed whereas S. pulchrum is well*
*decomposed and S.cuspidatum is moderately decomposed;*
*Stems and branches are clearly visible.*
*Source: Kettridge and Binley (2008)*

The underlying process is according to Ho et al. (1999), the sorption capacity of plant tissue for lead ions. This process increased the linear attenuation coefficient of the tissues. Kettridge and Binley (2008) used a single threshold value of the linear attenuation coefficient between the peat material between the fibres and the sphagnum stems of the sample to distinguish these two.

The flushing approach outlined by Kettridge and Binley (2008) proved that X-ray micro CT is capable of identifying any organic matter of peat samples of a reasonable sample size, it showed also that the focus was limited on the larger organic constituents. This is the case when a defined peak of the linear attenuation coefficient is not identifiable. This can occur in a more decomposed peat when there are few significant structures visible within the X-ray CT images.

Next to flushing a peat sample with lead(II)nitrate and scanning it with a X-ray micro CT scanner, two other imaging methods can be tentatively applied to image the fabric of peat.

Neutron CT is the first technique which will be applied on a peat sample. Zarebanadkouki et al. (2015) described this tool to image water and root distributions in soils, the technique will be explained in section 5.1. Furthermore X-ray phase CT will be performed on a peat sample. According to Bertrand et al. (2012), the main advantage of this technique is edge enhancement especially for materials presenting a low contrast in attenuation. The technique will be explained in section 5.2.

## 4.6 Site location

In this research peat from a site close to the Markermeer, the Netherlands is used. Markermeer is a shallow 3 to 5 meters deep lake in the central Netherlands, in between North Holland, Flevoland and the IJsselmeer. It is used as a freshwater reservoir to prevent flooding and droughts. In 2003 water from the Markermeer was used to keep the dikes surrounding Amsterdam wet in order to keep them safe because of the drought during the summer.


**Figure 8:** *Location of Uitdam;*
*Label 1: Peat from Katwoude;*
*Label 2: Peat from Uitdam*
*Source: "Google Maps" 2018*

For this research two peats are imaged, i.e. Katwoude and Uitdam. The characteristics of both peats will be explained in the next section.

## 4.7 Characteristics of the peat used

Both peats are stored in a climate room to reduce bio degradation. In this room the temperature is kept at 13°C and the relative humidity RH is kept at 68 %.
The first characteristic of peat which is extracted is the water content. This is determined by using an oven to dry the peat at 60 °C for 48 hours. The water content is calculated three times for both peats in order to compensate for soil variability. Moreover the specific gravity $G_s$ of the soil is calculated. This index property is measured using a helium pycnometer in accordance with ASTM-D5550-14. Next to this property, the organic content of the soil is assessed by ignition in a furnace at 500 °C. All the properties are reported in the following table.

| **Type of peat** | **Water content** [%] | **Specific gravity**[-] | **Organic content** [%] |
|---|---|---|---|
| Katwoude | 320 | 1.49 | 93 |
| Uitdam | 708 | 1.46 | 94 |

**Table 5:** *Index properties of the to be tested peats*

By using a Leica Stereo Explorer microscope both peats can be magnified, this is shown in figure 9 and 10. In figure 9 the peat which is called Uitdam is shown. The peat material between the fibres is massive and speckled as shown at label 4. Label 3 represents these speckles which are most probably minerals formed during decomposition as mentioned in section 4.3. Furthermore label 1 represents a fragment of wood. The quality of the picture is not that good but this wood remain is most probably semi-decomposed. Label 2 displays a light brownish material. This material is a semi-decomposed remain of grass. The other small structures which are not clearly visible on this picture could be some fibres made of remains of seeds, twigs, and leafs.

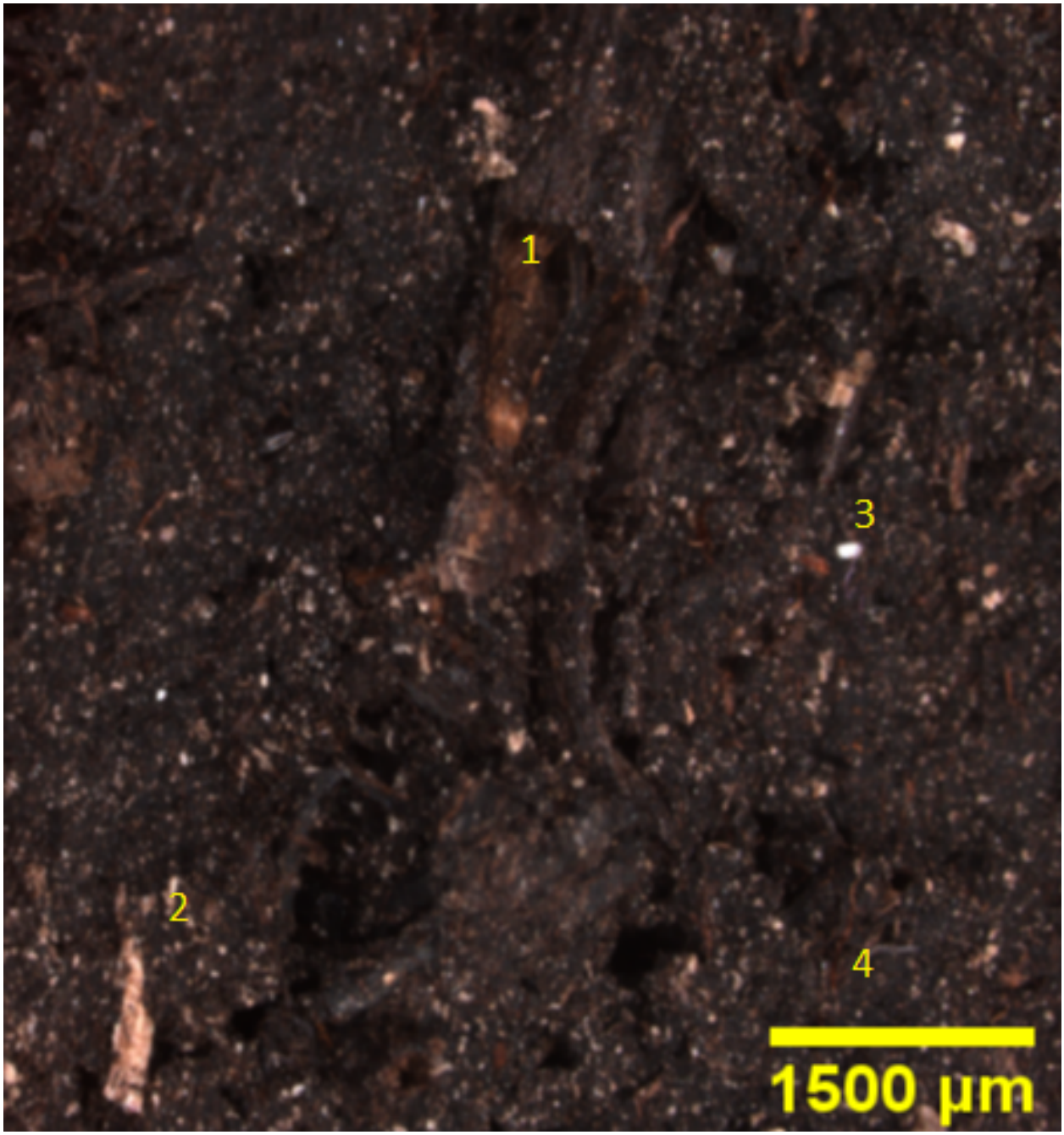


**Figure 9:** *Image of "Uitdam" peat using a Leica Stereo Explorer microscope.*
*Label 1 represents a big semi-degraded piece of wood;*
*Label 2 represents a light brownish remain of grass;*
*Label 3 represents a white speckle which is a mineral which has formed during decomposition of plant tissue;*
*Label 4 represents an example of the dark peat material between the fibres*

In peat of Katwoude lots of light brownish fragments are visible. The bigger fragments represents some remains of grass like label 1 shows, whereas the little brownish fragments represents fragments of grass. Label 2 represents the peat material between fibres and label 3 illustrates most probably a mineral which has formed during decomposition of plant tissue.

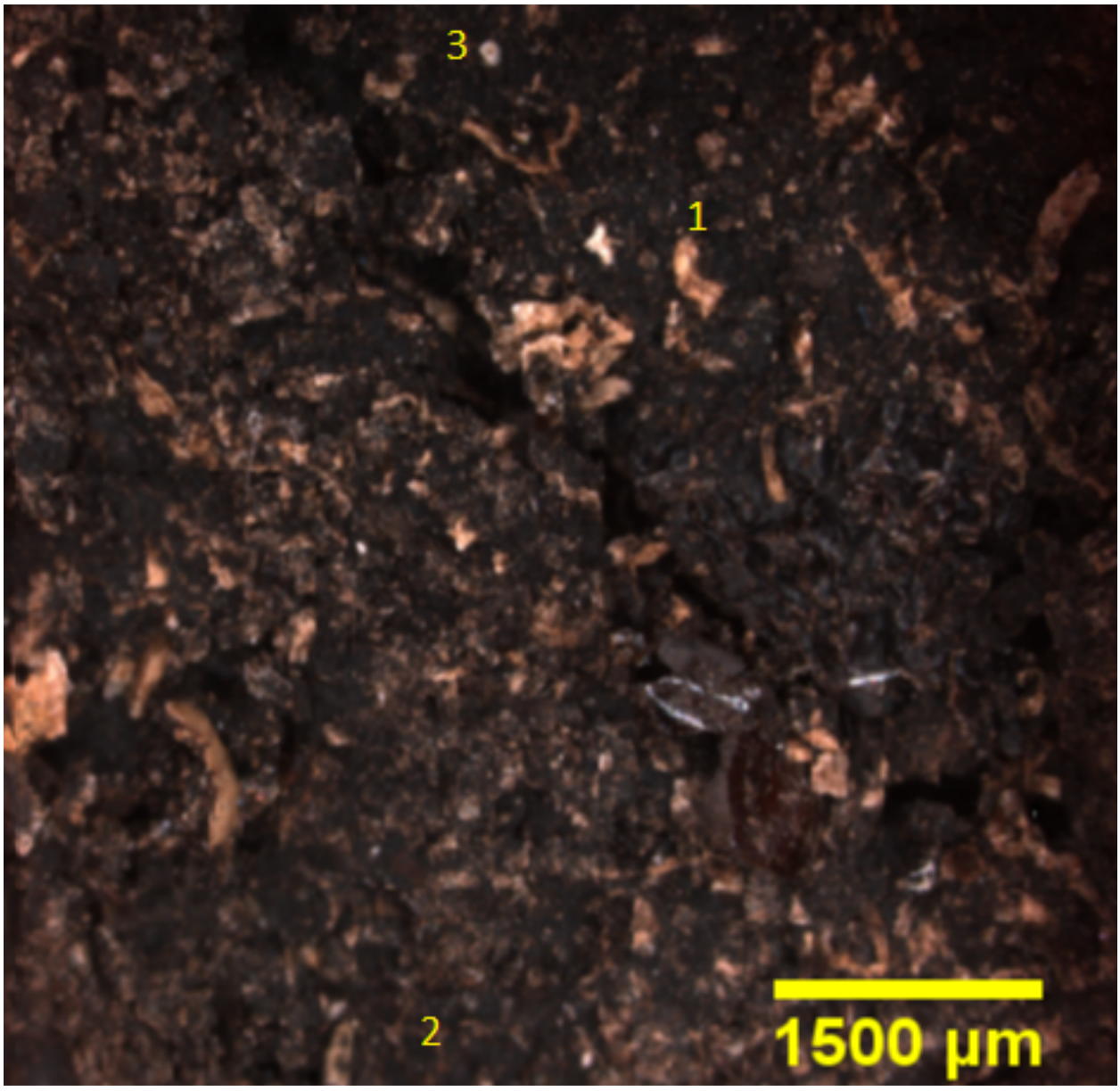


**Figure 10:** *Images of "Katwoude" peat using a Leica Stereo Explorer microscope.*
*Label 1 represents a remain of grass;*
*Label 2 represents the dark peat material between the fibres;*
*Label 3 shows a mineral which has formed during decomposition*

A sieving procedure is performed on the Uitdam peat which in order to illustrate the different types of fibres in peat. Figure 11 shows the remains of wood occurring in peat.


**Figure 11:** *Image of fragments of wood in Uitdam peat;*
*Fragments of wood occur at different sizes in the peat*

Furthermore some grassy material is found in this type of peat. The left picture of figure 12 shows the hairy grassy material. Label 1 shows that this material consists of small semi-decomposed hairy material. Furthermore label 2 shows a non-decomposed grass fibre. The right figure shows a small branch which occurs at different sizes in this type of peat.

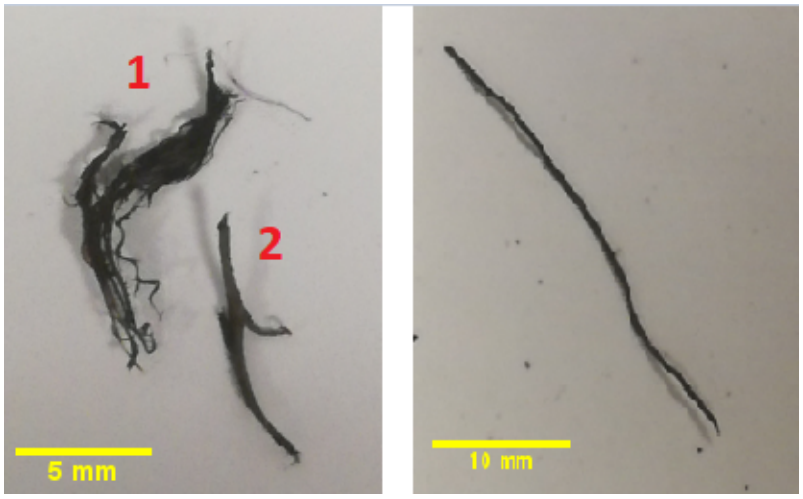


**Figure 12:** *Left: Image of grassy material found in Uitdam peat;*
*Right: image of a fragment of a branch in Uitdam peat;*

The material between the fibres of peat is a product (semi-)decomposed fibres and other organic material. This material is magnified using the Leica Stereo Explorer microscope as shown in figure 13.

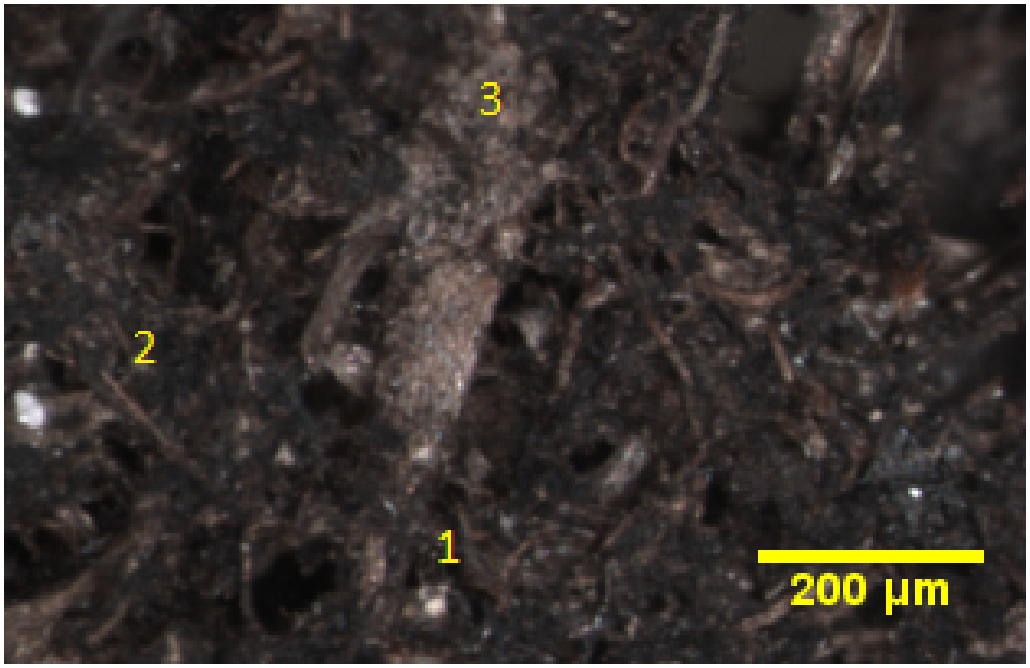


**Figure 13:** *Magnified peat material present between the fibres;*
*Label 1 shows a mineral;*
*Label 2 shows a remain of a grassy hairy fibre or branch;*
*Label 3 shows a remain of wood*

In the peat material minerals are found such as observed in figure 9, i.e. label 1. Furthermore lots of small fibres can be found representing label 2. It seems that this material consists of the remains of the grassy hairy fibres and branches showed in figure 12. Finally, label 3 shows a remain of wood which is brown in color.

## 4.8 Objectives and problem definition

The thesis objective is to image the fabric of peat coming from a site close to Markermeer, using neutron CT, X-ray CT and X-ray phase CT. Knowledge of the internal fibrous peat fabric is important to predict its behavior under loading conditions.
Following from the issues related to the success of the objective there are a number of research questions, such as: (1) Could the orientation and length of fibres be extracted out of the image data? (2) What type of fibres are presented in the peat: air-filled, water-filled or both? (3) Are there any differences to be observed by comparing X-ray phase CT and X-ray micro CT on the peat? (4) What is the next step to increase the knowledge of the behaviour of fibres under loading conditions?

In case wet peat cannot be properly imaged, dry peat will be used and the same research questions will be answered.

## 4.9 Hypothesis

"Neutron CT using the neutron beam at the Reactor Institute Delft (RID) is a better technique to image the fabric of peat than micro X-ray CT and X-ray phase CT."

## 4.10 Thesis outline

Firstly, chapter 5 describes the three different imaging techniques to image the fabric of peat, i.e. neutron CT, conventional X-ray micro CT and X-ray phase CT. In this chapter the theoretical attenuation coefficients of the different materials in peat are described as well. This coefficient describes the interaction of neutrons or X-rays with the present materials in peat per unit of thickness. Furthermore, this chapter describes the previous research performed on imaging plant tissue using both neutron CT and X-ray phase CT. Chapter 6 briefly explains the imaging equipment which will be used to image the fibres in peat. The workflow to image the fibres is shown in chapter 7. This chapter describes also the first trials performed on different peat samples using neutron radiography, which is used to determine the transmission of neutrons. Transmission is an inverse function of the attenuation coefficient, since peat has a high water content (which has a high attenuation coefficient), the resulting transmission of neutrons is low. A saturation process to saturate the peat sample with heavy water to decrease the attenuation coefficient did not work out. Therefore, a flushing procedure was performed to flush the peat with heavy water. This is described in chapter 8. Since this procedure proved to work out, the resulting reconstructed tomographic images were filtered using a 3D data visualization software, called Avizo. This is described in chapter 9. This chapter describes also the comparison of the neutron CT images with the X-ray micro CT images of the same sample. Furthermore, X-ray phase CT on a peat sample is explained in subsection 9.3. This scan was performed to reveal more fibres present in the peat compared to the previous scans.
Finally, the thesis is finished with a discussion, conclusions and recommendations.

# 5 Imaging techniques

To image the fibres of peat, three different imaging techniques will be used and are explained below: neutron CT, X-ray CT and X-ray phase contrast CT imaging.

## 5.1 Thermal neutron imaging

Zarebanadkouki et al. (2013) described the imaging technique neutron radiography as a tool to image water and root distribution in soils. This technique uses a neutron beam to image a sample. The transmitted beam gives information about the composition and thickness of the sample. Neutrons are neutrally charged and generally interact with light materials and penetrate in heavy materials. There are different type of neutrons, thermal and fast neutrons have in general a wavelength between $10^{-9}$ and less than $2.0 * 10^{-10}$ meter. The interaction and penetration are governed by the law of attenuation of radiation passing through a physical substance.

The law of attenuation is described by the Beer-Lambert law:

$$T = \frac{I}{I_0} = \exp - \sum_{i=1}^{i=n} (\Sigma_i d_i) \tag{2}$$

Here, $T$ is the transmission of the neutrons, $I$ the transmitted intensity of the beam $[m^{-2}s^{-1}]$, $I_0$, the intensity of the neutron beam at start $[m^{-2}s^{-1}]$, $d_i$, the thickness of the imaged sample$[m]$ and $\Sigma_i$, the macroscopic attenuation coefficient$[m^{-1}]$, which is a function of the interactions of neutrons with available materials per unit of thickness. This coefficient can be calculated using the different microscopic cross-sections found at the website of the National Institute of Standards and Technology(NIST).

The microscopic cross-section describes all processes between, in this case, neutrons and an atom. The equation for the calculations of the microscopic cross-section ($\sigma_{eff}$; $[cm^2]$) of an atom includes the sum of both the scattering and absorption cross-sections, i.e.

$$\sigma_{eff} = \sigma_{el} + \sigma_{in} + \sigma_{ab} \tag{3}$$

Here $\sigma_{el}$ is the elastic scattering cross-section, $\sigma_{in}$ the inelastic scattering cross-section and $\sigma_{ab}$ is the absorption cross-section (Bertrand et al. (2012)).

Before imaging peat with thermal neutrons, the macroscopic attenuation coefficients $\Sigma$ of both water and plant tissue are calculated. The coefficient of water is calculated because the water content of peat is high. For the calculation of the macroscopic attenuation coefficient of decomposed plant tissue present in the peat material between the fibres, table 2 of section 4.3 is used. For the macroscopic attenuation coefficient of non-decomposed plants cells in peat, table 3 and 4 of section 4.3 are used. Next to the calculations of the macroscopic attenuation coefficients of water and plant tissue, the coefficient for heavy water is calculated. This value is expected to be considerably lower than that of water and plant tissue because heavy water is almost transparent to neutrons, and therefore less absorbing than water and plant tissue. This is of importance for imaging peat because the goal is to get a contrast between the fibres and the fine peat material. The transmission of neutrons also depends on the thickness of the imaged sample as can be seen from equation 2. The smaller the sample the higher the transmission should be. This is of interest for chapter 7.

### 5.1.1 Attenuation coefficient

In order to calculate the macroscopic attenuation coefficient Σ, which corresponds to the total "equivalent area" of all target particles per unit volume, the microscopic cross-section needs to be divided by the atomic density Q.

$$Q = \frac{M}{\rho} \tag{4}$$

The final equation for determining the attenuation coefficient is shown below.

$$\Sigma = \frac{N_A * \sigma_{eff}}{Q} \tag{5}$$

Here, Σ is the attenuation coefficient $[cm^{-1}]$, $N_A$ is $6.022 * 10^{23}\ mol^{-1}$, $\sigma_{eff}$ is the microscopic cross-section$[cm^2]$, and Q is the ratio of the molar mass over the density of the molecule $[cm^3/mol]$

By knowing this, it is possible to calculate the theoretical attenuation coefficient of the peat material between the fibres of peat.

### 5.1.2 Theoretical attenuation coefficient of peat material between the fibres of peat

As described in section 4.7, the decomposed material is present in the peat material between the fibres. Following from the water content of around 700% given in section 4.7, the ratio between water and the decomposed organic matter can be estimated. The attenuation coefficient Σ of the peat material between the fibres is then empirically described using equation 6.

$$\Sigma_g = \frac{7}{8}\Sigma_w + \frac{1}{8}\Sigma_p \tag{6}$$

Here, $\Sigma_g$ is the attenuation coefficient of the peat material between the fibres $[cm^{-1}]$ which depends on the attenuation coefficient of water $\Sigma_w$, and the attenuation coefficient of decomposed plant tissue $\Sigma p$.

To calculate the attenuation coefficient of both water and decomposed plant tissue, the microscopic cross-section, molar mass and density of the representing compounds are needed following from equation 4 and 5 from the previous subsection.

In table 6 the values of the microscopic cross-sections and the atomic weight of atoms of natural water can be found.

| **Element** | **Atomic weight [g/mol]** | $\sigma_{el}$ $[10^{-24}\ cm^2]$ | $\sigma_{in}$ $[10^{-24}\ cm^2]$ | $\sigma_{ab}$ $[10^{-24}\ cm^2]$ |
|---|---|---|---|---|
| H | 1.0 | 1.757 | 80.260 | 0.330 |
| O | 16.0 | 4.232 | 0.001 | 0.000 |
| $H_2O$ molecule | 18.0 | 7.746 | 160.521 | 0.660 |

**Table 6:** *Input parameters for computing the macroscopic attenuation coefficient of natural water($H_2O$)*

The attenuation coefficient is calculated at 5.65 $cm^{-1}$.

Based on table 2 the average attenuation coefficient of the decomposed plant tissue can be calculated. First, the effective macroscopic attenuation coefficient $\sigma_{eff}$, is calculated for each element present in the compounds of the particles (table 7).

| **Elements** | **Atomic weight [g/mol]** | **Microscopic cross sections** $[10^{-24}\ cm^2]$ | | | |
|---|---|---|---|---|---|
| | | $\sigma_{el}$ | $\sigma_{in}$ | $\sigma_{ab}$ | $\sigma_{eff}$ |
| C | 12.0 | 5.551 | 0.001 | 0.0035 | 5.6 |
| H | 1.0 | 1.757 | 80.260 | 0.330 | 82.4 |
| O | 16.0 | 4.232 | 0.001 | 0.000 | 4.2 |
| N | 14.0 | 11.01 | 0.5 | 1.9 | 13.4 |
| S | 32.0 | 1.019 | 0.007 | 0.53 | 1.6 |

**Table 7:** *The representative elements present in the compounds of the plant and wood tissue with its atomic weight and microscopic cross sections*

The molar mass of the compound can be computed using table 7 by multiplying the index number of the element in the compound with the atomic weight of the element, and the density $\rho$ of the compounds is found in Stamm (1929) and Guimaraes et al. (2008). The final average attenuation coefficient can be calculated using the percentages of tissue in the peat material. This percentage is averaged using table 2 to one value in a way that by adding them up the final percentage is 100.

| **Compounds present** | **Percentage of tissue** | **Chemical formula** | **Molar mass** $[g/mol]$ | $\rho$ $[g/cm^3]$ | $\Sigma$ $[cm^{-1}]$ |
|---|---|---|---|---|---|
| Cellulose | 50 | $(C_6H_{10}O_5)_n$ | 162 | 1.5 | 4.9 |
| Lignin | 30 | $C_{30}H_{33}O_{11}$ | 569 | 1.45 | 4.5 |
| Water and proteins | 14 | $C_{72}H_{112}N_{18}O_{22}S$ | 1612 | 1.35 | 5.0 |
| Resins | 5 | $C_{20}H_{30}O_2$ | 302 | 1.1 | 5.7 |
| Waxes | 1 | $C_{29}H_{60}O$ | 424 | 1.2 | 5.5 |

**Table 8:** *The representative compounds of the plant and wood tissue with its molar mass, density and computed macroscopic cross sections*

The average attenuation coefficient $\Sigma$ of the (dry) decomposed plant tissue is 4.90 $cm^{-1}$.

By using equation 6, the estimated value of the macroscopic attenuation coefficient $\Sigma_{pm}$ of the peat material between the fibres is 5.6 $cm^{-1}$. This value means that the neutrons will be absorbed by the peat material between the fibres during neutron radiography according to the Beer-Lambert which was introduced in section 5.1.

### 5.1.3 Average theoretical attenuation coefficient the cell walls of the fibres

As described in section 4.3, a cell wall consists of a primary cell wall and a secondary cell wall. The primary wall consists of hemi-cellulose, cellulose and pectin. The percentages, chemical formula, molar mass, density and microscopic attenuation coefficient are shown in table 9.

| **Compounds present** | **Percentage of tissue** | **Chemical formula** | **Molar mass** $[g/mol]$ | $\rho$ $[g/cm^3]$ | $\Sigma$ $[cm^{-1}]$ |
|---|---|---|---|---|---|
| hemi-cellulose | 40 | $C_6H_{10}O_5$ | 162 | 1.50 | 4.9 |
| cellulose | 30 | $(C_6H_{10}O_5)_n$ | 162 | 1.50 | 4.9 |
| pectin | 30 | $C_6H_{10}O_7$ | 194 | 1.52 | 4.2 |

**Table 9:** *The representative compounds of the primary cell wall with its molar mass, density and computed macroscopic cross sections*
*Source: Chen (2014) and Kalluri et al. (2014)*

By using equation 5, the compounds present in the primary cell wall have an average attenuation coefficient $\Sigma$ of 4.7 $cm^{-1}$.

The secondary cell wall consists of hemi-cellulose, cellulose, lignin and protein. In general the compounds are present in an equal amount in the cell wall.

| **Compounds present** | **Percentage of tissue** | **Chemical formula** | **Molar mass** $[g/mol]$ | $\rho$ $[g/cm^3]$ | $\Sigma$ $[cm^{-1}]$ |
|---|---|---|---|---|---|
| hemi-cellulose | 25 | $C_6H_{10}O_5$ | 162 | 1.50 | 4.9 |
| cellulose | 25 | $(C_6H_{10}O_5)_n$ | 162 | 1.50 | 4.9 |
| lignin | 25 | $C_{30}H_{33}O_{11}$ | 569 | 1.45 | 4.5 |
| protein | 25 | $C_{72}H_{112}N_{18}O_{22}S$ | 1612 | 1.35 | 5.0 |

**Table 10:** *The representative compounds of the secondary cell wall with its molar mass, density and computed macroscopic cross sections*
*Source: Chen (2014) and Kalluri et al. (2014)*

The compounds present in the secondary cell wall have an average attenuation coefficient $\Sigma$ of 4.8 $cm^{-1}$. This is almost the same as the attenuation coefficient for the compounds present in the primary cell. Therefore the value of 4.8 $cm^{-1}$ is chosen to be the average attenuation coefficient of the compounds present in the cell wall. As described in section 4.3, the water content of the cell walls of the fibres is determined at 300 %. Based on this water content the empirical equation of the attenuation coefficient of the cell wall can be described using equation 7.

$$\Sigma_{cw} = \frac{3}{4}\Sigma_w + \frac{1}{4}\Sigma_c \tag{7}$$

Here, $\Sigma_{cw}$ is the attenuation coefficient of the cell wall $[cm^{-1}]$ which consists of the attenuation coefficient of water $\Sigma_w$, and the attenuation coefficient of the compounds present in the cell wall $\Sigma c$.

Inserting the attenuation coefficient of both water and the compounds present in the cell wall in equation 7, the average attenuation coefficient of the cell wall is 5.4 $cm^{-1}$. This means that the cell walls of the fibres interact with neutrons almost in the same way as

the peat material between the fibres does, and therefore there will be no contrast to be observed between between the peat material between the fibres and fibres using neutron radiography. By replacing the water present in the peat material between the fibres and free water in the peat by a liquid which has a low macroscopic attenuation coefficient in such a way that the peat fibres remain full of natural water or air. Heavy water is such a liquid with a low macroscopic attenuation coefficient.

### 5.1.4 Theoretical attenuation coefficient of heavy water ($D_2O$)

The same calculation for the microscopic cross-section and for the macroscopic attenuation coefficient for heavy water is performed as for natural water. This results in a macroscopic attenuation of 0.65 $cm^{-1}$ for heavy water. Table 11 displays the different attenuation coefficients for the described materials.

| **Material** | **Macroscopic attenuation coefficient** $[cm^{-1}]$ |
|---|---|
| $H_2O$ molecule | 5.65 |
| $D_2O$ molecule | 0.65 |
| Peat material | 5.60 |
| Cell wall | 5.40 |

**Table 11:** *Attenuation coefficients of different materials present in peat and heavy water ($D_2O$)*

In order to have a contrast between the peat fibres present in peat and peat material between the fibres in peat using thermal neutrons, the present water in the peat material between the fibres needs to be exchanged most probably with heavy water. In order to better understand the role of heavy water on neutron CT, a previous research performed by Zarebanadkouki et al. (2015) is briefly explained in the next subsection.

### 5.1.5 Previous research on imaging plant tissue with neutrons

Zarebanadkouki et al. (2015) used neutron CT to better understand the behavior of roots during uptake of water from soils. In this paper neutron tomography was used to monitor the flow of heavy water into a lupine root. This root was grown in a sandy-silt mix for 10 days. Figure 14 shows the cross-section of the sample. Here, the intensity of the color gives information about the attenuation coefficient. The more blue, the higher the heavy water content and the lower the attenuation coefficient as shown on the legend of the figure.

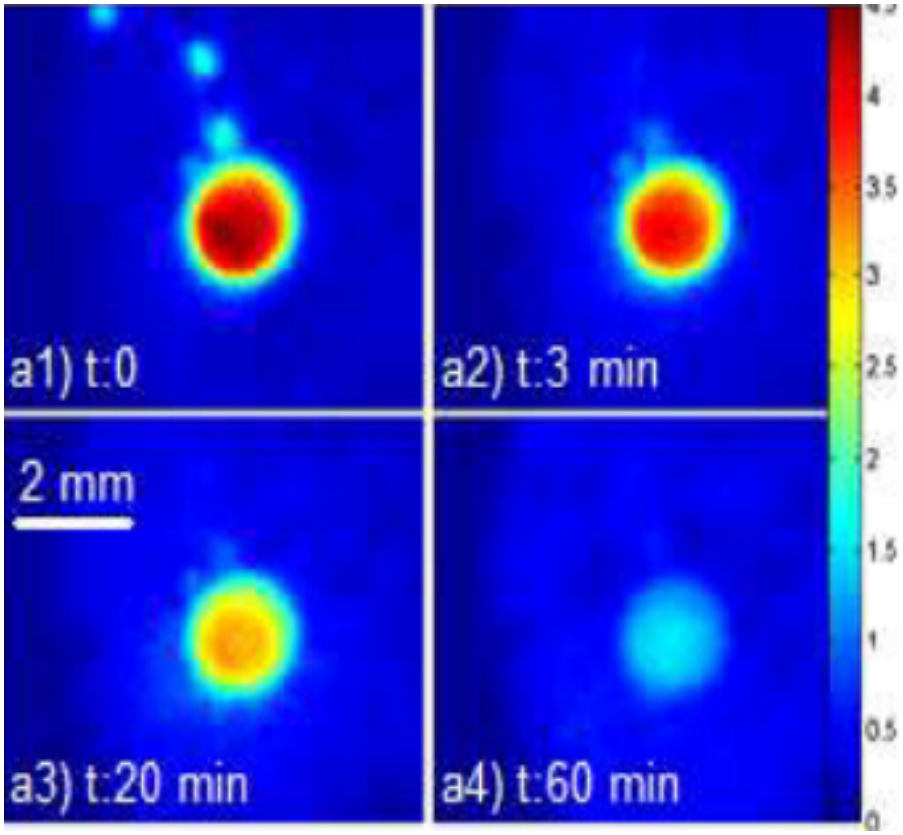


**Figure 14:** *Horizontal cross section of a 10 day old lupine root.*
*Here the neutron attenuation coefficient is displayed at different times after $D_2O$ injection, the colour bars refers to the neutron attenuation coefficient*
*Source: Zarebanadkouki et al. (2015)*

As one can see, the lupine root takes up heavy water in time resulting in a lower attenuation coefficient in the roots. So Zarebanadkouki et al. (2015) proved that neutron CT can be used to study the flow of water across a root tissue. As shown in subsection 4.7 no roots are found in the to be imaged peat and therefore it is not clear what the influence of heavy water will be on the peat samples. Ideally heavy water, as shown in the research of Zarebanadkouki et al. (2015), will be a good contrast agent assuming that fibres remain full of natural water or air inducing a contrast in attenuation between the fibres and the peat material between the fibres.

## 5.2 X-rays

X-rays have a wavelength between $10^{-9}$ and $10^{-10}$ meter which is 1000 times shorter than the wavelength of visible light. This means that the resolution with X-rays is higher than with visible light.

### 5.2.1 Basics of X-ray interaction with matter

X-rays have a high penetration depth and therefore they are useful to investigate the fibres of peat. X-rays will travel in straight lines through the peat because its interaction with peat(light elements) is weak.

The X-rays interact mainly with the electron shell of the present atoms in peat. According to Van Geet et al. (2000) CT images show the differences in density and the composition of peat using X-rays. X-rays interact in a similar way as neutrons with peat. This is described in equation 8.

$$n(Z, E) = 1 - \delta(Z, E) + i\beta(Z, E) \tag{8}$$

Here, $n$ is the index of refraction. This index describes the absorption and scattering of X-rays with peat. Furthermore $Z$ is the atomic number of the compounds present in the peat, $E$ is the energy in Electron Volt, $\beta$ is related to the photo-electrical cross-section, and $\delta$ is related to the electron density. When the propagation distance between the object and the detector is small, this refraction effect can be neglected. The obtained contrast primarily results from the decreased intensity of the X-ray beam traversing sample, according to Beer-Lambert law described in section 5.1.

The linear attenuation coefficient is related to $\beta$ as described in equation 9.

$$\mu_i = \frac{4\pi\beta}{\lambda} \tag{9}$$

Here $\lambda$ is the wavelength of the X-ray wave. The linear attenuation coefficient is dependent on the atomic number $Z$.
This leads to a contrast between compounds with different densities.

Equation 3 of the previous section is used to describe the total X-ray interaction cross-section between X-rays and an atom.

The interaction processes between X-rays and peat are shown in figure 15.

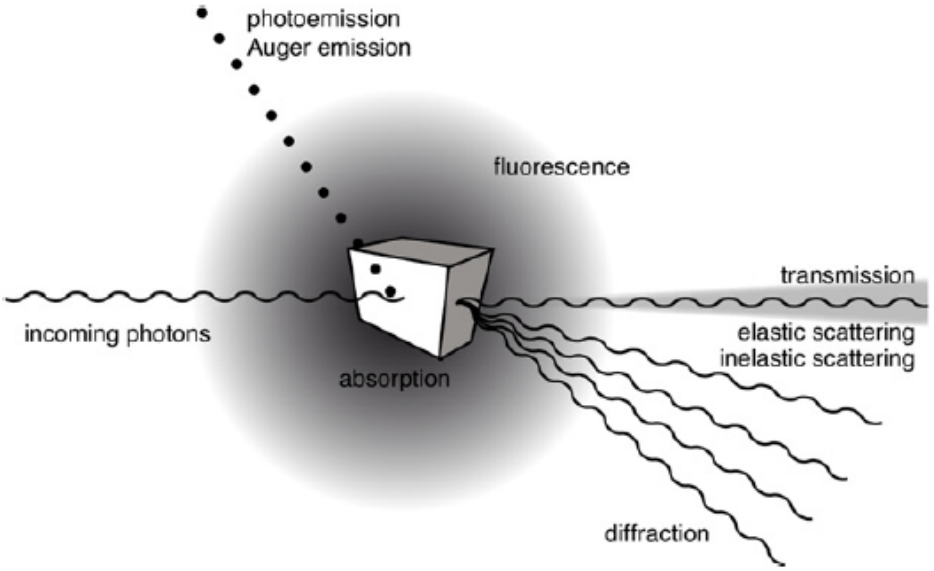


**Figure 15:** *Main interaction processes present in X-ray (photons) interaction with matter*
*Source: Bertrand et al. (2012)*

Peat consists of light elements therefore the refraction angle $\alpha$ will be small. However, by using phase contrast techniques this angle can be found. This angle is related to the gradient of the phase $\phi(x, y)$ of the refracted beam:

$$\alpha_x = \frac{\lambda}{2\pi} \frac{\delta\phi(x, y)}{\delta x} \tag{10}$$

Here, $\delta$ is related to the electron density $\rho_e$ according to:

$$\delta = \frac{r_0 \rho_e \lambda^2}{2\pi} \tag{11}$$

Here, $r_0$ is the electron radius.

The next figure displays the X-ray phase contrast CT setup. In this setup absorption and the free space of the X-ray beam is shown. Furthermore a schematic representation is shown of a sample with its absorption and phase contrast projections.

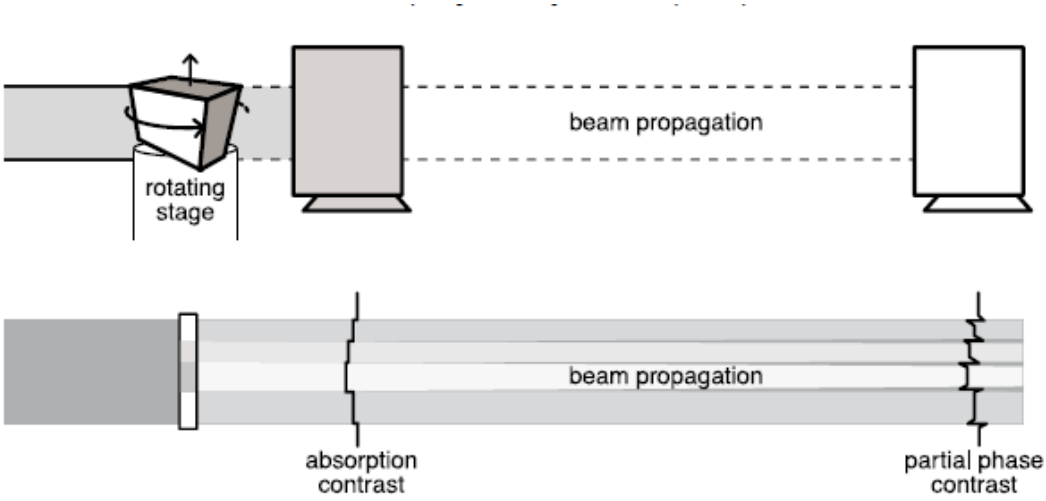


**Figure 16:** *(top) Phase contrast tomographic microscopy setup; Here, the detector can be moved closer and further away from the sample; (bottom) The phase contrast and absorption projections represented with a sample; Source: Bertrand et al. (2012)*

### 5.2.2 Different X-ray phase contrast techniques

As described in the previous section, the detection of the refraction angle and the refraction of the X-ray beam is the main goal of X-ray phase contrast techniques. Bertrand et al. (2012) divided the X-ray phase contrast technique into three categories: free-space propagation, interferometry and analyzer systems.

Free-space propagation displays a high spatial resolution and its setup can be easily done. Next to those advantages, edge enhancement can occur using free-space propagation. This effect becomes more clear using larger propagation distances. Edge enhancement increases the visibility of the internal boundaries of a sample, which is useful when imaging the fabric of peat.

Other approaches for phase retrieval use only one sample-detector distance. According to Wilkins et al. (1996) and Bertrand et al. (2012) the image contrast is sufficient to segment and post process images using this fixed distance for low absorbing materials like peat. This method will be performed on a peat sample at the Ghent University Centre for X-ray CT. Although these methods are not fully quantitative and are based on assumptions like a homogeneous composition of the scanned material as stated in Paganin et al. (2002), and the negligible absorption of the material stated in Groso et al. (2006). If one wants a fully quantitative result for a peat sample, tomographic data sets at multiple distances are acquired. However, this takes a lot of time to post process and segment the images.

The other above mentioned phase contrast methods are not used due to their demanding setups. Although they give decent results as well.

### 5.2.3 Previous research on imaging plant tissue with X-ray phase CT

Karunakaran et al. (2015) used X-ray phase contrast imaging to image plants. Plant parts and roots of a canola plant were scanned. In this paper it is concluded that phase contrast imaging results in good images to study the dynamic processes in plants. In order to compare X-ray absorption imaging with X-ray phase contrast imaging the stem of the canola plant was recorded with both techniques (fig. 17).

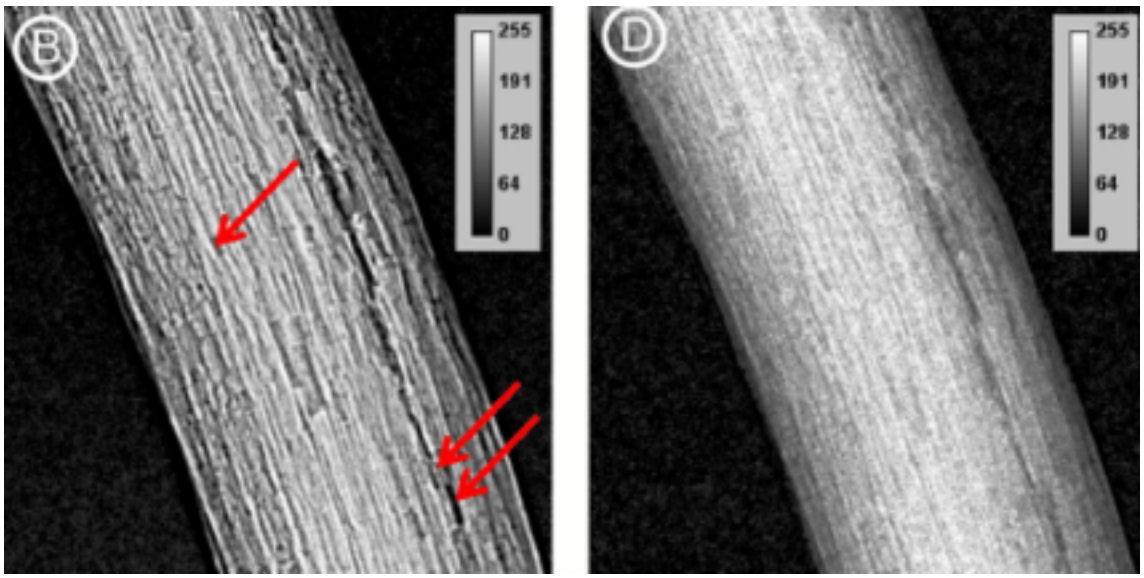


**Figure 17:** *Left: X-ray phase radiograph of a plant stem;*
*Right: X-ray absorption radiograph of the same stem;*
*The arrows indicate the vessels in the stem.*
*Source: Karunakaran et al. (2015)*

The phase contrast technique showed more line profiles across the stem as shown in figure 17. Furthermore the vessels in the stem were more distinct using phase contrast. The goal of Karunakaran et al. (2015) was also to compare both techniques while applying them on a so-called below ground level sample in order to image the soil root system. However, the difference between the X-ray phase contrast images and X-ray absorption images was not clear. Previous studies like, Seignez et al. (2010), showed that soil structure, density and porosity are of influence on the quality of the image. Karunakaran et al. (2015) concluded that a soil with a high organic content displays less contrast because of absorption of X-rays. Therefore, Karunakaran et al. (2015) put a root in a sandy loam sample. The result was a good contrast between the soil and the root because sandy loam has a low organic matter content.
Based on those findings imaging peat with the X-ray phase contrast technique could potentially result in a low contrast because peat has a high organic matter content.

# 6 Equipment to image the peat samples

As described in the previous section, there are three techniques to image the fibres of peat. The neutron CT procedure will be performed in the thermal neutron imaging station in Delft. This imaging station is explained in section 6.1. Furthermore, the peat will be scanned using a X-ray Micro CT scanner which is present in the geoscience section at Delft University of Technology. The properties of this scanner are described in section 6.2. Another X-ray micro CT scanner is present in Ghent, which is developed by the Ghent University Centre for X-ray CT. This scanner will also be used as a X-ray phase contrast scanner, and is described in section 6.3.

## 6.1 Thermal neutron imaging station at TU Delft

In this section the thermal neutron imaging station is described. This neutron imaging station is present at the Reactor Institute Delft (RID). This reactor is 2.3 Mega Watt swimming-pool type and is operated for more than 50 years as a source of neutrons and positrons. The reactor is mainly used for education and research purposes. The neutron imaging station which is used for this thesis is called FISH. Different sections of the university of Delft benefits from the neutron imaging and CT possibility in FISH to do non-destructive investigations (Zhou et al. (2018)).

The top-view of FISH is shown in the next figure (fig. 18).

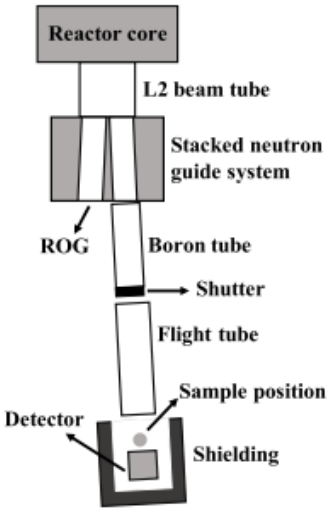


**Figure 18:** *Top-view lay-out of the neutron imaging station called FISH Source: Zhou et al. (2018)*

The average neutron flux density is $3*10^6\ cm^{-2}s^{-1}$ at the sample position stage. Furthermore, the wavelength of the thermal neutrons is $1.8*10^{-10}$ meter. The setup of FISH can be found in figure 19.

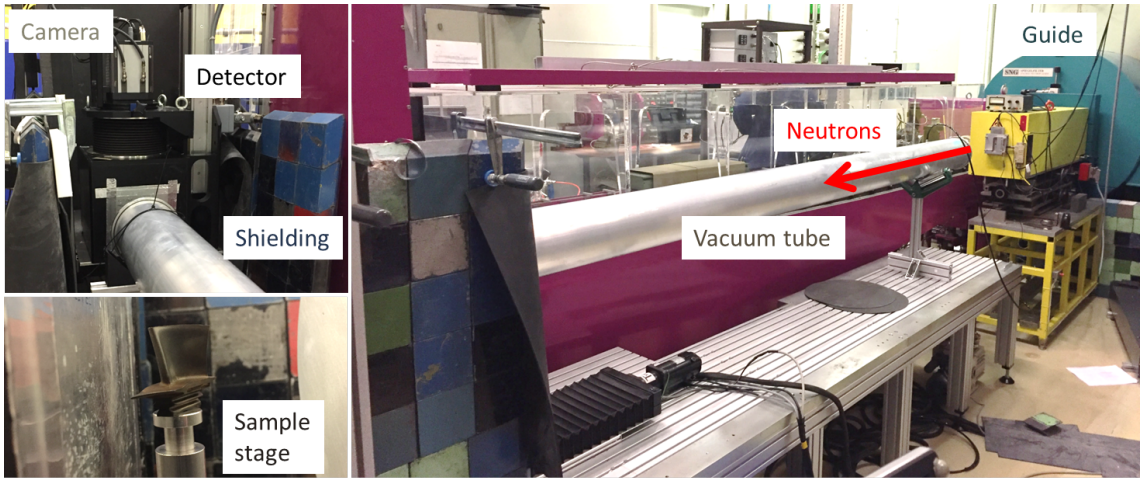


**Figure 19:** *FISH setup on L2 beam line*
*Source: Zhou et al. (2018)*

Zhou et al. (2018) described the detector system as a system based on scinitillators coupled to a CCD/sCMOS camera. A scintillator emits visible light which is reflected by mirror and it absorbs neutrons.

The voxel size of FISH is about 50 $\mu$m and the effective spatial resolution is 150 $\mu$m because at least 3 pixels are needed to distinguish an edge. The tomographic measurements which are performed in FISH consists of an X-number of projections, 10 dark current and 10 open beam images. Each image has an exposure time of 70 s. The images are reconstructed by using Octopus software.

## 6.2 Nanotom high resolution X-ray micro-CT scanner at TU Delft

This section describes the micro-CT scanner Phoenix Nanotom which is present at the department of geoscience and engineering at Delft University of Technology. The scanner is shown in figure 20.


**Figure 20:** *Phoenix nanotom micro-CT scanner.*
*Source: Baker Hughes a GE Company*

The nanotom scanner uses a phoenix with a voltage of 180 kV with a power of 15 Watt. The tube is internal cooled which reduces thermal effects. The detector area is 3072 x 2400 pixels which allows sample size of up to 250 x 240 $\mu$m.

## 6.3 Hector X-ray micro-CT scanner at Ghent University

This section describes the micro-CT scanner Hector developed by UGCT, the Ghent University Centre for X-ray CT. UGCT designs its own scanners and assembles them in concrete bunkers. The setup of Hector is shown in figure 21.

**Figure 21:** *Representation of the Hector setup.*
*Source: Ghent university centre for X-ray CT*

The micro focus source delivers a power of 280 Watt to ensure a high X-ray flux. The minimum focal spot size is 4 $\mu$m. The source-to-object (SOD) can be altered using the magnification stage. Furthermore tilted radiography and CT is possible due to its vertical and horizontal axis, covering an area of 80 x 80 cm$^2$. Moreover the rotation stage can carry loads of 80 kg.

# 7 Workflow of imaging peat samples

After having introduced the available imaging sources in the previous chapter, the imaging equipment will be used in this section. First, a workflow has been established (fig.22) which will be used to perform the imaging part of this project.

During the first trials peat with its natural water content is imaged in order to check the transmission of neutrons. If this value is higher than 20%, neutron CT will be used to image the sample. This means that the sample does absorb neutrons but in a moderate way. It is clear that the higher the transmission is, the better the analyzing part will be. Furthermore the peat will be dried and imaged in order to check the transmission of the dry peat material. After drying the sample it will be tried to saturate with heavy water in order to check the influence of heavy water on the transmission of neutrons keeping in mind that dry peat hardly takes up fluid. Since the aim is to image wet peat to better understand the role of fibres on the unusual behavior of the soil, i.e. high compressibility and friction angle, imaging dry peat is not of interest at this stage of the project.
If the transmission of the wet peat is lower than 20% using neutron radiography, a wet peat sample will be flushed with heavy water using a triaxial setup (fig.23) in order to decrease the attenuation coefficient of the peat material between the fibres. The goal of flushing is keeping the tissue of the fibres resistant for heavy water by keeping them full with natural water or air. Therefore, a contrast in transmission should be observable between the peat material between the fibres and the fibres itself because of the low attenuation coefficient of heavy water as described in chapter 5. If flushing does not work out, the dry sample will be imaged using neutron CT although the transmission of the dry peat material is not that high. In all three scenarios, i.e. imaging wet sample at natural water content, imaging flushed sample and imaging dry sample, the peat sample will be imaged in a wet and a dry state with X-ray micro CT in order to check the similarities and differences observable between the three scans.

If neutron CT does not give a satisfying result regarding imaging the fibres of peat, a sample will be prepared to be imaged using X-ray phase CT. The sample will be dried and imaged in the X-ray micro-CT in order to analyze the dry cell walls of the fibres and the dry peat material between the fibres. As described in section 5.2.2 X-ray phase CT uses only one sample-detector distance. The image contrast should be sufficient to segment and post process images using this fixed distance for low absorbing materials like peat. This scan is used to reveal more structures in peat compared to the other scans performed on peat.

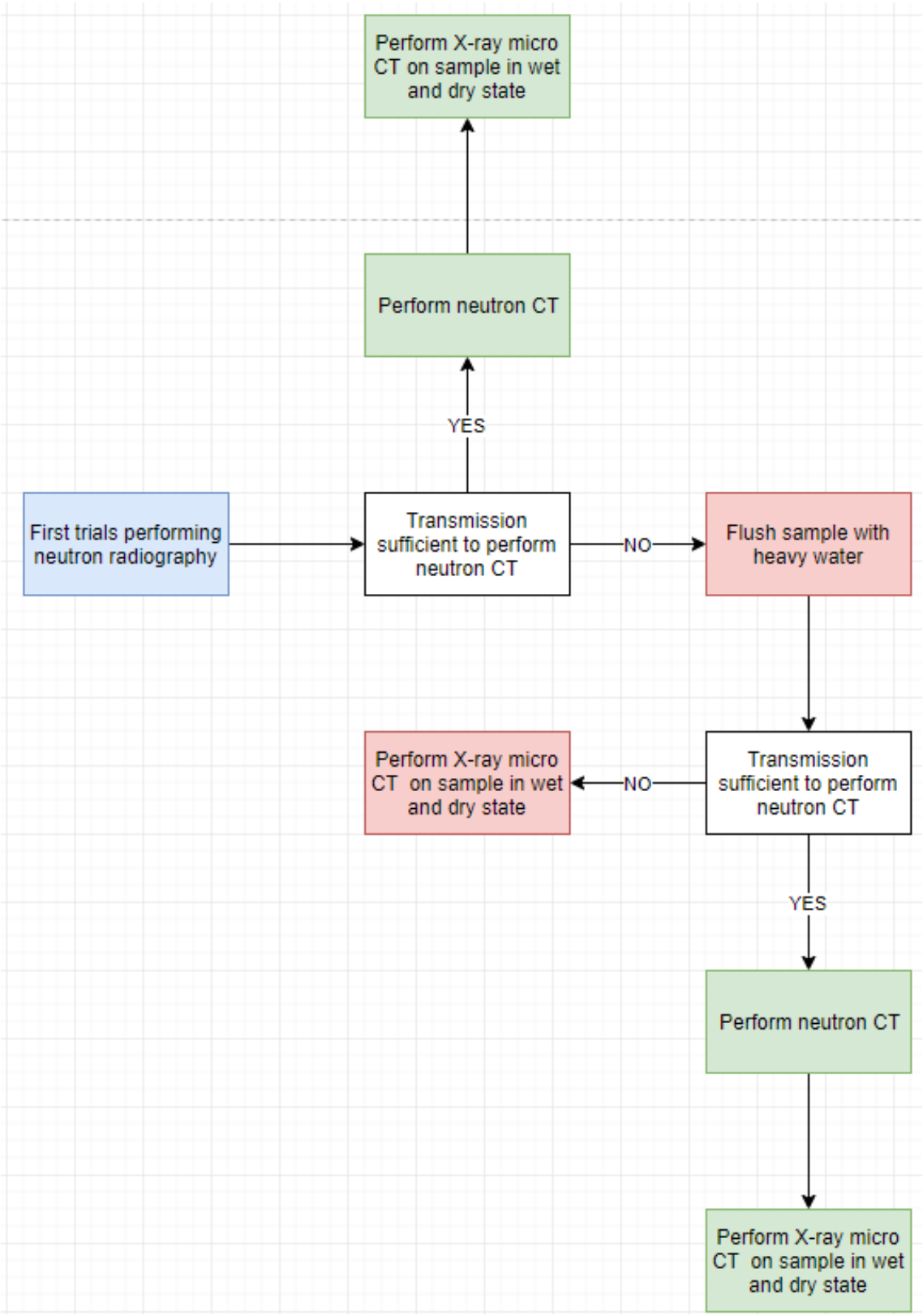


**Figure 22:** *Workflow for neutron imaging experiment starting with first trials*

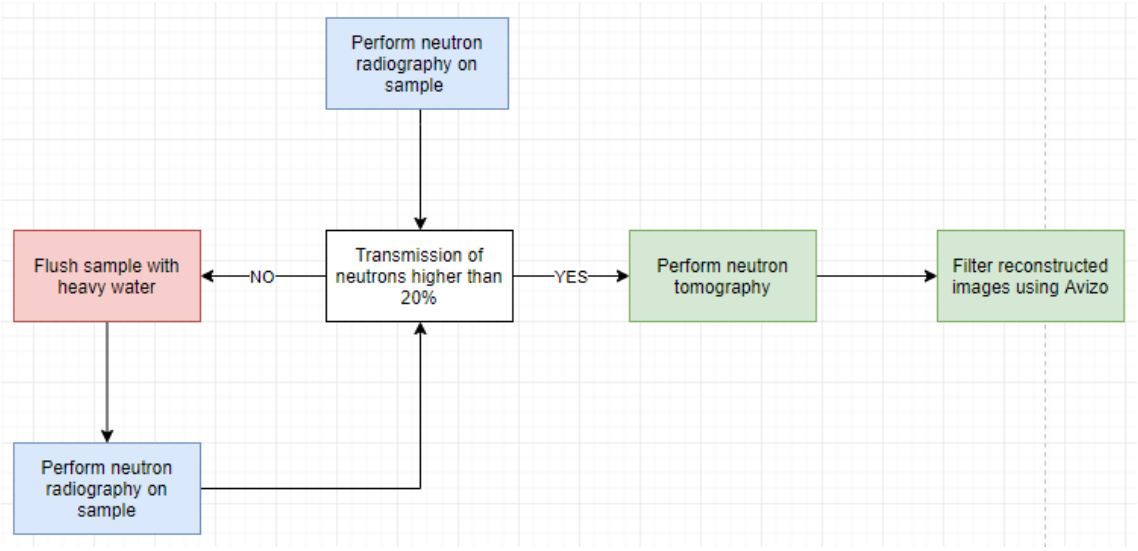


**Figure 23:** *Workflow to perform neutron CT finally*

## 7.1 First trials using neutron CT

As described in section 4.6, two type of peats will be tested, one called Katwoude and one Uitdam. During the trials both peats will be imaged with their natural water content. This will be done in order to verify the expected high attenuation coefficient, and therefore the low transmission of neutrons, as theoretically described in chapter 5. After computing the transmission of neutrons using both peats with their natural water content, heavy water will be used to saturate both peats in order to increase the transmission of neutrons during neutron radiography.

After performing neutron radiography on both peats, new smaller samples will be created and imaged again with neutron radiography. The samples will be dried and imaged again in order to check the transmission of its organic matter and fibres. Finally, heavy water will be used to try to saturate a wet and dry peat sample with heavy water keeping in mind that dry peat hardly takes up fluid.

### 7.1.1 Sampling method

An aluminum cylinder is used as a container to store the peat using neutron radiography. This sample holder is made of aluminum because aluminum shows low interaction probability with neutrons and therefore allowing a high penetration depth of the neutrons. The dimensions of the cylinder are shown in table 12. The peat is manually put in the sample holder.

| **cylinder** | **[cm]** |
|---|---|
| height | 6.7 |
| diameter | 3.0 |
| wall thickness | 0.22 |

**Table 12:** *Dimensions of used aluminum sample holder to store peat sample during imaging*

### 7.1.2 First trial using neutron radiography

The radiograph for the "Uitdam" peat is shown in figure 24, a similar image has been recorded for the Katwoude peat. The dark pixels of the radiograph correspond to peat at natural water content inside an 0.22 mm thick aluminum container. The peat sample absorbed neutrons following from the darkness inside the aluminum container. The trial confirms the high attenuation coefficient of peat components calculated in 5.1.2 and 5.1.3. The transmission of the peat sample contained in its aluminum container is calculated using equation 12.

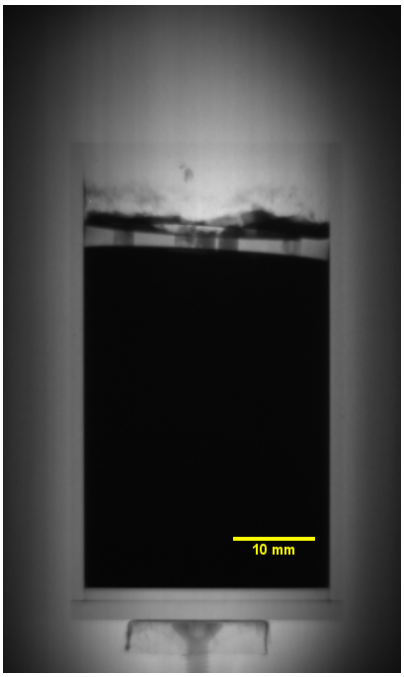


**Figure 24:** *Neutron radiograph of Uitdam peat with its natural water content stored inside an aluminum container;*
*Diameter: 3.0 cm*
*Wall thickness: 0.22 cm*

$$T = \frac{I - I_{dark}}{I_0 - I_{dark}} \tag{12}$$

In order to normalize the transmission of neutrons the dark field is subtracted from both images of the sample in the beam( $I$) and open beam ($I_0$) images. The intensities are derived from the radiographs using the open source image analysis program ImageJ. The transmission coefficient for both peats enclosed in a 3.0 cm thick aluminum cylinder is shown in table 13.

| | **Mark**$[H_2O]$ | **Katw**$[H_2O]$ |
|---|---|---|
| Transmission[-] | 0.02 | 0.03 |

**Table 13:** *Transmission results following from the neutron radiographs of a first trial using Uitdam peat and Katwoude peat respectively*

It is very low in both cases, despite the limited thickness of the peat sample (3 cm).

### 7.1.3 Second trial using heavy water

After verifying the high absorption of neutrons by the peat sample, heavy water will be used to saturate both peats in order to decrease the absorption of neutrons and increase the transmission of neutrons. As described in section 5.1.4 heavy water has a low attenuation coefficient, and therefore a high transmission of neutrons following from the Beer-Lambert law.
To saturate both peats with heavy water, a cylinder with a height of 6.7 cm is filled up to 2.0 cm with heavy water(fig. 25). The peat is pushed on top of the heavy water and once the aluminum cylinder is full of peat, a small film of heavy water is poured on top of the sample. To enhance the heavy water uptake, the peat sample is put in a vacuum tank for 24 hours. The principle of this experiment is diffusion. According to Dahal and Adhikari (2012) the mutual diffusion coefficient of heavy water and water is quite similar to the value of self-diffusion of heavy water. So heavy water will most probably diffuse in the natural water present in the sample and therefore the attenuation coefficient of the peat material between the fibres will decrease. A contrast should be visible on the radiographs between the fibres and the surrounding peat material.

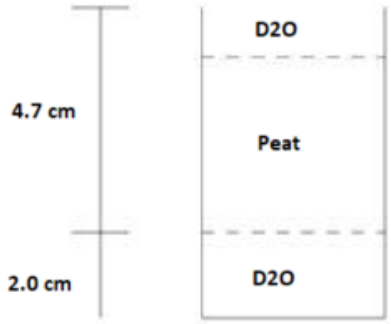


**Figure 25:** *Schematic representation of the aluminium cylinder attempting to saturate peat with heavy water($D_2O$);*
*The aluminum cylinder is filled up to a height of 2.0 cm with heavy water($D_2O$);*
*This sample is put in a vacuum tank for 24 hours to enhance the heavy water uptake by the peat*

The same calculation is performed as described in the previous subsection. The radiograph for the Uitdam peat is shown in figure 26.

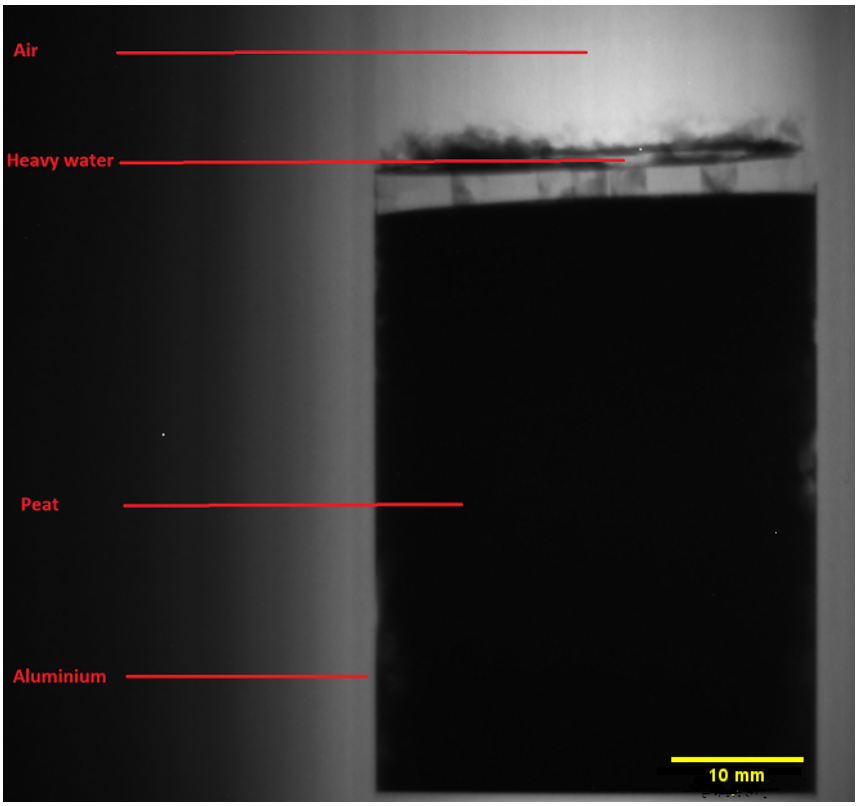


**Figure 26:** *Neutron radiograph of Uitdam peat of trial trying to saturate peat sample with heavy water($D_2O$) stored inside an aluminum container;*
*Diameter: 3.0 cm*
*Wall thickness: 0.22 cm*

The corresponding radiograph of the "Uitdam" peat shows a dark colour indicating a high absorption of neutrons. The result of the transmission calculation is shown in table 14.

| | **Mark**[$D_2O$] | **Katw**[$D_2O$] |
|---|---|---|
| Transmission[-] | 0.04 | 0.05 |

**Table 14:** *Transmission results following from the neutron radiographs of second trial trying to saturate both Uitdam peat and Katwoude peat with heavy water($D_2O$)*

The transmission increased with 0.02 for both peats after the attempt to saturate both peats with heavy water. It is clear that the increase in transmission is too little to observe different structures in the peat. The saturation attempt did not work out. A more elaborated saturation procedure is needed, see sections 8.1 and 8.2. Before flushing a peat sample with heavy water, the influence of the thickness of the peat sample and the wall thickness of the aluminum cylinder on the transmission will be checked first.

## 7.2 Trial using a thinner sample holder and imaging the dry sample

Since the Beer-Lambert law is a function of both the attenuation coefficient and the thickness of the sample, the optimum sample thickness needs to be found. During the previous trials a sample diameter of 3.0 cm including an aluminum wall thickness of 0.22 cm was used. For this trial the outer diameter of the aluminum container is 1.5 cm, the cylinder wall thickness is 0.12 cm (table 15) in order to observe the difference between the transmission of neutrons in the previous trials and the trials described in this section.

| **cylinder** | **[cm]** |
|---|---|
| height | 1.5 |
| diameter | 1.5 |
| wall thickness | 0.12 |

**Table 15:** *Dimensions of used aluminum container to store peat sample during imaging*

For the trials in this subsection Uitdam peat is used. For the remaining part of this thesis this type of peat will be the only one being used because it is extensively present in the lab under well-preserved conditions. In order to observe the influence of the sample diameter and wall thickness a wet peat sample with its natural water content is imaged first with neutron radiography. Then, the sample is air-dried and imaged before attempting to re-saturate the peat sample with heavy water while keeping in mind that it is almost impossible to re-saturate dry peat.

### 7.2.1 Wet sample at natural water ($H_2O$) content

The radiograph of the wet peat sample is shown in figure 27. According to section 7.1, the dark pixel inside the aluminum container represents a high absorption of neutrons. The lighter spots inside the peat represent pores. In order to quantify the transmission of neutrons, equation 12 of subsection 7.1.2 is used. The corresponding transmission result is 0.02. This value is the same for the Uitdam peat using the aluminum container with a diameter of 3.0 cm, as described in section 7.1.2. The decrease in wall thickness and sample diameter did not improve the transmission result. Therefore, the focus will be put on decreasing the attenuation coefficient of the peat material between the fibres assuming that the fibres keep their natural water content inducing a contrast of transmission between both components because this coefficient is the only factor which influence the transmission of neutrons considering the Beer-Lambert law (at relatively small sample sizes).

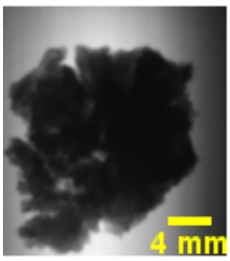


**Figure 27:** *Neutron radiograph of Uitdam peat with its natural water content stored inside a container made of aluminum foil*
*Diameter : 1.5 cm and Wall thickness: 0.12 cm*

The sample will be dried in order to check the transmission of the dry peat material between the fibres.

### 7.2.2 Dry sample

After drying the sample the weight decreased from 3.04 grams to 0.38 grams and the sample shrunk. Using equation 12 of subsection 7.1.2. the transmission of neutrons is 0.10. This means that the dry organic decomposed matter and fibres absorb neutrons. The transmission increased compared to the previous subsection due to the high amount of empty pores in the dry sample.

### 7.2.3 Sample re-saturated with heavy water($D_2O$)

In order to check the influence of heavy water on the transmission of neutrons in practice, the previous protocol was used to try to re-saturate the sample with heavy water. Since peat is hard to saturate once it has dried out, this is challenging. The dry peat is submerged in heavy water and put in a vacuum tank for 96 hours to enhance the fluid uptake. The sample did not swell, however its weight in grams has more than doubled(table 16). Neutron radiography was performed on the sample and equation 12 from section 7.1.2 is used to calculate the transmission of neutrons. The transmission turned out to be 0.09 which means that most of the neutrons are absorbed by the sample. This is inline with the test on the dry sample. Heavy water decreased the transmission of neutrons little due to the fact that heavy water is almost transparent to neutrons (not fully).

| **Sample** | **Weight (grams)** |
|---|---|
| *dried* | 0.38 |
| $D_2$O | 0.88 |

**Table 16:** *Weight of the sample after both drying and re-saturation with heavy water*

## 7.3 Conclusion after first trials

Since the transmission is a function of both the thickness of the tested sample and the macroscopic attenuation coefficient, it is important to get these two parameters as optimum as possible. Following from section 7.2 the sample diameter including the wall thickness of the aluminum container should not be thicker than 3.0 cm because this range of diameters or thicknesses was shown (0-3 cm) not to affect the attenuation coefficient much following from the Beer-Lambert law and the trial described in section 7.2. Next to this, the attenuation coefficient of the peat material between the fibres should be as low as possible in order to have a contrast with the fibres in the peat sample. Heavy water is a proper liquid to enhance the contrast because of its low attenuation characteristic.
By knowing this, another difficulty needs to be solved. This difficulty is to diffuse the heavy water in the natural water of the peat material between the fibres. To perform this, a flushing procedure will be established using a triaxial cell. This procedure is described in the next chapter.

# 8 Flushing of peat with heavy water

As described in the previous section, heavy water will be used to flush a peat sample. Since the peat material has a theoretical average attenuation coefficient of 5.6 $cm^{-1}$ as described in subsection 5.1.2, it absorbs neutrons and the corresponding neutron radiograph is dark. Furthermore the primary and secondary cell walls of the fibres have an average attenuation coefficient of 4.8 $cm^{-1}$ and therefore there is hardly no contrast visible between the peat material between the fibres and the cell walls of the fibres on the neutron radiographs. The aim of flushing peat with heavy water is to get a contrast in transmission of neutrons between the peat material between fibres and the peat fibres itself. As already mentioned in subsection 7.1.3, the mutual diffusion coefficient of heavy water and water is similar to the value of self-diffusion of heavy water. So heavy water will most probably diffuse in the natural water present in the peat and therefore the attenuation coefficient of the peat material between the fibres decrease.

For this flushing approach a triaxial test set-up is used. In geo-engineering the purpose of performing triaxial tests is to determine the mechanical properties of the soil. A triaxial test is performed on a cylindricial sample.

## 8.1 Sampling method and flushing procedure

A sample of 38 mm in diameter is obtained using a rotary drill to drill the desired sample out of the block of peat. The purpose of drilling is to disturb the sample as little as possible, in order to come close to the in-situ conditions of its fibre structure. However, the edges of the sample will be disturbed due to drilling moreover the obtained sample will be moderately pushed in a sample holder and further disturbed. However, at this stage of the research limited attention is put on imaging undisturbed samples.
To explain the flushing procedure a triaxial setup is shown in figure 28.

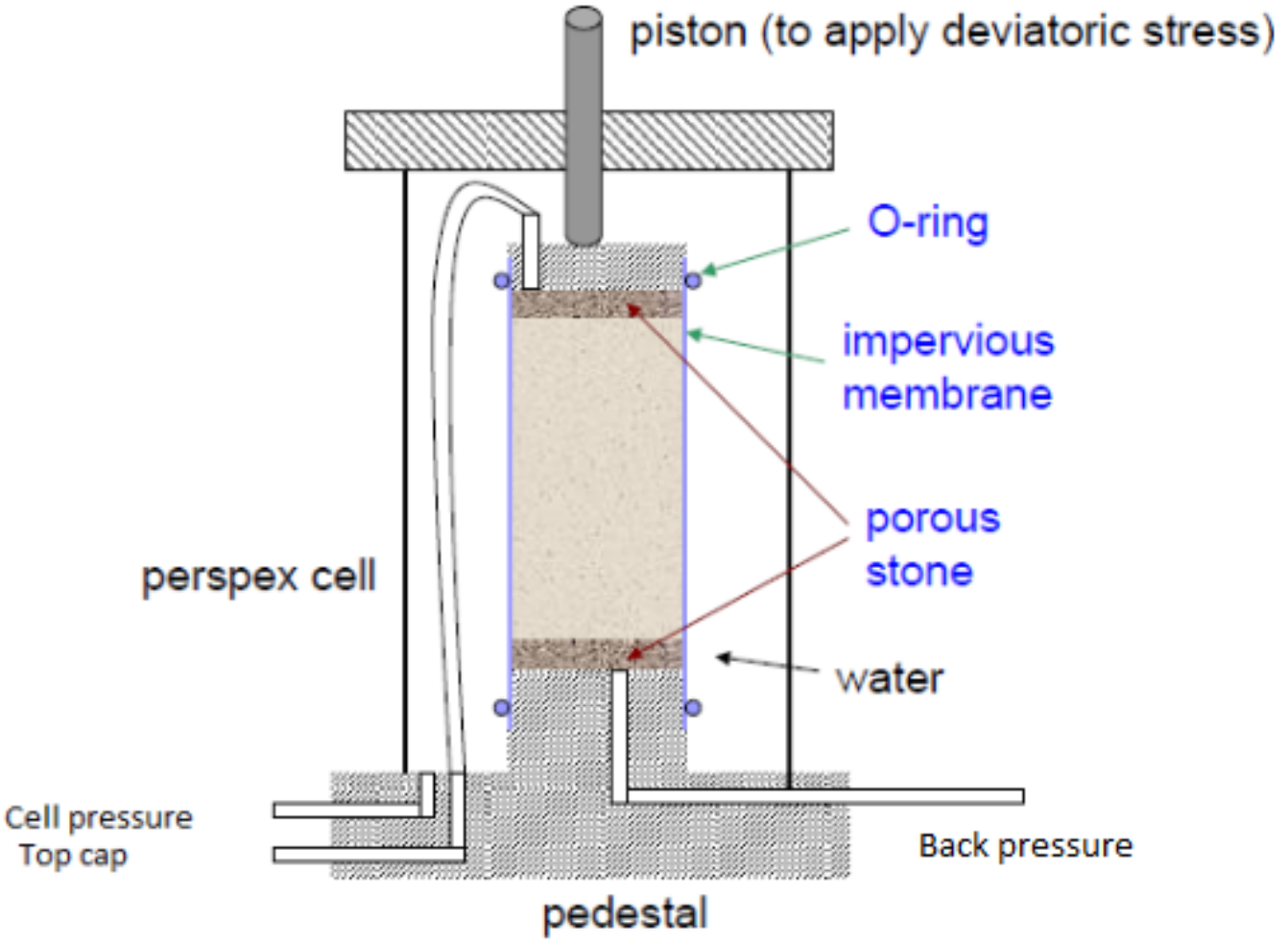


**Figure 28:** *Triaxial set-up;*
*A sample is present in between two porous stones;*
*Around the sample a latex membrane is present;*
*The pressure inside the perspex cell is controlled by a GDS controller;*
*The back pressure controller contains of heavy water to saturate the sample from bottom to top;*
*The top cap allows water to flow out of the sample during flushing.*

A triaxial test subjects a cylindrical soil sample to radial stresses. The piston applies the axial stress on the sample. The deviatoric stress shown in figure 28 is the difference between the axial stress and the confining pressure in the cell. This set-up can be adjusted in order to flush the peat sample. The piston will not be fixed and does not carry any load because the goal is to flush the peat sample from bottom to top with heavy water. The first component of the flushing setup is the porous sandstone. This porous disk will be put on the pedestal and is fully saturated in order to avoid air bubbles to block heavy water of flowing in the sample. On top of this porous disk the sample will be placed with another porous disk on top of it. A latex membrane will be placed around the sample in order to keep the sample in place and prevent any leakage of heavy water. This membrane will be fixed on the footing of the pedestal, using two latex O-rings. Finally, the top cap will be placed on the upper porous disk. This top cap allows for water flowing out during flushing. The cell will be filled with de-aired water, this water will be around the sample and controls the pressure in the cell. To control this pressure a GDS standard cell pressure

volume controller will be used during flushing. Another volume controller will be used to control the back pressure of the setup. This pressure is normally applied to the specimen pore-water to cause air in the pore space to compress and to pass into solution in the pore-water to increase the saturation of the specimen (McCarthy and McCarthy (1977)). The controller will be filled with heavy water in order to flush the sample from bottom to top. In order to flush the sample from bottom to top a pressure gradient has to be generated between the pores and heavy water. Since the pore pressure will not be measured during this experiment, the gradient will be manually determined by slowly increasing the back pressure. This will be performed in a slow manner in order to prevent destroying the fibres. The volume of heavy water which will be used is 1.1 time the volume of the cylinder, i.e. 75 mL. The accuracy of the controllers is $\pm 1kPa$ on pressure and $\pm 300mm^3$ on volume. The test will be performed in a controlled environment at temperature T of 13°C and a relative humidity RH of 68%.

## 8.2 Flushing execution

The setup to flush the peat is shown in figure 29. The two controllers are shown on the left side of the figure. The cell pressure controller is placed on top of the back pressure controller. The two controllers are connected to two valves of the triaxial cell (on the right side of the figure). Inside the cylindrical triaxial cell the sample is placed. The cell is placed on a footing in order to catch the liquid mix which will flow out of the cell in a beaker. This mixture will flow via the available top cap which is put on top of the upper porous disk as described in the previous subsection. The lines which connect the cell to the controllers are de-aired before starting the flushing procedure.

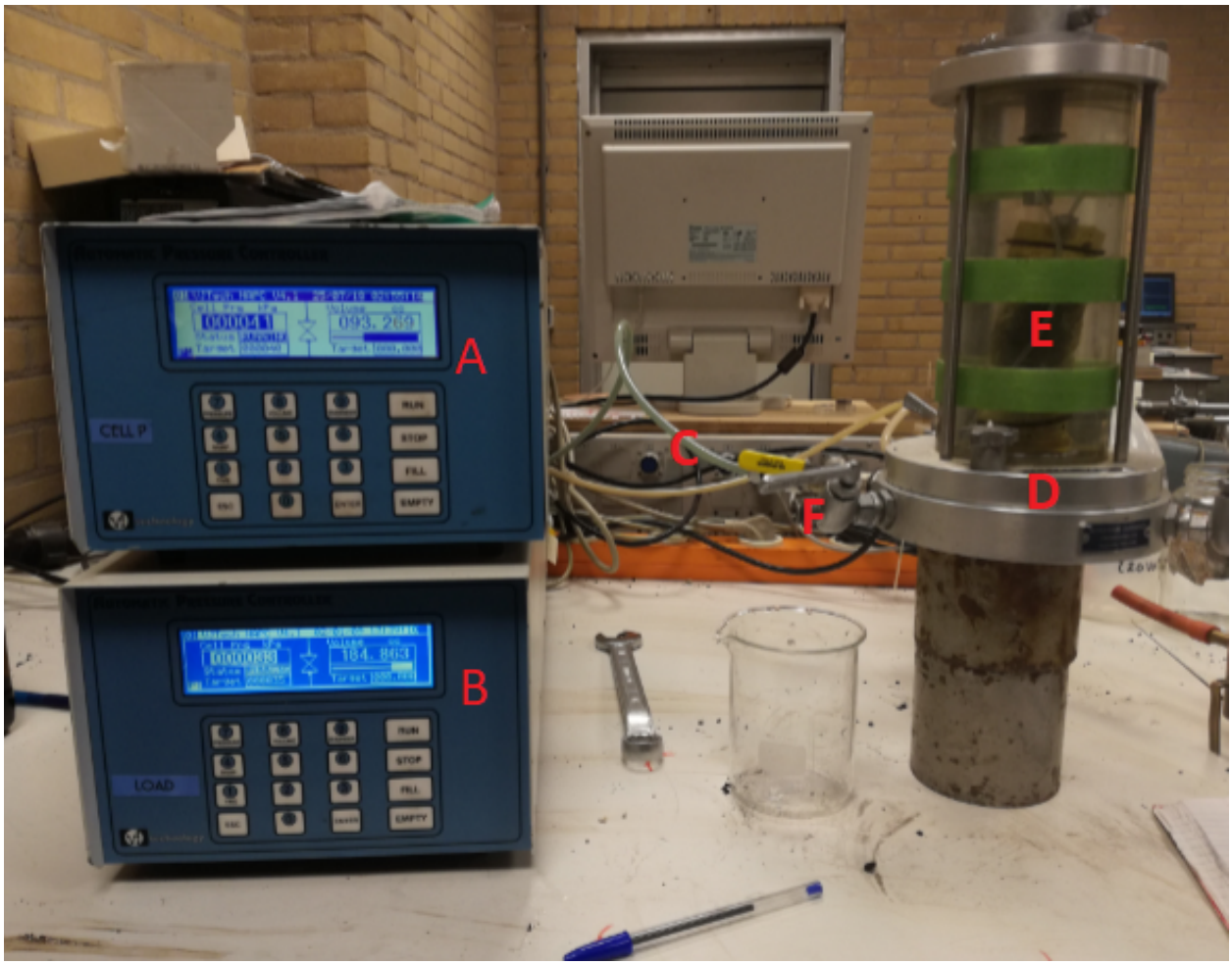


**Figure 29:** *Flushing setup using a triaxial cell and two controllers;*
*A) Controller which controls the cell pressure of natural water within the perspex cell;*
*B) Controller which controls the volume of heavy water during flushing;*
*C) Two hoses which connect respectively the cell and back pressure controller to the triaxial cell;*
*D) The triaxial cell;*
*E) Peat specimen surrounded by a latex membrane and water;*
*F) Valve which allows the liquid mixture for flowing in the beaker*

The pressure controllers are both manually controlled in order to be able to adjust the pressure in a way that heavy water flows slowly from bottom to top by generating a small pressure gradient between the bottom (inlet of heavy water) and the top of the pore pressure circuit (top cap) by leaving valve F open. This allows the liquid to escape from the sample as heavy water enters the sample. The flushing procedure took 3.5 hours as shown in figure 30 and 31. In figure 30 the blue graph represents the evolution of the cell pressure in time during flushing, whereas the orange graph represents the evolution of the back pressure in time during flushing. Both pressures increased almost linearly during the first hour of the experiment before reaching an almost constant value. The cell pressure increased in a way to maintain the difference between the cell and back pressure constant to about 5 kPa. This was performed in such a way as to keep the effective stress during flushing.

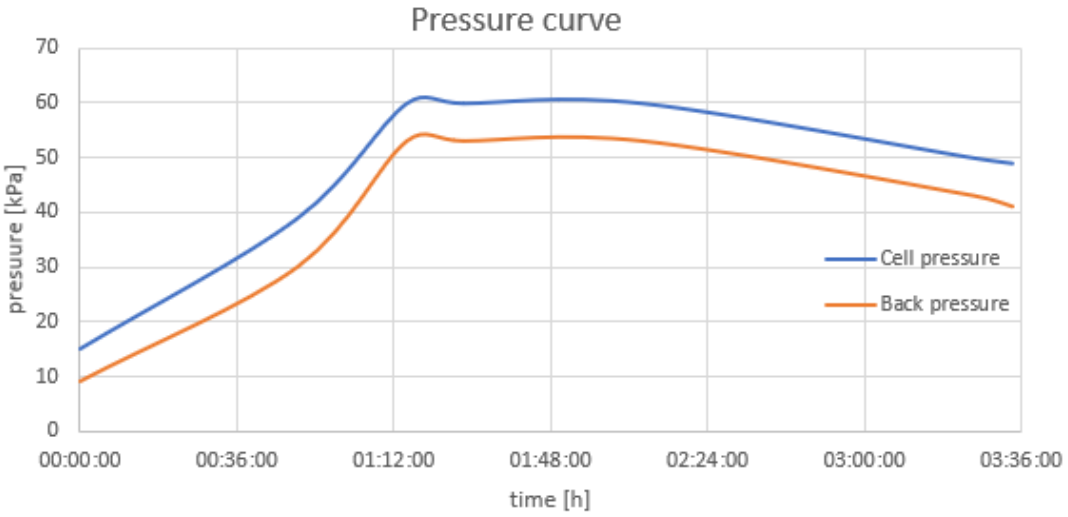


**Figure 30:** *Graph representing both the amount of cell and back pressure applied to the peat sample during flushing with heavy water*

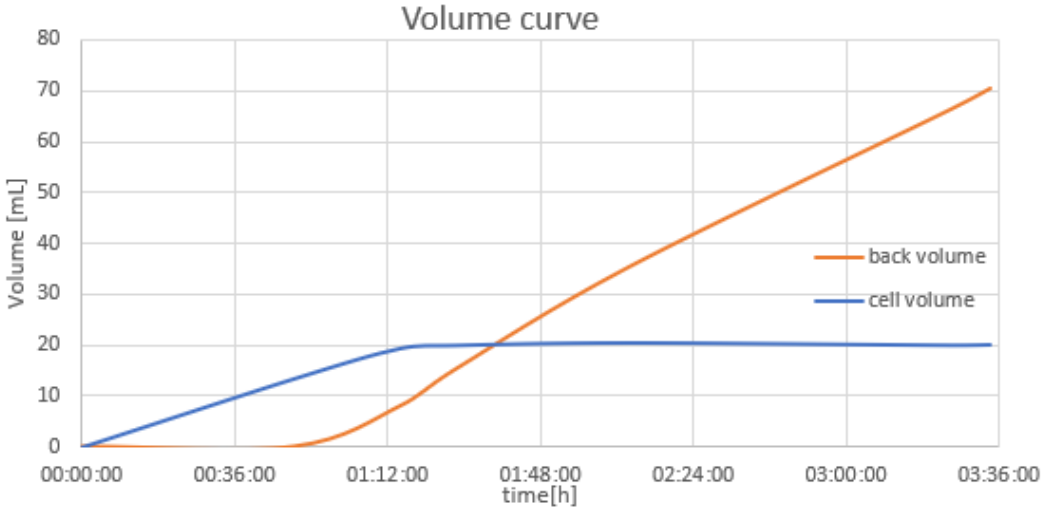


**Figure 31:** *Graph representing both the amount of cell and back volume used during flushing the peat with heavy water*

As mentioned in the introduction of this chapter, the pore pressure was not measured, and

therefore the pressure gradient between the pores and the heavy water was not measured but since a liquid mixture was flowing out the valve (label F in fig. 29) this gradient was high enough to rise the heavy water in the sample. The liquid mixture which flew out of the representative valve (label F in fig.29) is caught in a beaker and will be imaged using neutron radiography in order to measure its transmission. This will be performed in order to calculate the amount of heavy water which is present in the sample after flushing.

## 8.3 Determination volume of heavy water in sample

In this subsection the volume of heavy water in the flushed sample is calculated. This is of importance to make sure that flushing went well. A decent volume of heavy water needs to be present in the sample to decrease the attenuation coefficient of the peat material between the fibres. First the volume of the peat sample before and after flushing will be calculated. This is described in section 8.3.1. Next, the Beer-Lambert law will be used to calculate the attenuation coefficient of the collected liquid mixture during flushing the peat sample with heavy water. Based on this coefficient of the liquid mixture, the fraction of heavy water in the liquid mixture will be calculated in section 8.3.3. Following from the total volume of the liquid mixture, the volume of heavy water in the liquid mixture will be calculated using the fraction of heavy water in the liquid mixture. Finally, based on the total volume of heavy water used during flushing the amount of heavy water in the peat sample after flushing will be calculated.

### 8.3.1 Volume calculation of peat sample

As described in section 8.2, the diameter of the peat sample decreased due to the increase in cell pressure during flushing. The dimensions of the peat sample can be found in table 17, dividing them into an initial condition representing the dimensions before flushing, and a final condition representing the dimensions of the sample after flushing.

| **Dimensions of peat sample** | **Initial condition** | **Final condition** |
|---|---|---|
| height [cm] | 6.0 | 6.0 |
| radius [cm] | 1.90 | 1.71 |

**Table 17:** *Dimensions of peat sample of both before and after flushing it with heavy water*

Equation 13 is used for calculating the volume of a cylindrical specimen like the peat sample.

$$Volume = \pi * radius^2 * height \tag{13}$$

The result of the volume calculation is shown in table 18. The volumes of the peat sample before and after flushing are indicated. Furthermore the volume of heavy water ($D_2O$) which is used during flushing is shown in this table. This volume is of importance to calculate the amount of heavy water in the peat sample (subsection 8.3.3). Finally, the volume of the collected liquid mixture is indicated in table 18. This volume will be used to calculate the amount of heavy water in the mixture by knowing the fraction of heavy water. (subsection 8.3.3.).

| | **Peat sample before flushing** | **Peat sample after flushing** | **$D_2O$ used during flushing** | **Liquid collected** |
|---|---|---|---|---|
| Volume[mL] | 68 | 55 | 70 | 82 |

**Table 18:** *Different volumes of the peat sample before and after flushing with heavy water, the amount of heavy water($D_2O$) used during flushing, and the amount of liquid which was collected during flushing*

### 8.3.2 Measured attenuation coefficient of heavy water and collected liquid mixture using neutron radiography

As described in chapter 7, neutron radiography is used to check whether a sample absorbs neutrons or not. Subsection 5.1.4 described the theoretical attenuation coefficient of heavy water. This theoretical coefficient differs from the attenuation coefficient of heavy water in practice, i.e. in the neutron beam. As mentioned in chapter 5 the theoretical attenuation coefficient is calculated by including both the absorption and the scattering processes. However, in practice, some of the scattered neutrons also arrive on the detector which results in a higher measured transmission of neutrons than the theoretical transmission. Therefore, the measured attenuation coefficient is lower than the theoretical one, following from the Beer-Lambert law.

In order to measure the attenuation coefficient of heavy water before passage through the peat sample in the neutron beam, a small cuvette of glass is filled with heavy water. Furthermore a cuvette is filled with the collected liquid mixture. Both cuvettes are put in the neutron beam to determine the attenuation coefficient of both.

The average transmission T could be obtained using ImageJ. The values of both the transmission and thickness t of the cuvette walls are shown in table 19.

| **Parameter** | **Heavy water** | **Collected liquid mixture** |
|---|---|---|
| Transmission T of neutrons[-] | 0.906 | 0.541 |
| Thickness t of cuvette[cm] | 0.2 | 0.2 |

**Table 19:** *Observed transmission T, and total cuvette thickness to calculate attenuation coefficient* $\Sigma$ *of both the heavy water and collected liquid mixture*

To calculate the attenuation coefficient of respectively heavy water and the collected liquid mixture in the beam, the Beer-Lambert law can be rewritten in order to calculate both attenuation coefficients as shown in equation 14.

$$\Sigma = \frac{-lnT}{t} \tag{14}$$

Here, $\Sigma$ is the attenuation coefficient, T is the transmission of the neutrons and t is the thickness of the cuvette. The attenuation coefficient of both liquids are shown in table 20.

| **Parameter** | **Heavy water** | **Collected liquid mixture** |
|---|---|---|
| Attenuation coefficient $[cm^{-1}]$ | 0.50 | 3.07 |

**Table 20:** *Calculated attenuation coefficient of both the heavy water and collected liquid mixture*

The measured attenuation of heavy water is lower than the theoretical value (0.65 $cm^{-1}$) calculated in chapter 5 due to measured scattered neutrons on the detector as mentioned above. By knowing these coefficients the amount of heavy water in the liquid mixture can be calculated.

### 8.3.3 Calculation amount of heavy water in peat sample

Since the collected liquid mixture contains only heavy water and natural water, the fraction of both liquids in this mixture can be calculated. This is performed using the attenuation coefficient $\Sigma$ of the liquid mixture, heavy water and natural water using equation 15.

$$A_{D2O} = \frac{\Sigma_{MIX} - \Sigma_{D2O}}{\Sigma_{H2O} - \Sigma_{D2O}} \tag{15}$$

Here, $A_{D2O}$ is the fraction of heavy water in the collected liquid mixture, $\Sigma_{MIX}$ is the attenuation coefficient of the liquid mixture, $\Sigma_{D2O}$ is the attenuation coefficient of heavy water, and $\Sigma_{H2O}$ is the attenuation coefficient of natural water. The fraction of both the heavy water($D_2O$), and natural water($H_2O$) present in the liquid mixture are shown in table 21.

| **Liquid** | **Fraction[-]** |
|---|---|
| $D_2O$ | 0.48 |
| $H_2O$ | 0.52 |

**Table 21:** *Fraction of both the heavy water($D_2O$) and the natural water ($H_2O$) in the collected liquid mixture*

By knowing the fraction of heavy water in the liquid mixture, the volume of heavy water in the mixture can be calculated using the total volume of the mixture which is shown in table 18. Furthermore by subtracting this volume from the total volume of heavy water used during flushing, the volume of heavy water in the peat sample can be calculated. The volume of heavy water for both cases is shown in table 22.

| | **Liquid residual** | **Peat sample** |
|---|---|---|
| Volume of $D_2O$ [mL] | 39.5 | 30.5 |

**Table 22:** *Volume of heavy water($D_2O$) in both the collected liquid residual and the peat sample*

The percentage of heavy water present in the peat sample can be calculated using the ratio of the volume of heavy water in the sample over the total volume of the sample after flushing, as shown in equation 16.

$$A_{D2O} = \frac{V_{D2O}}{V_P} * 100\% \tag{16}$$

Here, $A_{D2O}$ is the percentage of heavy water in the peat sample after flushing, $V_{D2O}$ is the volume of heavy water in the peat sample as shown in table 22, and $V_P$ is the total volume of the peat sample as shown in table 16. The amount of heavy water present in the peat sample is 55% after inserting the values in equation 16. As described in the introduction of this chapter, the heavy water has most probably diffused in the natural water present in the peat sample because of their almost similar mutual diffusion coefficient. This coefficient is quite similar to the value of self-diffusion of heavy water and therefore heavy water has diffused in the natural water. As mentioned earlier, ideally heavy water has decreased the attenuation coefficient of the peat material between the fibres present in the peat inducing a contrast in attenuation between the peat material and the fibres.

In order to verify this, a small sample will be sampled out of the flushed peat sample. This sample holder is made of aluminum and its dimensions are shown in table 23.

| **cylinder** | **[cm]** |
|---|---|
| height | 3.4 |
| diameter | 1.8 |
| wall thickness | 0.15 |

**Table 23:** *Dimensions of used aluminum container to store peat sample during neutron imaging*

The peat sample will be imaged with thermal neutrons performing neutron CT. The images will be reconstructed first and filtered using Avizo software version 9.4.

# 9 Imaging results of neutron CT, X-ray micro CT and X-ray phase CT

In this chapter the CT images are filtered using Avizo version 9.4. Section 9.1 describes what is observed on the different CT images of the peat sample described in section 8.3.3. This will be done by comparing the neutron CT images of the wet sample with the X-ray micro CT images of both the wet and the dry sample. The aim is to figure out what type of fibres are revealed by neutron CT of Uitdam peat after careful saturation with heavy water. Section 9.2 describes the filtering process which will be performed on the neutron CT images. The aim is to extract some morphological parameters of the fibres. This will be compared to the result of the filtering process of the X-ray micro CT images of the wet sample. Then another peat sample is imaged using X-ray phase CT in Ghent. On this scan smaller fibres are visible and they are extracted digitally. This scan will be compared to the X-ray micro CT scan of the sample in a saturated and a dry state performed at TU Delft.

## 9.1 Result of imaging the peat sample with neutron CT

As described in chapter 8, the aim of flushing a peat sample with heavy water was to get a contrast between the fibres and the peat material between the fibres. There are six scenarios which could allow in order to extract the 3D volumes of the fibres revealed by the neutron CT scan and calculate some morphological parameters which can be envisaged in figure 32.
The first scenario is that the fibres took up heavy water. Since the attenuation coefficient of heavy water is lower than the attenuation coefficient of the peat material and the cell walls of the fibre, there should be a contrast visible on the tomographic image. The second scenario illustrates that the fibres are filled with a mixture of heavy water and natural water. The difference in attenuation between the peat material and the cell walls of the fibres with the liquid mixture is too low to observe a contrast. The third scenario illustrates that the fibre is air-filled and none of the heavy water entered the cell walls of the fibre. There will be a contrast in attenuation between air(dark region), the cell wall and the peat material on the tomographic image. Scenario 4 illustrates that the fibre is natural water-filled and none of the heavy water entered the cell walls of the fibre. This results in a contrast of attenuation between natural water (bright color), the cell wall and the peat material. The fifth scenario illustrates that the cell walls of the fibre took up heavy water and the fibre is air-filled. Therefore there is only a contrast between air which is dark and both the cell wall and peat material which will display the same bright color. Finally, scenario 6 illustrates that the fibre is natural water-filled and the cell walls of the fibre took up heavy water. As described in scenario 5, there is only a contrast in attenuation between the natural water which is brighter than the cell wall and peat material on the tomographic image.
Note that air is dark on the tomographic images of neutron CT and natural water is bright on the reconstructed images of neutron CT. This is the opposite of what was described in chapter 7 because here natural water is dark on the transmission images because of its high attenuation coefficient for neutrons.

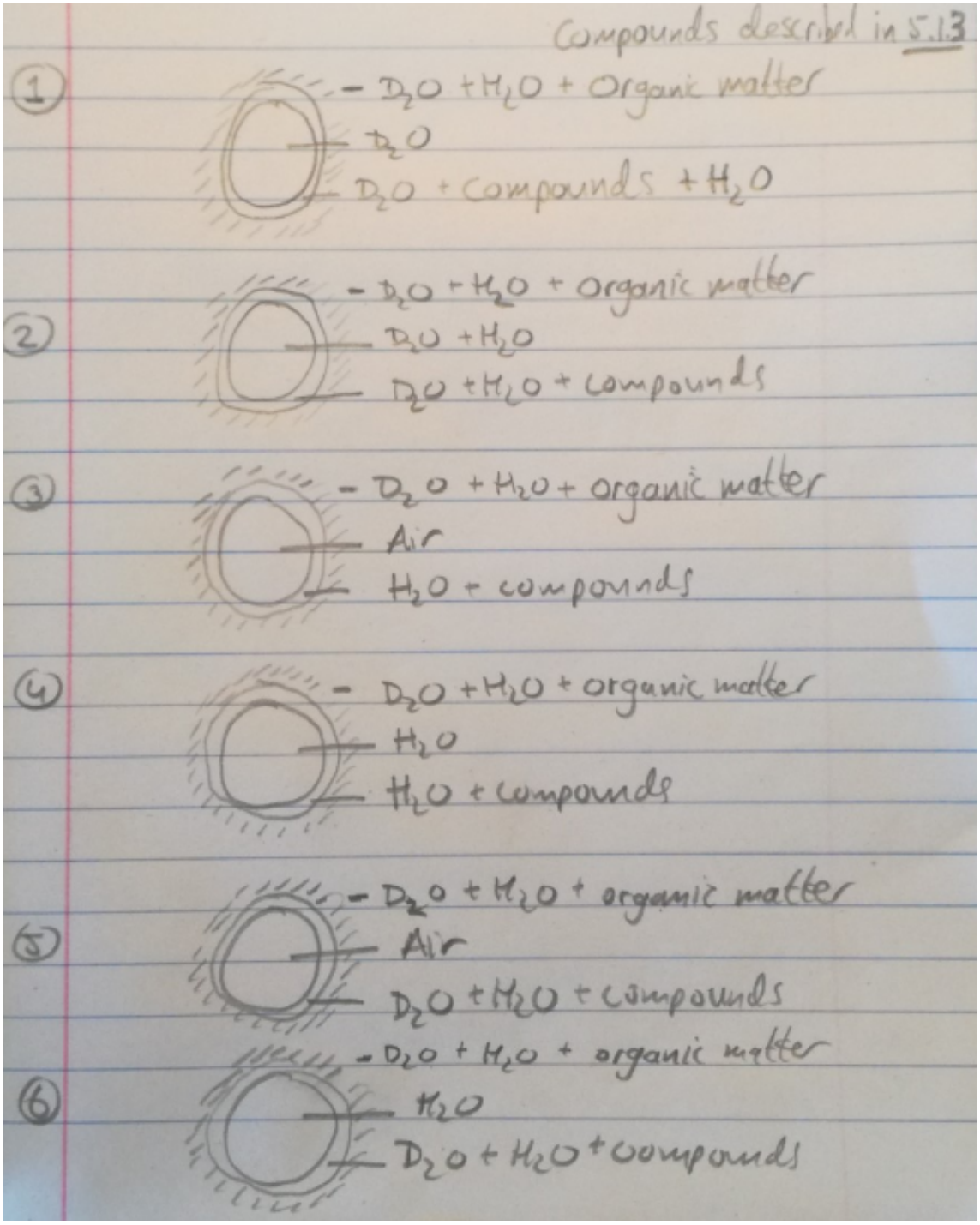


**Figure 32:** *Different scenarios of a conceptual neutron CT image of a fibre; The peat material consists of heavy water, natural water and organic matter*

In the following figure three tomographic images of the neutron CT scan of peat saturated with heavy water are shown. The slices show dark spots inside a grey matrix.

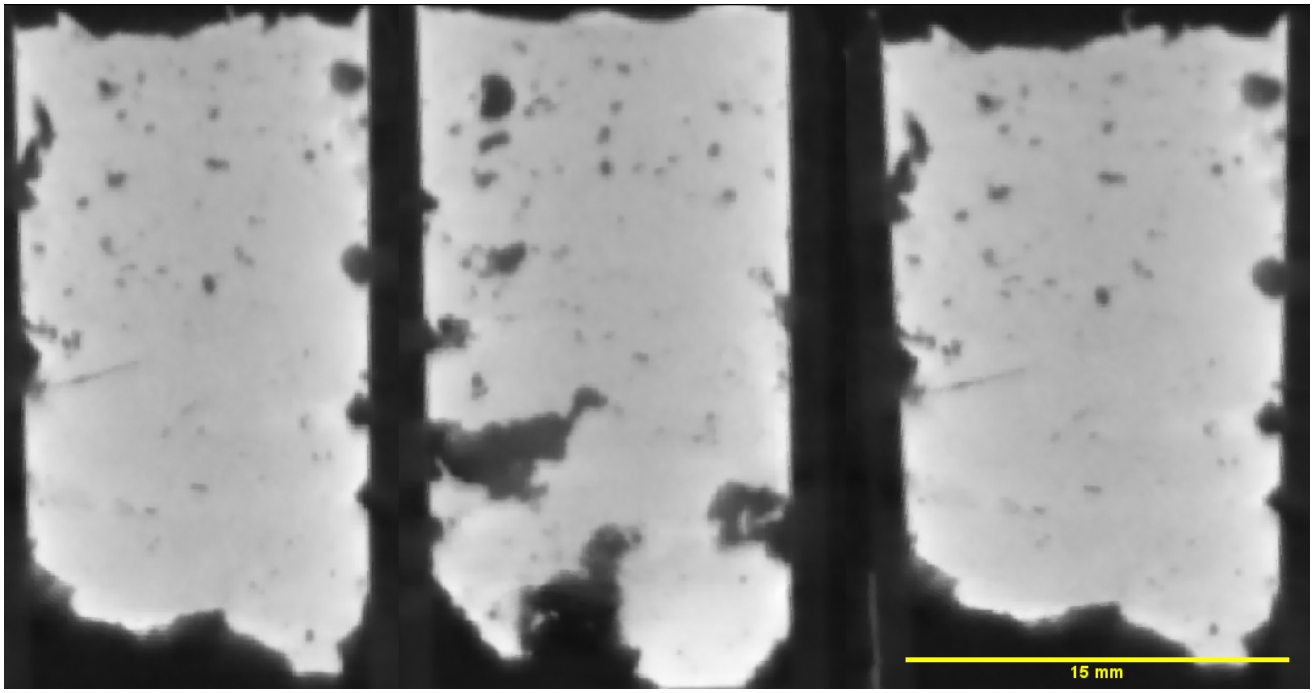


**Figure 33:** *tomographic images of peat sample using neutron CT;*
*Some dark regions are air- or heavy water-filled pores whereas the grey bulk represents the peat material between the fibres containing a mixture of heavy water, natural water, and organic matter*

The dark spots could be either air-filled or heavy water-filled fibres because air and heavy water have a low attenuation coefficient which results in a dark region on the tomographic images. The abundant grey colour on the cross-section is the peat material between the fibres. The natural water filled fibres are not visible on the tomographic image. The transition between the abundant grey color and the cell walls of the air-filled or heavy water filled fibres is not visible.

The attenuation coefficient of the peat material between the fibres can be theoretically described by first adjusting the relation which describes the attenuation coefficient between natural water and decomposed matter as shown in subsection 5.1.2. This relation needs to be adjusted due to the present heavy water in the sample after flushing. This approach will be outlined in this section.

As described in the previous chapter, the flushed sample contains 55 percent heavy water. Based on the initial water content of 700%, the volume of the peat particles can be estimated, which is one eighth of the total volume. The volume of both the fibres and the organic matter present in the peat material between the fibres can be calculated using table 18 from subsection 8.3.1 and is assumed to remain the same during flushing, i.e. 8.5 $cm^3$. In order to divide the peat particles in both fibres and organic matter, the tomographic images of figure 33 are used. Here, lots of air-filled and or heavy water-filled fibres inside the greyish peat material between the fibres are shown. Furthermore peat consists of natural water filled fibres and therefore the fibre content is assumed to be 20% of the total amount of peat particles. Therefore a volume of 80% of the calculated particles are present in the peat material between the fibres, which represents the volume of decomposed plant tissue. This represents 6.8 mL of the total volume of the particles. Equation 17 illustrates the relation to calculate the attenuation coefficient of the peat

material between the fibres.

$$\Sigma_g = a\Sigma_l + b\Sigma_p \tag{17}$$

Here, $\Sigma_g$ is the attenuation coefficient of the peat material between the fibres $[cm^{-1}]$ which consists of the attenuation coefficient of a liquid mixture containing both natural water and heavy water $\Sigma_l$, and the attenuation coefficient of decomposed plant tissue $\Sigma p$. Furthermore $a$ represents the estimated ratio of the liquid volume over the total volume of the peat material between the fibres, and $b$ represents the ratio of the peat particles over the total volume of the peat material between the fibres. These unknowns can be calculated as follows:

$$a = \frac{V_t - V_p}{(V_t - 0.2 * V_p)} \tag{18}$$

$$b = 1 - a \tag{19}$$

Here, $V_t$ is the total volume of the flushed peat sample, i.e. 55 $cm^3$, and $V_p$ is the volume of particles, i.e. 8.5 $cm^3$. By inserting these values the unknowns are found, i.e. $a = 0.87$ and $b = 0.13$.

The attenuation coefficient of the liquid mixture can be described as follows:

$$\Sigma_l = c\Sigma_{D_2O} + d\Sigma_{H_2O} \tag{20}$$

Here, $c$ is the fraction of heavy water present in the liquid mixture, $\Sigma_{D_2O}$ is the attenuation coefficient of heavy water, $d$ is the fraction of natural water present in the liquid mixture, and $\Sigma_{H_2O}$ is the attenuation coefficient of natural water.
To calculate $c$ and $d$ the following relations are established.

$$c = \frac{eV_t}{(V_t - 0.2V_p)} \tag{21}$$

$$d = 1 - c \tag{22}$$

As shown in equation 21, $c$ is a function of both the volume of heavy water, i.e. $eV_t$ ($e$ is the percentage of heavy water present in the sample, i.e. 55), and the volume of the peat material between the fibres, i.e. $V_t - 0.2V_p$. By filling in equations 21 and 22 both unknowns are retrieved, i.e. $c = 0.56$ and $d = 0.44$.

Now the attenuation coefficient of the peat material between the fibres can be calculated using equation 17 including all the above calculated parameters, i.e. 3.0 $cm^{-1}$.
Since this value is based on a few assumptions like the attenuation coefficient of the decomposed plant tissue, and the volume of decomposed plant tissue in the peat material between the fibres, the error of the calculated attenuation coefficient of the peat material is high. Therefore the value of this attenuation coefficient is considered to have an error in the order of about 20%. Now the attenuation coefficient lies in the following interval:

$$2.4cm^{-1} < \Sigma_g < 3.6cm^{-1} \tag{23}$$

Furthermore the attenuation coefficient of the cell walls can be calculated. There are two scenarios, one scenario illustrates that the walls took up heavy water whereas in the second scenario they did not take up heavy water. The latter is calculated in section 5.1.3 and resulted in an attenuation coefficient of 5.4 $cm^{-1}$. The same calculation for scenario one will be performed as described above for the peat material between the fibres. The relation of the attenuation coefficient for the cell walls from subsection 5.1.3 is used. Note that in case of uptake of heavy water the cell walls still contain around 50 % of natural water. By filling in the values the attenuation coefficient lies in the following interval:

$$2.7cm^{-1} < \Sigma_g < 4.1cm^{-1} \tag{24}$$

If the cell walls did not uptake heavy water, there should be a contrast visible between the peat material between the fibres and the fibres itself. Looking at label 1 of the tomographic image of figure 34 this is not visible. There is only a transition between the fibre and the greyish peat material. The difference in attenuation between the peat material and the cell walls which took up heavy water, is low (eq. 23 and 24) and therefore there is no contrast visible between both. Finally, one can conclude that the cell walls of the fibres took up heavy water. The dark color of the fibres is most probably air but it could also be heavy water due to its low attention coefficient. To verify if the dark color is indeed air, the sample has been kept saturated and scanned with the micro CT scanner at TU Delft. A tomographic image similar to the one shown in figure 34 is shown in figure 35. Label 1 represents the same fibre as shown on the neutron CT tomographic image. The fibre is dark which is air because this technique is based on density differences as explained in chapter 5. The higher the density of a material the brighter the color will be on the tomographic image. Around label 1 there is a white halo visible. This is the cell wall which has a greater density than the peat material between the fibres. This will be theoretically calculated.

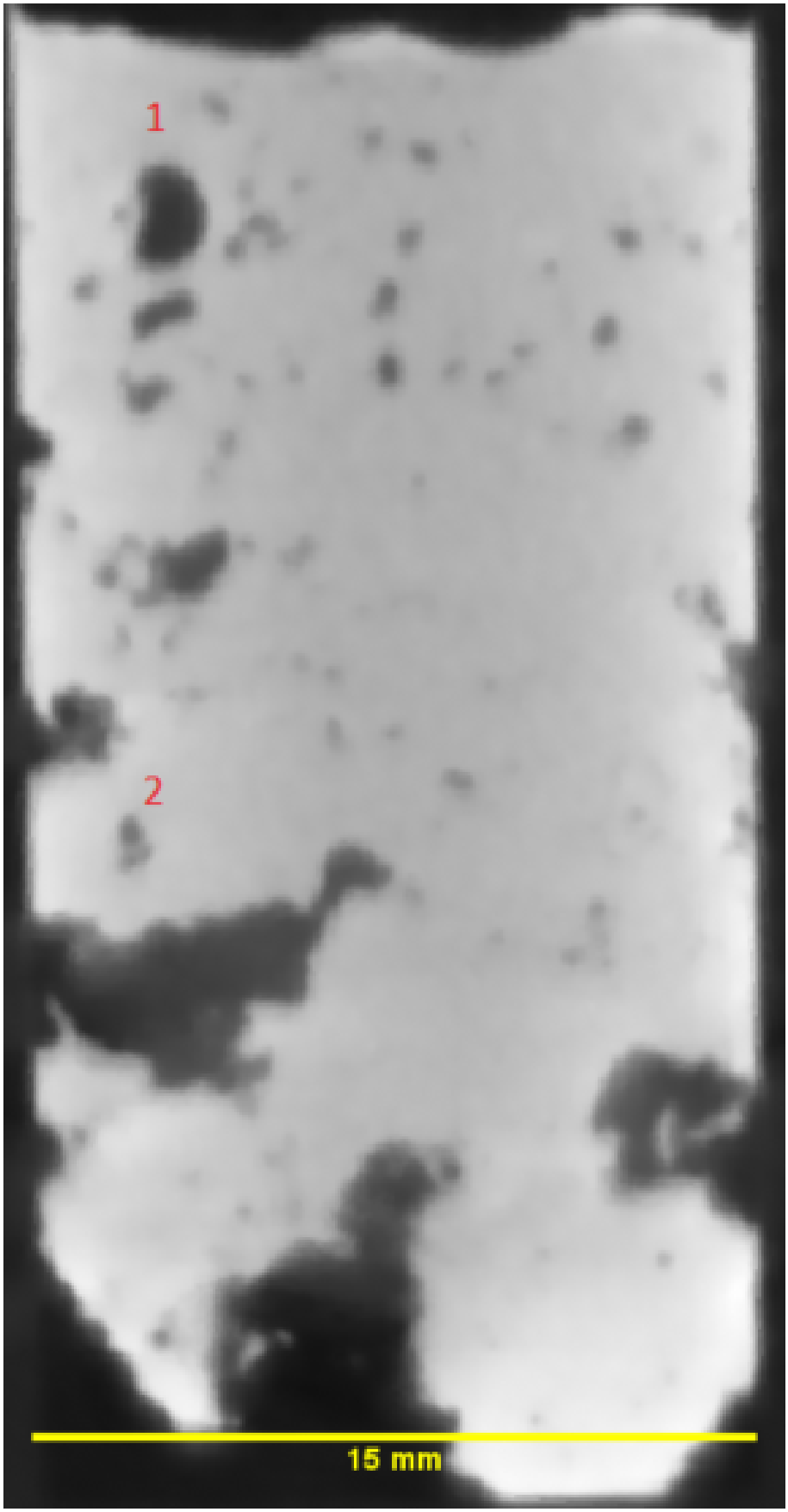


**Figure 34:** *Labelled pore on tomographic image which represents a fibre filled with air; The greyish bulk is the peat material between the fibres which is a mixture of heavy water, natural water and decomposed plant tissue*

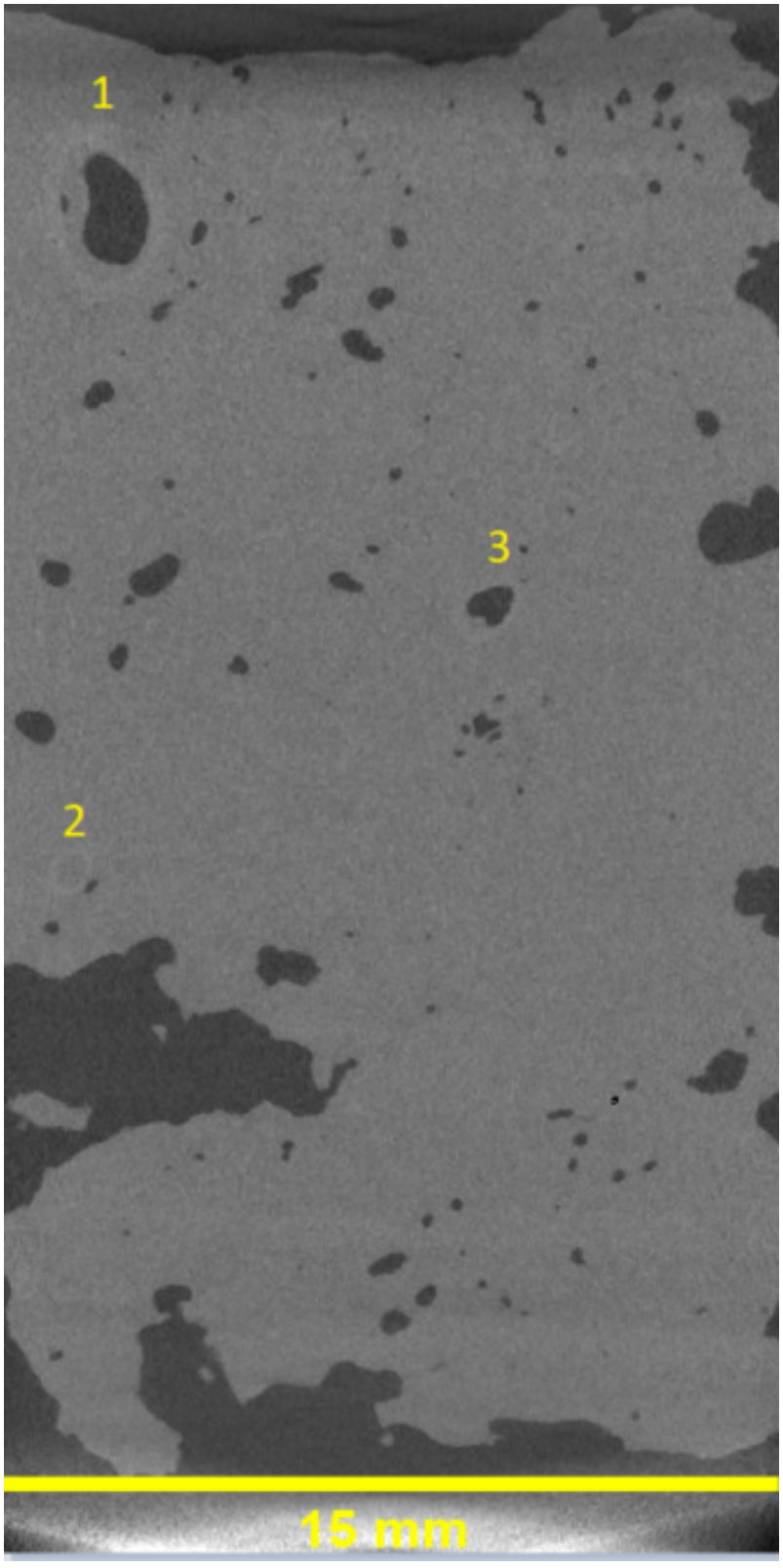


**Figure 35:** *tomographic image of peat sample using X-ray micro CT;*
*Some dark regions are air filled pores whereas the grey bulk represents the peat material between the fibres which is a mixture of heavy water, normal water and organic matter;*
*Label 1 represents the fibre filled with air as shown on figure 34;*
*Label 2 shows a white a halo surrounding the same colour as the peat material between the fibres which is also shown on figure 34;*
*Label 3 represents a small hollow structure which is not found on figure 34*

To quantify the density difference between the peat material and the cell walls, the relation to calculate the attenuation coefficient of the cell walls given in subsection 5.1.3 can be used for the estimated average density of the walls, i.e.

$$\rho_{cw} = \frac{3}{4}\rho_w + \frac{1}{4}\rho_c \tag{25}$$

Here $\rho_{cw}$ is the density of the cell wall $[g/cm^3]$ which consists of the density of the mixture of heavy water and natural water $\rho_w$, and the density of the compounds present in the cell wall $\rho_c$. For this case the calculation will only be performed for the cell walls in case of uptake of heavy water as proven above. Equation 25 can be filled in using an average density of the present compounds in the cell wall of 1.5 $g/cm^3$ as shown in chapter 5. This results in a density $\rho_{cw}$ of 1.16 $g/cm^3$. The density of the peat material between the fibres can be calculated in the same way the density of the cell wall is calculated, i.e. using equation 17 and 20 by replacing the attenuation coefficient for the density. This results in the next relation:

$$\rho_g = 0.87(0.56\rho_{D_2O} + 0.44\rho_{H_2O}) + 0.13\rho_p \tag{26}$$

Here $\rho_g$ is the density of the peat material between the fibres $[g/cm^3]$, $\rho_{D_2O}$ is the density of heavy water, $\rho_{H_2O}$ is the density of natural water, and $\rho_p$ is the density of the decomposed particles in the peat material. From table 8 of subsection 5.1.2 the average density of the decomposed plant tissue in the peat material is 1.4 $g/cm^3$. Moreover the density of the heavy water 1.1 $g/cm^3$. By filling in the values in equation 26, the density of the peat material between the fibres is found to be equal to 1.10 $g/cm^3$.
The difference $\Delta$ in density between the average density of the cell walls and the peat material between the fibres can be determined using equation 27.

$$\Delta = \frac{\rho_{cw} - \rho_g}{\rho_g} * 100\% \tag{27}$$

By filling in this equation, the density difference is computed at 5.4 %. Since the two densities are based on a few assumptions like the determination of the water content in the peat material between the fibres, the error of the difference in density is in the order of about 20% high. Therefore the value of this difference is considered to have an error of 20 %. Now the difference in density lies in the following interval:

$$4.5\% < \Delta < 6.5\% \tag{28}$$

The difference in density between the cell walls and the peat material between the fibres is high enough to observe a contrast on the tomographic image of the micro CT scan because this technique can distinguish a density difference of less than 0.5%. The white halo structures observed in figure 35 are the cell walls.

Label 2 shows the same white halo as shown in label 1. The difference of this white halo compared to the one shown labelled 1, is the color inside the structure on the tomographic image. The tomographic image displays the same colour inside the structure as the greyish peat material between the fibres. This is most probably a natural water-filled fibre. This fibre is also visible on the tomographic image of the neutron CT scan (fig. 34), i.e. label 2. Here the fibre shows the same dark color as for label 1, it is however a water-filled fibre as shown on figure 35. A reason for the dark color on the neutron tomographic image of

this labelled fibre is that during the time between scanning the sample with neutron CT and X-ray micro CT, water could have moved within the sample. This may result in a water-filled fibre on the tomographic image of the micro CT scanner.

To verify if the white halo structures visible on the tomographic image in figure 35 are indeed cell walls, the sample has been dried to verify and scanned using the micro CT scanner.

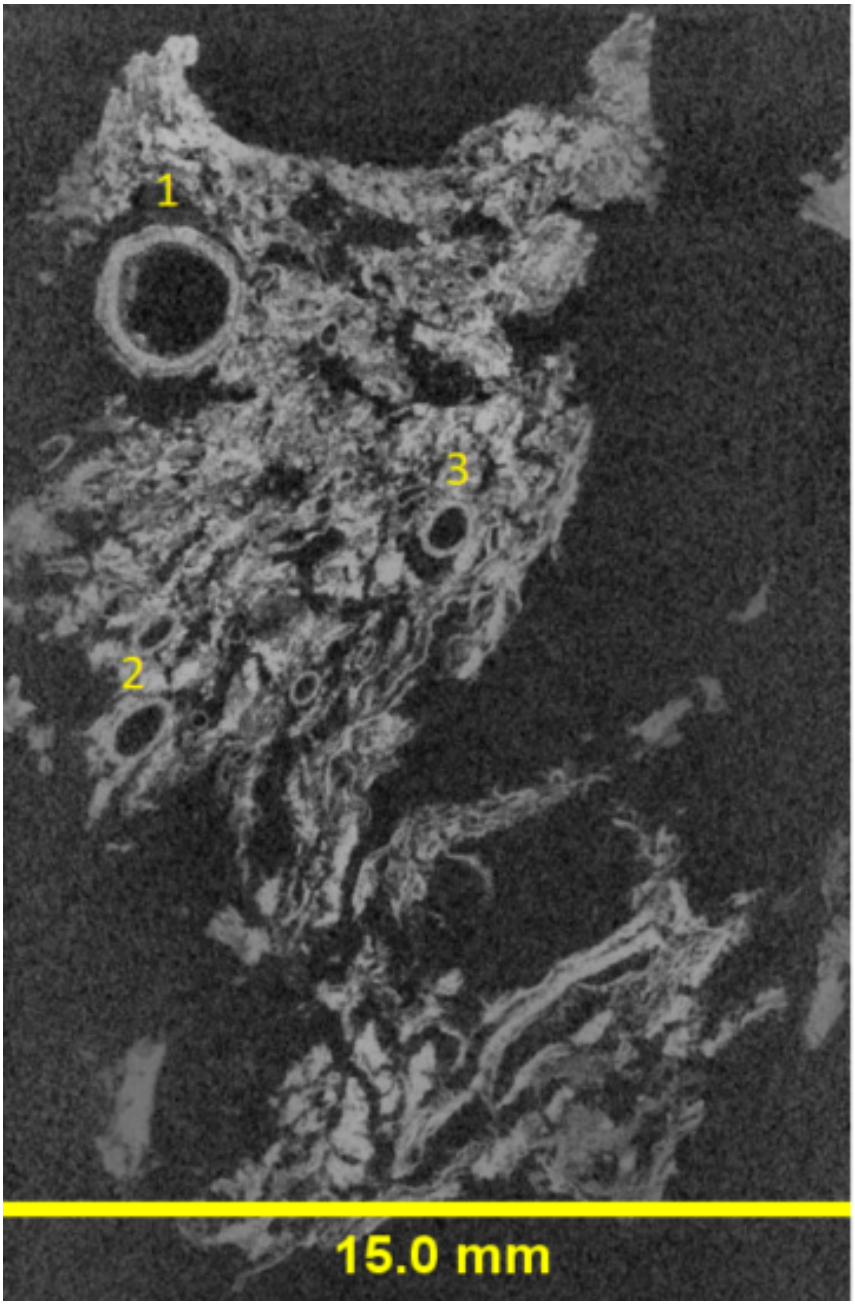


**Figure 36:** *tomographic images of dry peat sample using X-ray micro CT;*
*Air filled pores are observed in the greyish bulk which represents*
*the dry peat material between the fibres composed of decomposed plant tissue;*
*Label 1 represents the fibre filled with air as shown on figure 34 and 35;*
*Label 2 represents the white halo structure, which is a cellular wall;*
*Label 3 represents a small hollow fibre which is not found on figure 35*

The tomographic image corresponding to the sections shown in figure 34 and 35 is searched and is shown in figure 36. A perfect correspondence between images cannot be obtained. The same labels are used to distinguish the same fibres on the three scans. As one can observe the sample has shrunk differentially. Label 1 represents the air-filled fibre displayed on the tomographic images of both the neutron CT section and the micro CT section of the wet sample. The cell wall is thick on the dry scan and without any inner structure; the primary and secondary wall cannot be distinguished. As shown in subsection 5.1.3 both components of the cell wall have the same density. After drying the structure labelled 2 has lost its inner water. It appears clearly on the scan. Furthermore all the fine material between the air-filled fibres visible on the wet scans is revealed on the the dry scan. It consists of a fine organic tissue.

So based on the tomographic image of the neutron CT imaging it is not possible to observe the cell walls of the fibres because there is no transition between the peat material between the cell wall and the air to be observed in figure 34. The cell walls took up heavy water which resulted in a decrease of attenuation and therefore the difference in attenuation between the cell walls of the fibres and the peat material was too low to observe a contrast. The white halo structures visible on the micro CT scan of the wet sample are the cell walls of the fibres. On this scan not only air-filled fibres are visible, which is the case for the tomographic images of the neutron CT, but also natural water filled-fibres.

## 9.2 Filtering process of neutron CT images and X-ray micro CT images to display a 3D picture of the fibre network

The reconstructed neutron CT images are filtered in order to visualize geometry of the few fibres visible on the scans in 3D. Image thresholding based on selected grey values was not successful. Beam hardening was probably not corrected properly. As a result, fibres falling close to the claimed surface of the sample appear with the same grey color as the core of the sample, as shown in figure 37. Therefore other filters were tried to highlight the fibres.

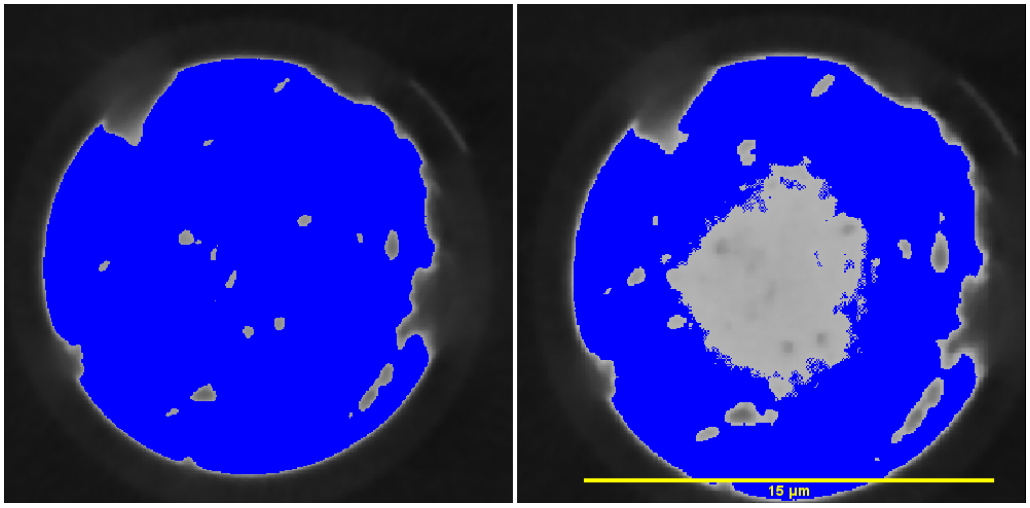


**Figure 37:**
*Unsuccessful thresholding of neutron CT images resulted in the same grey color (right image) for fibres as for the core of the sample due to not properly correcting beam hardening*

The DoB filter turned out to be the most suitable filter; it highlights the edges of the dark volumes on the neutron CT images. The explanation of this filter can be found in appendix A. Finally, the volume rendering tool is used to create a 3D view of some of the fibres. This view is shown in figure 38. Here label 1 represents the hollow structure also shown in figure 34, 35 and 36. The two labelled fibres are the clearest on this 3D picture of the geometry of the few fibres visible on the scans. Furthermore lots of structures like label 3 can be observed. These structures could be fibres because the tomographic image displayed on figure 34 visualizes small air-filled pores, i.e. dark regions on the cross-section. In order to make sure whether these structures are fibres or not, a new peat sample will be created and imaged with X-ray phase CT in Ghent. This will be performed to reveal more fibres. This is described in the next section. Some morphological characteristics of the fibres can be extracted using the measuring tool in avizo are shown in table 24. For fibres 1 and 2 the orientation of both fibres is taken using the vertical as reference direction. The width and length are measured manually using the measuring tool in avizo. As the fibres have a none regular geometry, this measurement is subjective.

| **Fibre** | **Orientation** [°] | **Width[cm]** | **Length[cm]** |
|---|---|---|---|
| Label 1 | 120 | 0.6 | 1.6 |
| Label 2 | 68 | 0.2 | 1.0 |

**Table 24:** *Morphological properties of the two selected fibres;*
*The orientation is taken using the vertical as reference;*
*The width and length are measured using the measuring tool in avizo*

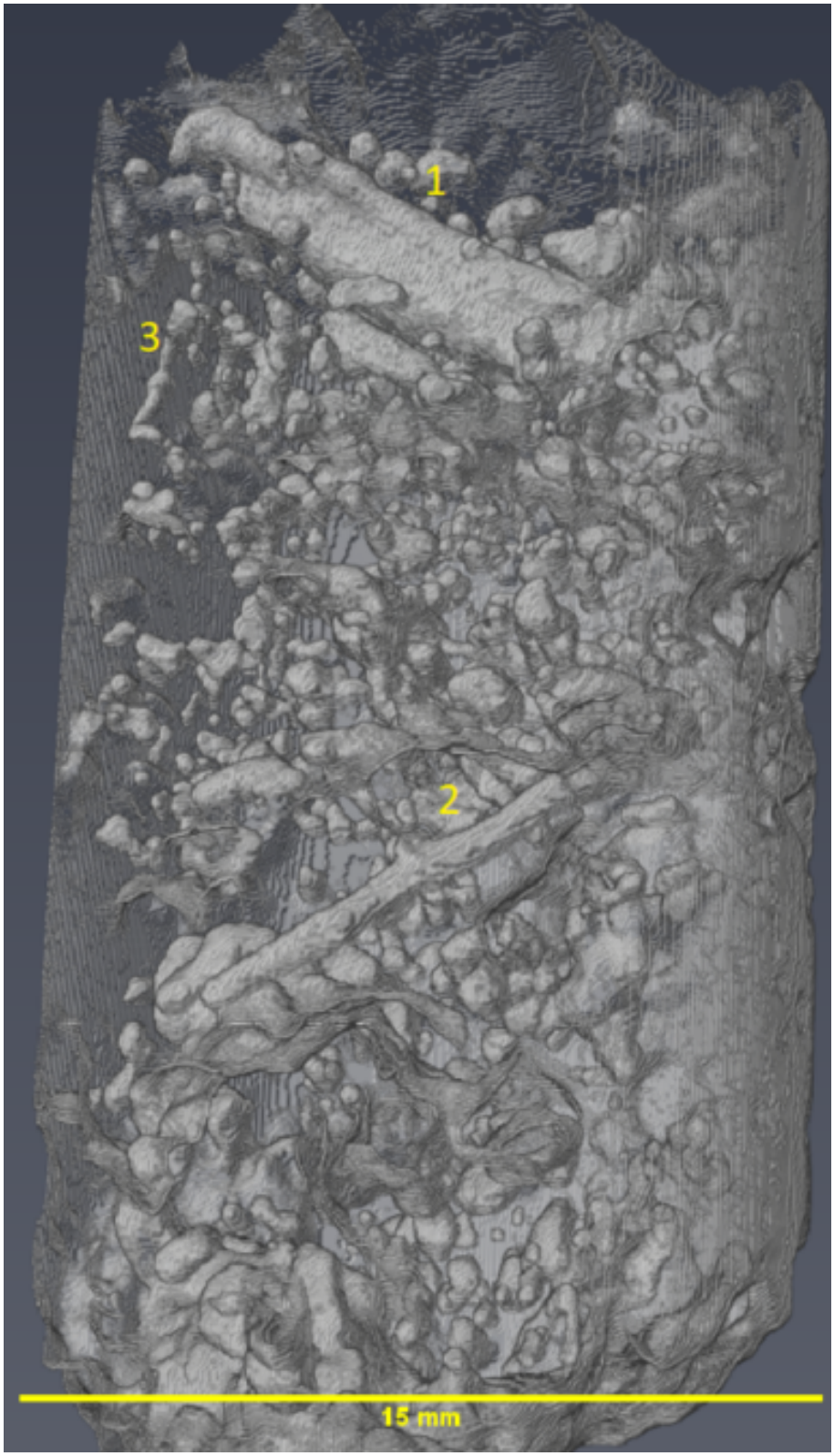


**Figure 38:**
*3D representation of the filtered images of the flushed peat sample imaged with neutron CT after applying the DoB filter in avizo;*
*Label 1 represents the hollow air-filled fibre observed on the tomographic images;*
*Label 2 represents an air-filled fibre which is also displayed on the tomographic images of the X-ray micro CT scan;*
*A lot of structures like label 3 are observed, these structures could be fibres*

The fibre marked with label 1 on figure 38 can also be filtered using the X-ray micro CT images. These images are filtered using the procedure displayed in appendix B. Thresholding was applied to extract the white halos corresponding to the walls of the fibres. Then, Avizo measure tool was used to obtain the volume of the white halos, and filter the halos based on their volume. The resulting view of label 1 fibre is shown on figure 39.

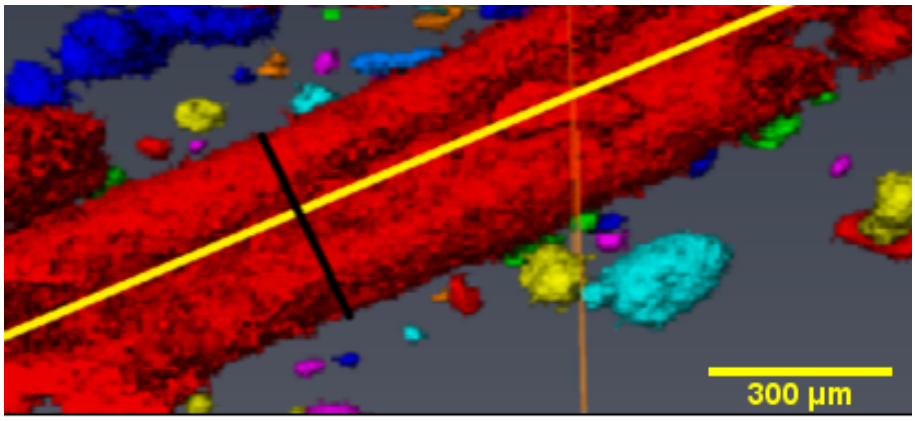


**Figure 39:** *Approach to measure the morphological parameters of a fibre; The yellow line represents the length of the fibre whereas the black line represents the width of the fibre.*

The length and width of the fibre can be measured manually and are compared to these obtained from the neutron CT scan. Results are found to be consistent.

| **Imaging method** | **width of fibre[cm]** | **length of fibre[cm]** |
|---|---|---|
| X-ray micro CT | 0.23 | 1.6 |
| Neutron CT | 0.21 | 1.6 |

**Table 25:** *Comparison of properties of the same fibre in saturated condition using both neutron CT and X-ray micro CT*

Since only the big air-filled fibres are visible on the neutron CT scan, the peat is imaged with X-ray phase tomography.

## 9.3 Analyzing white halo structures on the tomographic image using X-ray phase CT

For this study a small plastic sample holder is used to store the peat sample during imaging. This holder is preferred to an aluminum holder because it does not filter out weak low energy rays. The scanner settings of Hector, described in section 6.3, are shown in table 26.

| **Scanner settings** | **[mm]** |
|---|---|
| Source-Detector-Distance(SDD) | 1667 |
| Source-Object-Distance(SOD) | 76 |
| Voxel size | $9.0*10^{-3}$ |

**Table 26:** *Scanner settings of Hector with its high Source-Detector-Distance*

As one can see a large sample-detector distance is used for phase retrieval. As mentioned in subsection 5.2.2, the image contrast should be sufficient to segment and post process the corresponding images using this fixed distance.

The peat sample was kept saturated and imaged using X-ray micro CT in order to compare both methods. As one can observe from figure 40, where the upper image is a tomographic image of the X-ray phase CT data and the lower image a tomographic image of the X-ray micro CT data, the main benefit of X-ray phase CT, edge enhancement, did not occur. As described in section 5.2.3, Karunakaran et al. (2015) concluded that a soil with a high organic content, like peat, displays low contrast using X-ray phase CT. In the case of imaging peat, reconstruction of the X-ray phase data could not be performed without filtering because otherwise it would be hard to observe the patterns of the organic content of peat. This is due to a low difference in attenuation coefficients of the different materials present in peat. Filtering leads to losing the edge enhancement (Josipovic (2019)).

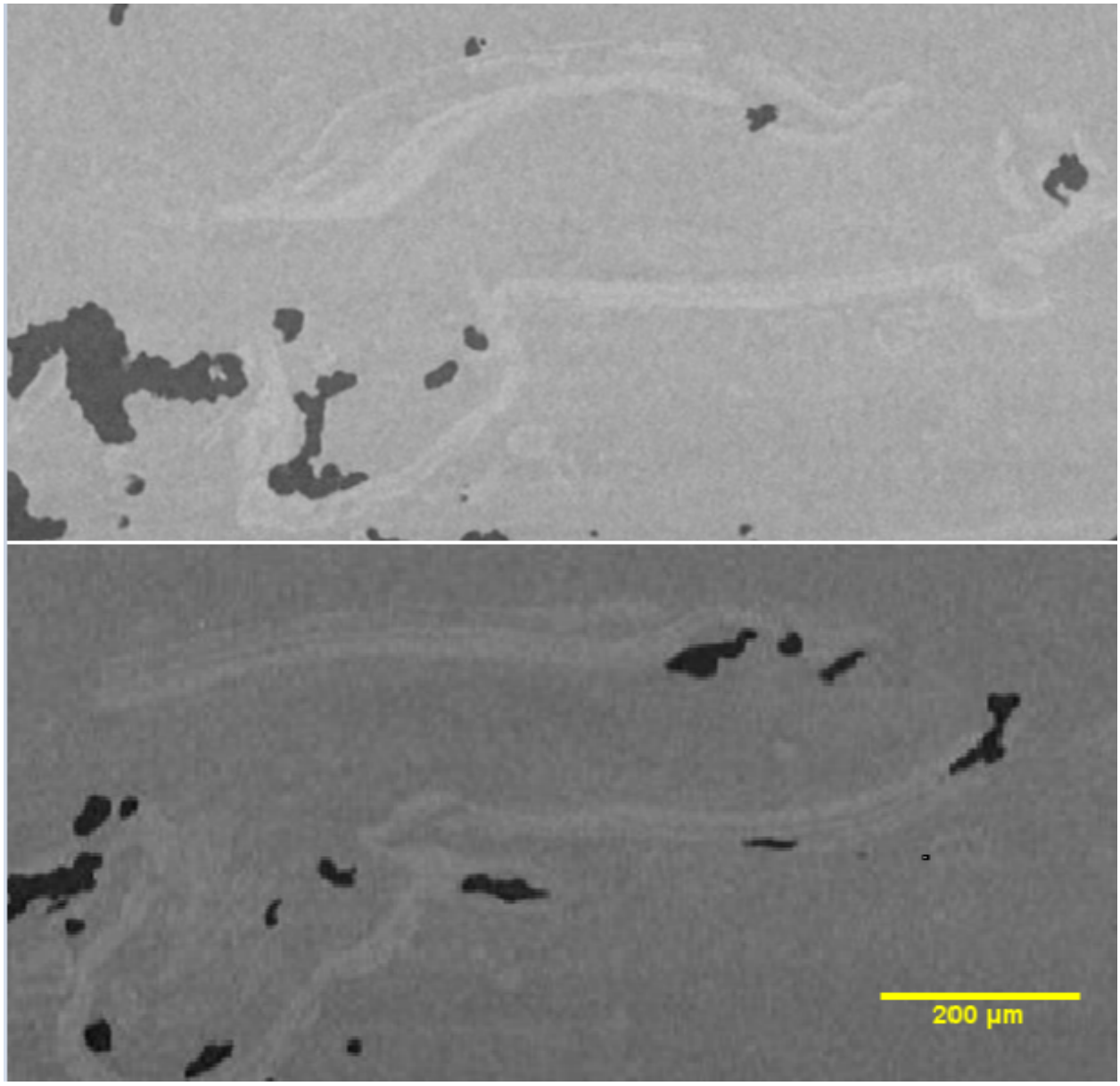


**Figure 40:**
*Comparison of tomographic image of peat sample imaged with X-ray phase CT at UGhent and X-ray micro CT at TU Delft*
*Upper: Small region of tomographic image of peat sample imaged with X-ray phase CT at UGhent; Lower: Small region of tomographic image of peat sample image with X-ray micro CT at TU Delft*

The filtering process to highlight the white halo structures is shown in appendix B. First the attention is put on the smaller fibres which are less visible on the other scans. The images were thresholded and filtered using the filter by measure tool in avizo. This filter was used to remove both the biggest and smallest artifacts of the 3D volume. Finally the volume rendering tool could be performed, generating a 3D view of the fibres. These fibres are dilated and closed generating a smoother surface of the fibres. The final 3D result of the network of the smaller fibres in front of a tomographic image in YZ-direction is shown in figure 41.

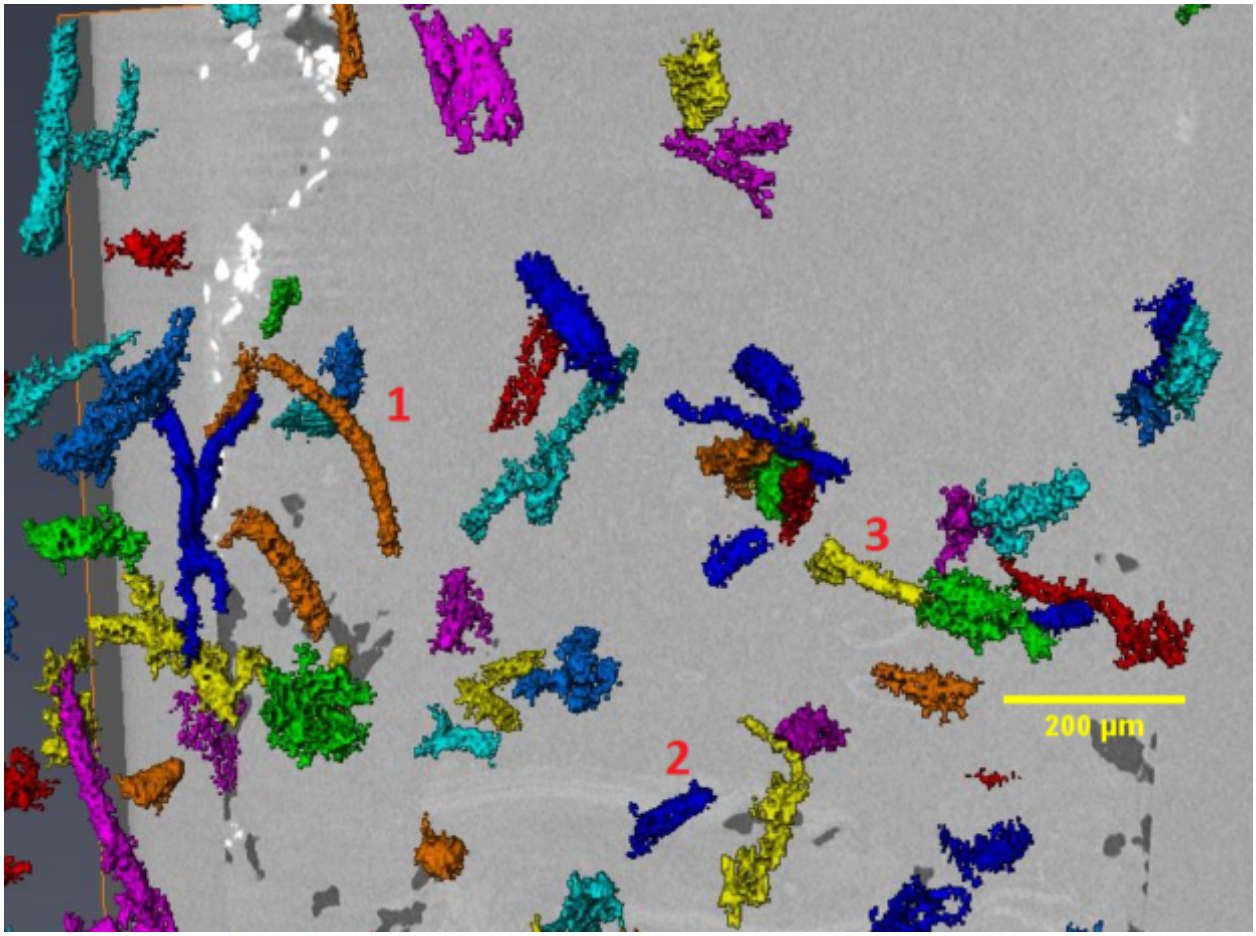


**Figure 41:** *3D representation of the fibre network using X-ray phase CT in front of a tomographic image in YZ-direction; The fibres are not orientated in one direction as the labelled fibres show*

As one can observe the fibres are not orientated in one direction. The three labelled fibres illustrate this. Some are curved and their direction cannot be simply measured automatically with avizo. As a result the main orientation of the fibres cannot be extracted. The fibres shown in this figure can be measured manually. The fibre displayed at label 1 is very thin, i.e. around 20 $\mu$m, and has a length of around 250 $\mu$m. This fibre could be a partial decomposed remain of grass as shown in figure 9 and 12 of section 4.7. Since the fibres are filtered in a certain range, the fibres have almost all the same characteristics in this figure.

The white halo structures shown on the tomographic images can be analyzed further by comparing the cross-section with the 3D view of the sample. Figure 42 shows a marked white halo which represents a water-filled fibre on the 3D volume of the fibres illustrated

on the left image. The length of this fibre is around 0.3 mm. This peat contains lots of these fibres with an approximate average length of 0.1-0.3 mm. Furthermore the peat from Uitdam contains of bigger fibres too, as shown in figure 9 and 11 of section 4.7. These fibres can be highlighted by using a different input value for the filtering by measure tool in avizo. In this case the smaller fibres are filtered out using this filter. Figure 43 displays a fibre of a length of around 4 mm. The left picture displays the tomographic image whereas the right picture displays the 3D representation of the fibre in front of this cross-section. As one can observe the fibre is water-filled because of the same characteristics as described above.

Moreover, air-filled white halo structures are visible on the tomographic images. One of these fibres is shown on figure 44. As one can observe from the left image, the white halo highlighted with the red square surrounds air which represents a dark colour on the tomographic image. On the right image one can observe the air-filled fibre in 3D. The fibre has a length of around 4 mm and a thickness of around 1.2 mm. Based on these characteristics of the fibre this could be a remain of wood. To verify this, a tomographic image of the dry sample is analyzed, shown in figure 45.

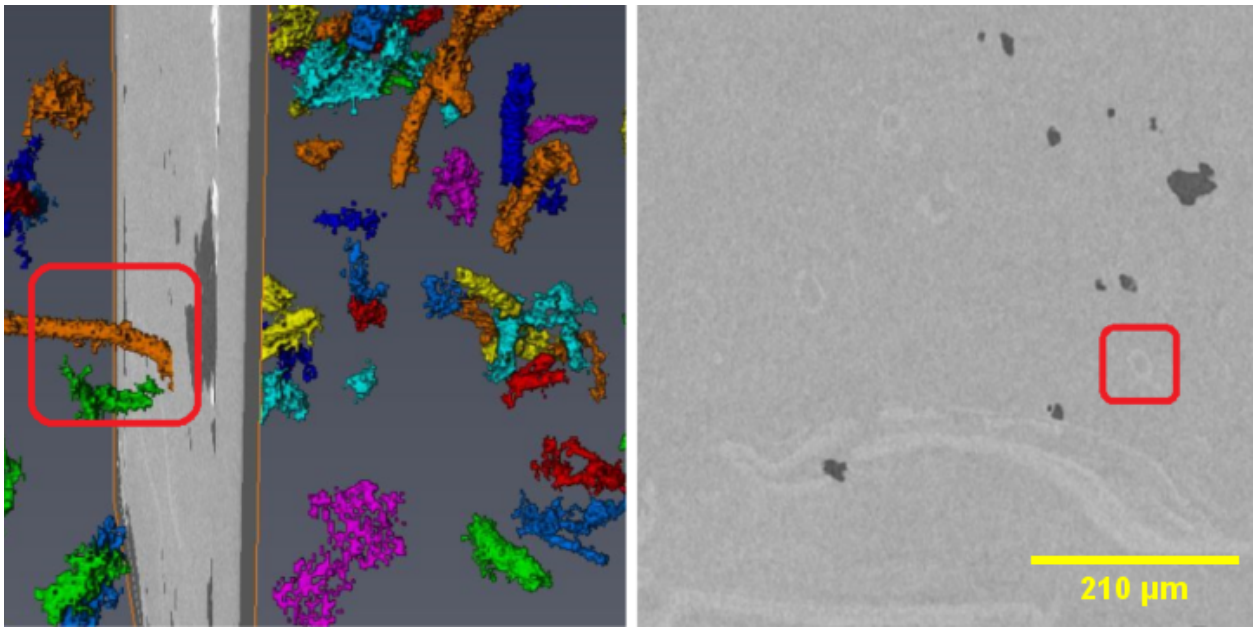


**Figure 42:** *left: 3D representation of the fibre network using X-ray phase CT; in front of a tomographic image in XZ-direction; right: tomographic image in XZ-direction; A white halo structure is highlighted on both images*

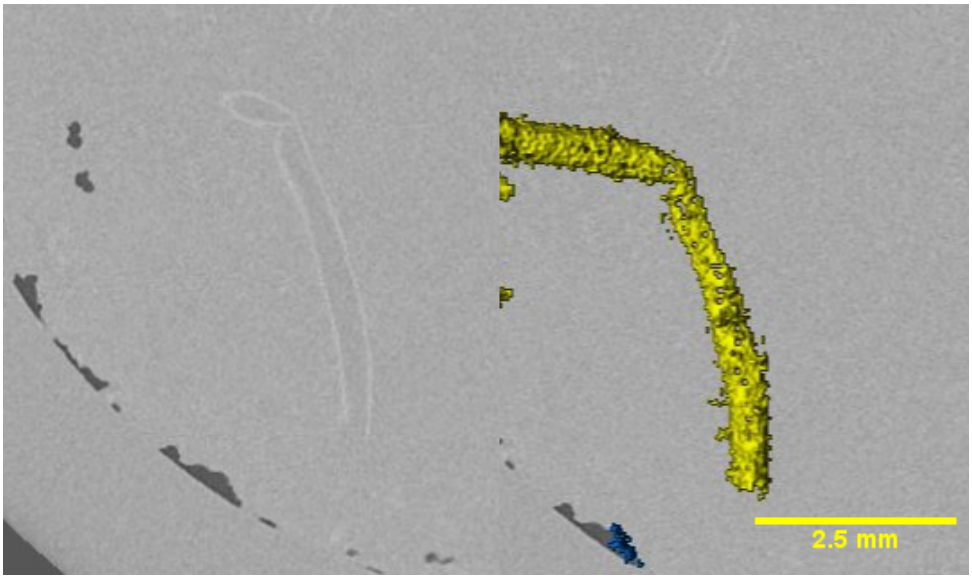


**Figure 43:** *left: tomographic image in XZ-direction, a white halo structure is observed; right: 3D view of the representative water-filled fibre of the tomographic image in front of the cross-section*

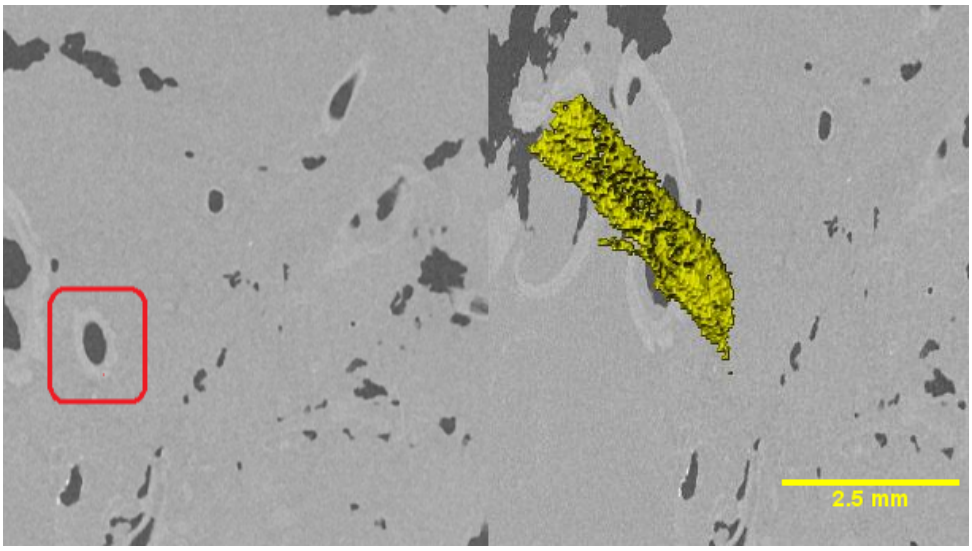


**Figure 44:** *left: tomographic image in YZ-direction, red square represents a white halo structure surrounding air; right: 3D view of the representative air-filled fibre of the tomographic image in front of the cross-section*

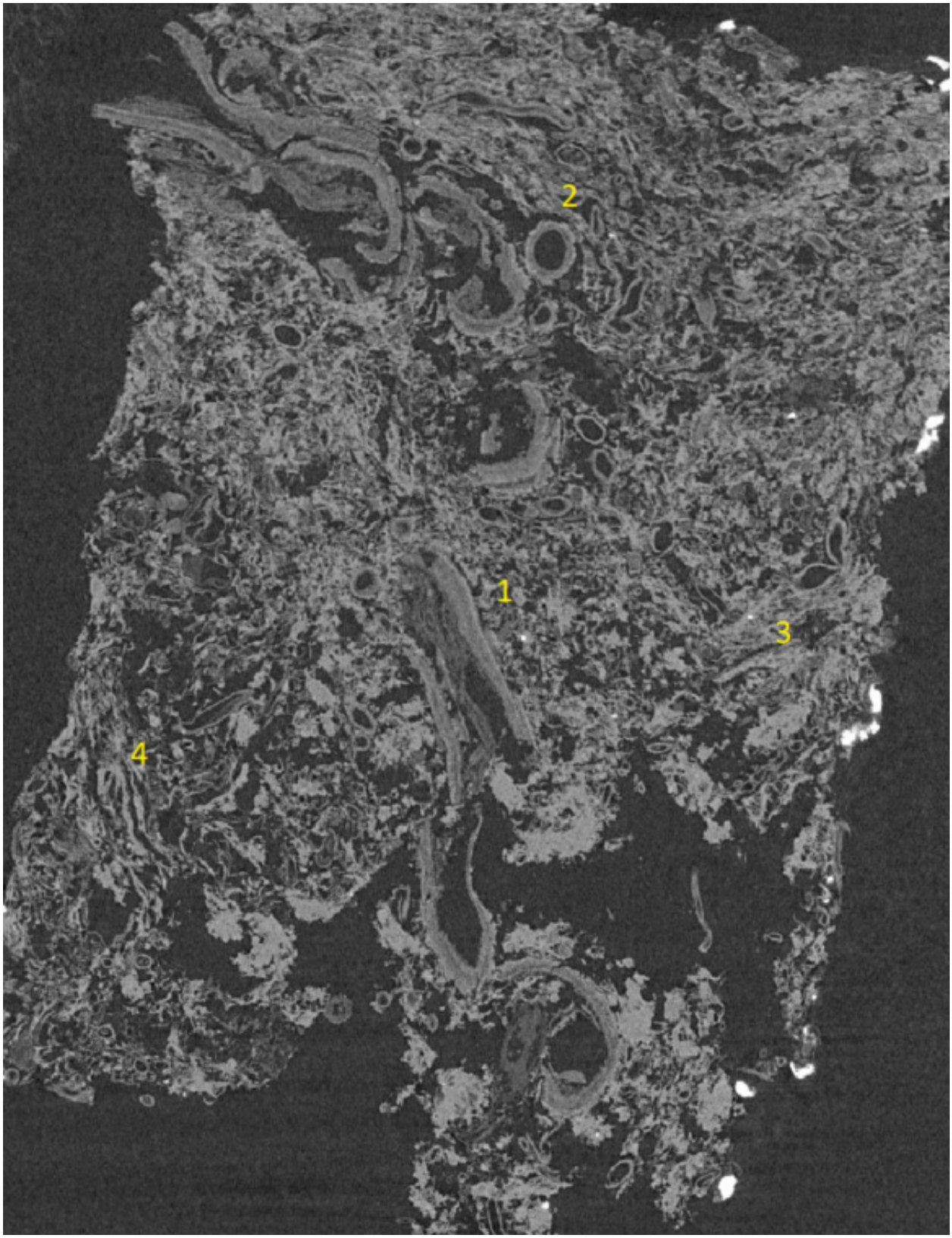


**Figure 45:** *tomographic image in XZ-direction representing the dry sample imaged with X-ray micro CT;*
*Label 1 represents a wood remain as shown in figure 9 of section 4.7 and showed in figure 44;*
*Label 2 represents a fibre filled with air as shown in figure 43;*
*Label 3 represents the peat material between the fibres in peat;*
*Label 4 represents a remain of grass as shown in figure 9 and 11 of section 4.7*

The described fibre of figure 43 turned out to be a wood remain representing label 1 on figure 45. This is because of the fact that the fibre is not filled with air after drying it. Wood has this characteristic and moreover the spatial properties of this tissue corresponds to the wood displayed on figure 9 of section 4.7. Label 2 represents an air-filled fibre. This is an example of the fibre outlined in figure 43. After drying the water inside the cell evaporated, and therefore the cell is filled with air. Label 3 represents the remain of peat material between the fibres after drying. This material is fine and composed of decomposed organic matter and semi-decomposed grassy matter, as shown in figure 13 of section 4.7. Finally label 4 represents a small remain of grass. Next to this, some other small fibres are shown on the tomographic image of the dry sample. These fibres are not shown on the cross-section of the wet scan because these fibres do not have thick cell walls, and therefore there is no density difference between the fibre and the peat material between the fibres.

# 10 Discussion

During this thesis a peat coming from a site called Uitdam, which is a lake in between Noord-Holland and Flevoland, is imaged using three methods, i.e. neutron CT, X-ray micro CT, and X-ray phase CT. The aim of this research was to image the fibres of peat to better understand the role of them in the unusual behavior of the peat material. For this research all (partly-decomposed) plant and wood tissue with a rod-like shape were treated as a fibre. Next to these fibres peat consists of a material, which is a mixture of water and decomposed plant and wood tissues. The fibres are cellular structures which are either water-filled, air-filled, or a combination of both. The tube has a primary cell wall and a secondary cell wall which is much thicker than the primary wall. The main compounds in the cell wall are cellulose and lignin. The goal of imaging peat with the above mentioned methods is to highlight the fibres from the peat material between the fibres in the peat.

Neutron radiography performed on an aluminum cylindrical peat sample with a diameter of 3.0 cm resulted in an attenuation coefficient, which describes the absorption of the neutrons by the sample, which was too high to observe structures from the radiographs. Since peat has a high water content it absorbs neutrons because water has a high attenuation coefficient. Furthermore the decomposed plant tissue and the cell walls of the fibres have almost the same attenuation coefficient as water. Therefore, it is impossible to observe any structure from the radiographs. The transmission of neutrons does not only depend on the attenuation coefficient of the peat but it also depends on the thickness of the sample, as described by the Beer-Lambert law. Therefore, samples with smaller diameters were imaged but neutron radiography resulted in the same amount of transmission of neutrons. To gain a contrast between the fibres and the peat material between the fibres, heavy water was used to replace the natural water. This was performed because heavy water has a low attenuation coefficient for neutrons, and therefore it should increase the transmission of neutrons. After trying to saturate peat with heavy water using a vacuum tank which did not work out because peat still had a high natural water content, a flushing procedure was established. Here, a triaxial set up was used. Heavy water was stored in a controller which controlled the back pressure. The goal was to get a pressure gradient between the pores and the back pressure allowing heavy water to flow in the sample from bottom to top. This procedure proved to work and the sample could be imaged with neutrons. Since heavy water and natural water have almost the same mutual diffusion coefficient, heavy water diffused in natural water. After imaging the liquid which flew out of the sample during flushing, the attenuation coefficient of the peat material between the fibres after flushing could be calculated. The value decreased enough to gain a contrast between the fibres and the peat material.
The flushed peat was imaged and the transmission increased allowing to perform neutron CT on the sample. Using avizo version 9.4 the reconstructed images were analyzed. In these images the peat material between the fibres and the air-filled fibres were clearly visible. A tomographic image of imaging the sample with neutron CT is shown on the left image of figure 46. However the walls of the fibres were not visible. A reason for this could be that the cells walls picked up some heavy water which resulted in a decrease of attenuation coefficient of the cell walls inducing an equal attenuation coefficient as for the peat material between the fibres. Furthermore the calculation of the attenuation coefficient of both the peat material between the fibres and the cell walls could be wrong because of the estimation of the fibre content done during the calculations.

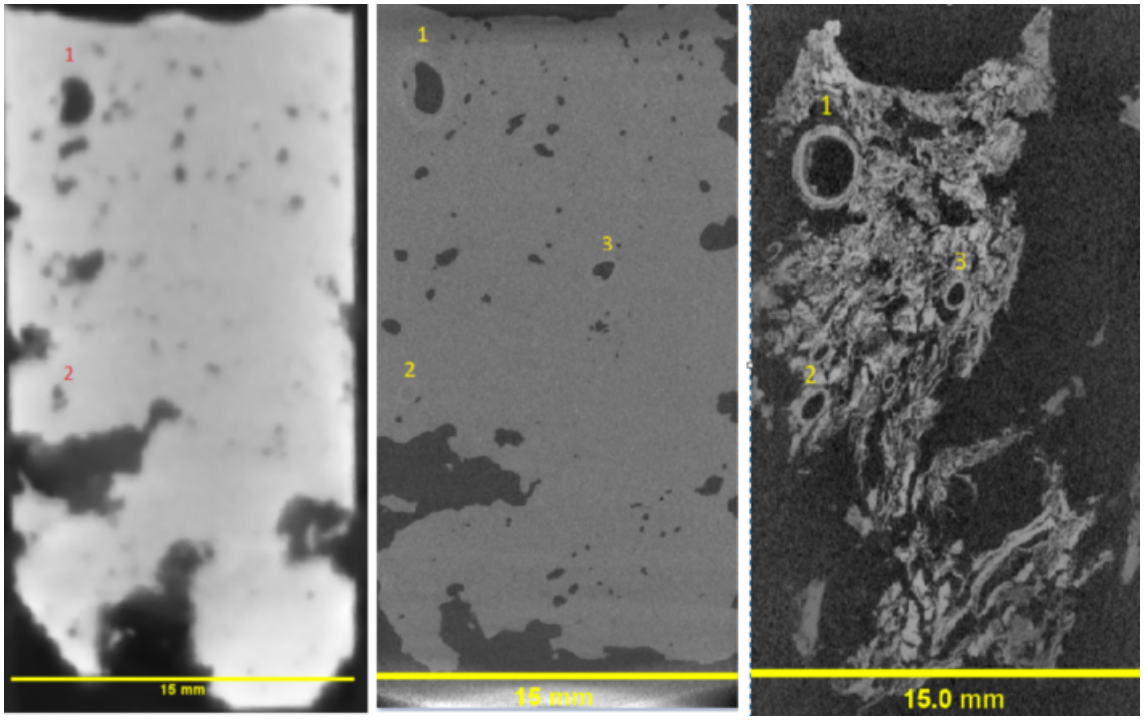


**Figure 46:** *tomographic images of different imaging techniques; Left: tomographic image of imaging peat with neutron CT; Middle: tomographic image of imaging peat with X-ray micro CT; Right: tomographic image of peat sample in dry state imaged with X-ray micro CT*

The same sample was also scanned in its wet and dry state using X-ray micro CT, a tomographic image of both scans is shown on the middle and right images of the figure above. In both cases the cell walls of empty fibres were observed, e.g. label 1. On the wet scan some white halo structures were visible in addition to the holes associated to air-filled hollow fibres, e.g. label 2. The X-ray micro CT scan of the same sample in a dry state showed that these halos correspond to the walls of plant fibres, e.g. label 2. The white halo shows up on the wet micro CT scan because the density of the cell walls is higher than the density for peat material between the fibres and water. On the dry micro CT scan of the sample, the structure of the dry peat material between the fibres appears. The material between the large tubular fibres is not amorphous but made of thin fragments of organic tissues.

The neutron tomographic images could be filtered using avizo version 9.4. From the 3D view only a few fibres were distinguished. Therefore, a new sample was scanned using X-ray phase CT in Ghent to reveal more fibres. This approach uses a large sample-detector distance which results in a high image contrast for low absorbing materials, like peat. However the resulting tomographic images, shown in figure 47, did not show any contrast enhancement compared to the tomographic images of the X-ray micro CT scan on the same sample. A previous research described by Karunakaran et al. (2015) showed that if a soil has a high organic content it displays less contrast between the edges of fibrous material and the material between this material. Furthermore reconstruction of the X-ray phase data could not be performed without filtering because otherwise it would be hard to observe the patterns of the organic content of peat. This is due to a low difference in attenuation coefficients of the different materials present in peat. Filtering leads to losing the edge enhancement.

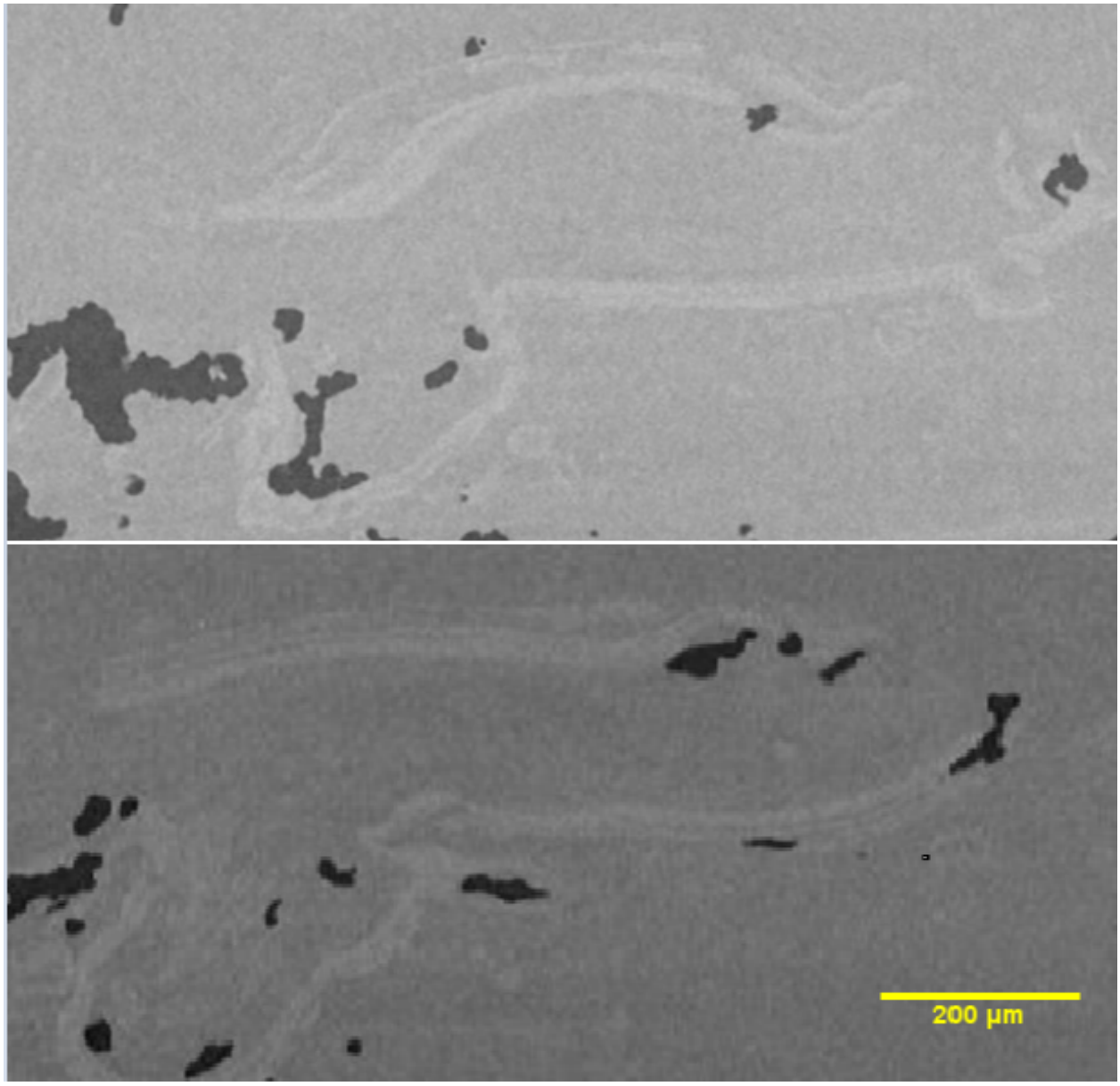


**Figure 47:**
*Comparison of tomographic image of peat sample imaged with X-ray phase CT at UGhent and X-ray micro*
*Upper: Small region of tomographic image of peat sample imaged with X-ray phase CT at UGhent;*
*Lower: Small region of tomographic image of peat sample image with X-ray micro CT at TU Delft*

The X-ray phase CT scan had a better resolution, i.e. 9$\mu$m, compared to the micro CT scan performed on the first sample, i.e. 15$\mu$m. Therefore, smaller fibres were better shown on X-ray phase contrast CT images. The fibres were found to be randomly orientated as shown in figure 48. The sample was dried and scanned using X-ray micro CT. The tomographic images of both scans were compared in order to better understand the origin of the fibres. On the dry scan other small fibrous structures were visible.

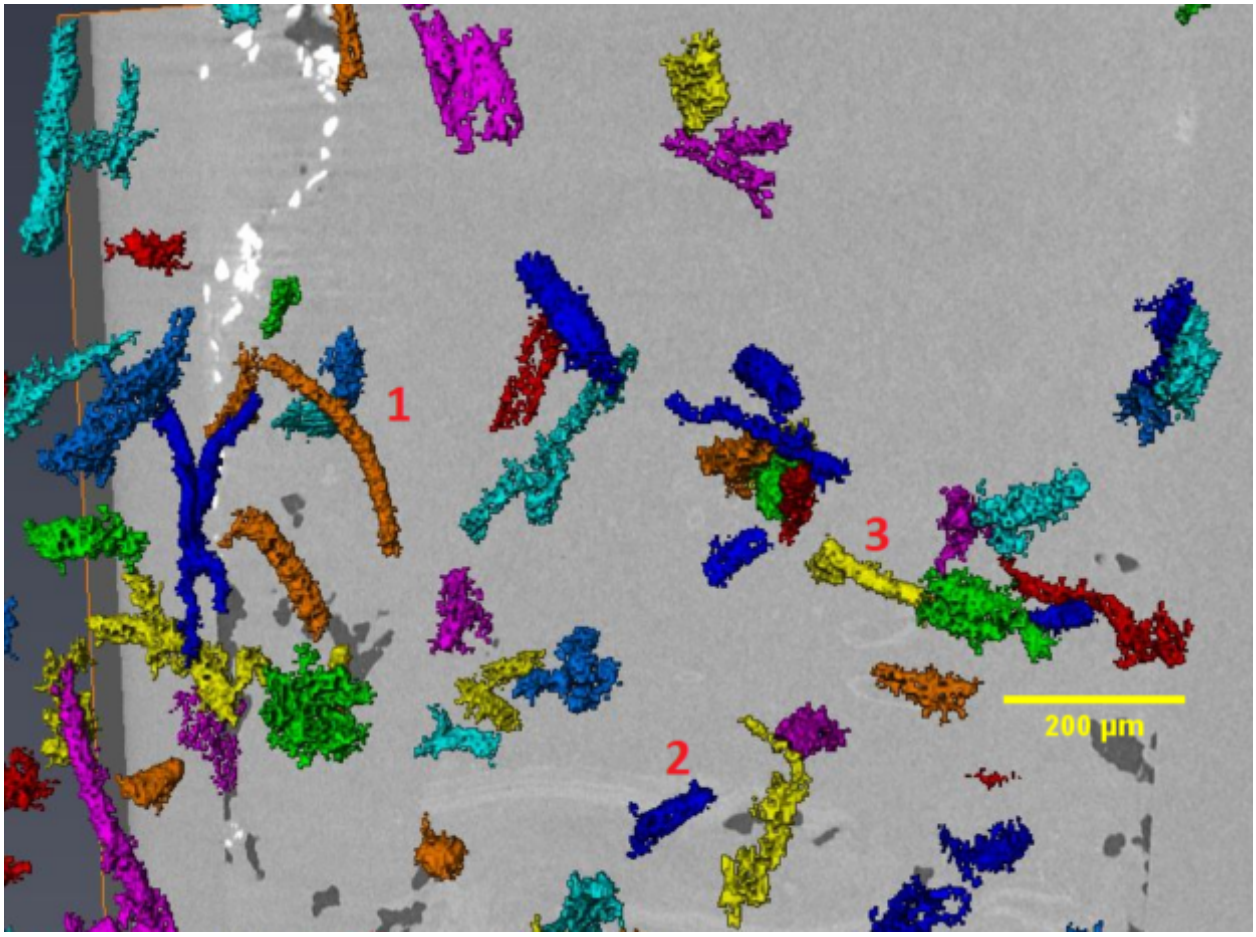


**Figure 48:** *3D representation of the fibre network using X-ray phase CT in front of a tomographic image in YZ-direction; The fibres are not orientated in one direction as the labelled fibres show*

# 11 Conclusions and Recommendations

This study focused on imaging the fibres of peat from a site called Uitdam located in the Netherlands. To do so, neutron CT at the Reactor Institute Delft, X-ray phase CT at the Ghent University Centre for X-ray CT, and X-ray micro CT at the geoscience section of TU Delft were performed on different samples. To perform neutron CT the sample was flushed with heavy water to get a transmission contrast between the peat material between the fibres and the fibres itself.

The result of performing neutron CT on the flushed peat sample was not convincing because only air-filled tubular fibres could be distinguished from the peat material between the fibres in the tomographic images. Furthermore only the big fibres could be distinguished from the peat material because of the high resolution of the neutron station, i.e. 150$\mu$m. The length and width of the tubular fibres could be extracted which answers the first research question of this thesis. However, the micro-CT scan of the dry sample performed at TU Delft, revealed the presence of many other fibrous structures which were invisible on the neutron CT scan. Since most of the fibres in peat are water-filled, the neutron CT images were of limited interest. The elongated white halo visible on the X-ray micro CT scan of the wet sample at TU Delft revealed to be water-filled tubular fibres. Therefore, both air-filled tubular and water-filled tubular fibres could be distinguished from the X-ray micro CT scan which answers the second research question of this thesis. The X-ray micro CT scan of the same sample in a dry state showed that the white halos correspond to the walls of fibres.

To reveal more fibres X-ray phase CT in Ghent was performed on a new sample. The white halo visible on the grey-sections were filtered using avizo version 9.4. The tubular fibres were found to be randomly orientated. The main benefit of X-ray phase CT, the edge enhancement, did not occur on the tomographic images. It was lost during reconstruction of the data because filtering was performed on the raw data during reconstruction otherwise it would be hard to observe the patterns of the organic content of peat. This is due to a low difference in attenuation coefficients of the different materials present in peat. Therefore, the third research question can be answered negatively because the same structures are visible on the scans of Ghent and Delft.

To conclude, neutron CT showed only the big air-filled fibres imaging a heavy water flushed peat sample whereas X-ray micro CT showed the cell walls of both air-filled and water-filled fibres as a white halo on the tomographic image. Therefore, the hypothesis stated in section 4.9 is rejected. Furthermore, X-ray phase CT did not show its main benefit, i.e. edge enhancement, due to a too low difference in attenuation coefficient of the different materials present in peat. The tubular fibres found on the X-ray micro CT images were found to be randomly orientated

To perform further research on the behavior of fibres of wet peat under loading conditions one should question if it is sufficient to track white halos of tubular fibres to better understand displacement of peat fabric. If so, I would propose to image a peat sample while running in-situ geotechnical tests on it. Keep the sample saturated and perform X-ray micro CT scans. This test can be performed at UGhent, using the same scanner as used for this research. The scanner (Hector) can carry loads of up to 80 kg. Furthermore to better understand the heavy water uptake of the cell walls of the fibres, one could put a tubular fibre in heavy water. This can be performed in order to observe the heavy water uptake of the fibre in time while imaging it with neutron CT as Zarebanadkouki et al. (2013) showed with a lupine root.

# References


Bertrand, L., Cotte, M., Stampanoni, M., Thoury, M., Marone, F., and Schöder, S. (2012). Development and trends in synchrotron studies of ancient and historical materials. *Physics Reports*, 519(2):51–96.

Böttinger, M., Meier-Fleischer, K., and Ulmen, C. (2013). Tutorial: Interactive 3d visualization in earth system research with avizo green 8.0. *DKRZ/KlimaCampus Hamburg*.

Buades, A., Coll, B., and Morel, J.-M. (2005). A non-local algorithm for image denoising. In *Computer Vision and Pattern Recognition, 2005. CVPR 2005. IEEE Computer Society Conference on*, volume 2, pages 60–65. IEEE.

Chen, H. (2014). Chemical composition and structure of natural lignocellulose. In *Biotechnology of lignocellulose*, pages 25–71. Springer.

Dahal, U. and Adhikari, N. P. (2012). Molecular dynamics study of diffusion of heavy water in normal water at different temperatures. *Journal of Molecular Liquids*, 167:34–39.

Davison, B. H., Parks, J., Davis, M. F., and Donohoe, B. S. (2013). Plant cell walls: basics of structure, chemistry, accessibility and the influence on conversion. *Aqueous pretreatment of plant biomass for biological and chemical conversion to fuels and chemicals*, pages 23–38.

Drzymulska, D. (2016). Peat decomposition–shaping factors, significance in environmental studies and methods of determination; a literature review. *Geologos*, 22(1):61–69.

Francis, W. and Peters, M. C. (2013). *Fuels and fuel technology: a summarized manual*. Elsevier.

Frandsen, W. H. (1997). Ignition probability of organic soils. *Canadian Journal of Forest Research*, 27(9):1471–1477.

Gore, A. J. P. (1983). *Mires–swamp, bog, fen, and moor*. Elsevier Scientific Publishing Company.

Groso, A., Abela, R., and Stampanoni, M. (2006). Implementation of a fast method for high resolution phase contrast tomography. *Optics express*, 14(18):8103–8110.

Grosse-Brauckmann, G. (1996). Classification of peat and peatbogs in germany and its botanical, ecological and pedological foundations. In *Proceedings of 10th International Peat Congress," Peatlands Use-Present, Past and Future*, volume 27, pages 21–38.

Guide, A. U. (2013). Visualization sciences group. SAS.

Guimaraes, G. C., Coelho Junior, M. C., and Garcia Rojas, E. E. (2008). Density and kinematic viscosity of pectin aqueous solution. *Journal of Chemical & Engineering Data*, 54(2):662–667.

Ho, Y., McKay, G., et al. (1999). Batch lead (ii) removal from aqueous solution by peat: equilibrium and kinetics. *Trans IChemE*, 77(part B):165–173.

Josipovic (2019). Private discussion about losing edge enhancement on the grey cross-section of x-ray phase ct.

Kalluri, U. C., Yin, H., Yang, X., and Davison, B. H. (2014). Systems and synthetic biology approaches to alter plant cell walls and reduce biomass recalcitrance. *Plant biotechnology journal*, 12(9):1207–1216.

Karunakaran, C., Lahlali, R., Zhu, N., Webb, A. M., Schmidt, M., Fransishyn, K., Belev, G., Wysokinski, T., Olson, J., Cooper, D. M., et al. (2015). Factors influencing real time internal structural visualization and dynamic process monitoring in plants using synchrotron-based phase contrast x-ray imaging. *Scientific Reports*, 5:12119.

Kettridge, N. and Binley, A. (2008). X-ray computed tomography of peat soils: Measuring gas content and peat structure. *Hydrological Processes: An International Journal*, 22(25):4827–4837.

Klavins, M., Sire, J., Purmalis, O., and Melecis, V. (2008). Approaches to estimating humification indicators for peat. *Mires & Peat*, 3.

Kramer, P. J. (1955). Water content and water turnover in plant cells. *Encyklopedia of Plant Physiology (ed. Ruhland, W.)*, 1:194–217.

Kurbatov, I. (1968). The question of the genesis of peat and its humic acids. In *Transactions of the 2nd international peat congress, Leningrad*, volume 1, pages 133–137. HMSO Edinburgh.

McCarthy, D. F. and McCarthy, D. F. (1977). *Essentials of soil mechanics and foundations*. Reston Publishing Company Virginia.

Mesri, G., Stark, T., Ajlouni, M., and Chen, C. (1997). Secondary compression of peat with or without surcharging. *Journal of Geotechnical and Geoenvironmental Engineering*, 123(5):411–421.

Mikucioniene, D., Cepukone, L., Salmeia, K. A., and Gaan, S. (2019). Comparative analysis of peat fibre properties and peat fibre-based knits flammability. *Autex Research Journal*, 19(2):157–164.

Paganin, D., Mayo, S., Gureyev, T. E., Miller, P. R., and Wilkins, S. W. (2002). Simultaneous phase and amplitude extraction from a single defocused image of a homogeneous object. *Journal of microscopy*, 206(1):33–40.

Seignez, N., Gauthier, A., Mess, F., Brunel, C., Dubois, M., and Potdevin, J. L. (2010). Development of plant roots network in polluted soils: an x-ray computed microtomography investigation. *Water, Air, & Soil Pollution*, 209(1-4):199–207.

Stamm, A. J. (1929). Density of wood substance, adsorption by wood, and permeability of wood. *The Journal of Physical Chemistry*, 33(3):398–414.

Terzaghi, K., Peck, R. B., and Mesri, G. (1996). *Soil mechanics in engineering practice*. John Wiley & Sons.

Van Breemen, N. (1995). How sphagnum bogs down other plants. *Trends in ecology & evolution*, 10(7):270–275.

Van Geet, M., Swennen, R., and Wevers, M. (2000). Quantitative analysis of reservoir rocks by microfocus x-ray computerised tomography. *Sedimentary Geology*, 132(1-2):25–36.

Wilkins, S., Gureyev, T. E., Gao, D., Pogany, A., and Stevenson, A. (1996). Phase-contrast imaging using polychromatic hard x-rays. *Nature*, 384(6607):335.

Zarebanadkouki, M., Carminati, A., Kaestner, A., Mannes, D., Morgano, M., Peetermans, S., Lehmann, E., and Trtik, P. (2015). On-the-fly neutron tomography of water transport into lupine roots. *Physics procedia*, 69:292–298.

Zarebanadkouki, M., Kim, Y. X., and Carminati, A. (2013). Where do roots take up water? neutron radiography of water flow into the roots of transpiring plants growing in soil. *New Phytologist*, 199(4):1034–1044.

Zhou, Z., Plomp, J., van Eijck, L., Vontobel, P., Harti, R. P., Lehmann, E., and Pappas, C. (2018). Fish: a thermal neutron imaging station at hor delft. *Journal of Archaeological Science: Reports*, 20:369–373.

Zwanenburg, C. and Barends, F. (2005). Unravelling the anisotropy of peat. In *Proceedings of the international conference on soil mechanics and geotechnical engineering*, volume 16, page 469. AA Balkema Publishers.

# Appendices

## A Determination of fibres using neutron tomographic data

After imaging the peat sample using neutron CT, the obtained dataset was reconstructed using "Octopus" software. This dataset could be filtered using "Amira Avizo" software version 9.4. This is a 3D data visualization software. Avizo was developed primarily for the visualization of medical, chemical or biological data. A typical application of avizo is the possibility of interactively extracting and rendering 3D representations of skin, bones and tumors using CT data. Starting in 2007, Avizo was extended for applications in earth sciences – initiated and coordinated by the German Climate Computing Centre (DKRZ) (Böttinger et al. (2013)).

### A.1 tomographic images

To analyze the tomographic images of the dataset the ortho slice tool can be selected. This tool displays one tomographic image out of the total dataset. Three orientations can be selected, i.e. XZ, YZ and XY. The XZ-orientation is selected most commonly because it displays the vertical cross-section of the displayed slice number. It is possible to scroll through all the cross-sections present in the dataset using this tool. An example of a grey ortho slice in XZ-direction using the above described sample is shown in figure 49.

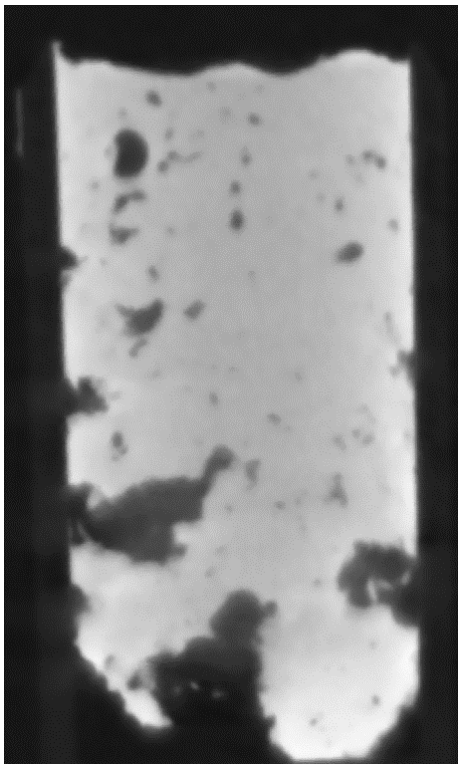

**Figure 49:** *Example of a tomographic image in XZ-direction using neutron CT images*

## A.2 Filtering of the images

Filtering is applied to improve the image quality and facilitate the post processing. Morevover filtering is performed to remove noise by applying neighborhood operations(Guide (2013)).

### A.2.1 DoB filter

The DoB-filter was applied on the neutron CT images. This filter calculates the difference between two local averages computed over cubic neighborhoods of different kernel sizes (Difference Of Boxes) applied on the same image. A kernel is an example of a convolution matrix. During convolution each element of the image will be added to its local neighbours. This will be weighted by the kernel.

The DoB operation applied to a 1D step edge is shown in figure 50.

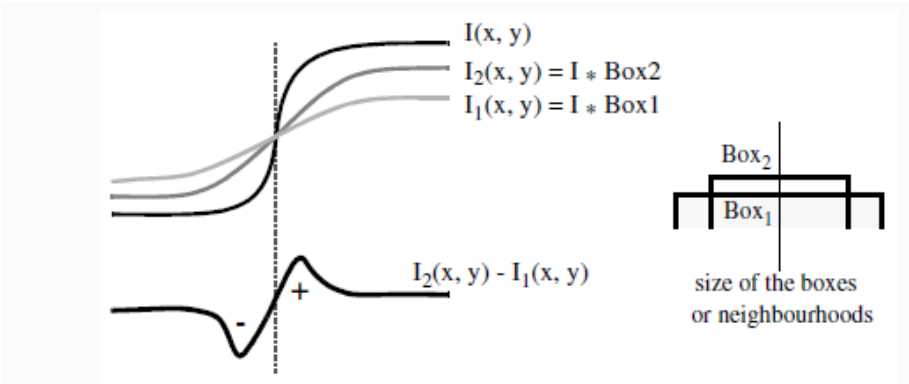


**Figure 50:** *DoB approximation;*
*Source: Avizo help*

The DoB Filter does not compute the Laplacian of an image, but it is a good approximation and has the main advantage of not generating isolated points. To keep a correct representation of the edges and a maximum of detail, small kernels need to be used. The deviation between the two masks has a direct effect on the edges. If the difference is too large, the edges are very thick and all small details disappear. If the difference is small, the edges are very thin and details more precise. After trial and error the best result occurred while setting the difference at 1 pixel. This 3D result is shown in figure 52. The input values which were used for analyzing the peat sample are shown in figure 51.

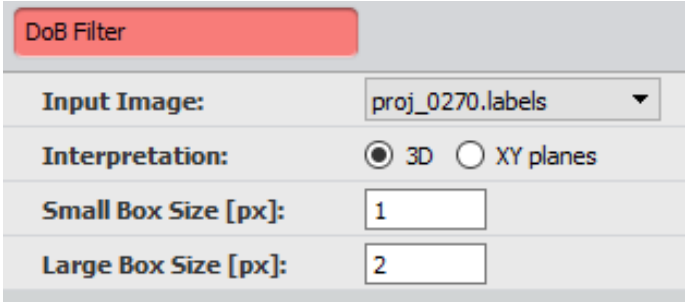


**Figure 51:** *3D rendered volume of DoB filtered neutron CT images*

## A.3 Volume rendering

To get a 3D image of the DoB-filtered dataset the volume rendering tool was selected as shown in chapter 9. This resulted in the following 3D rendered volume of the DoB filtered dataset.

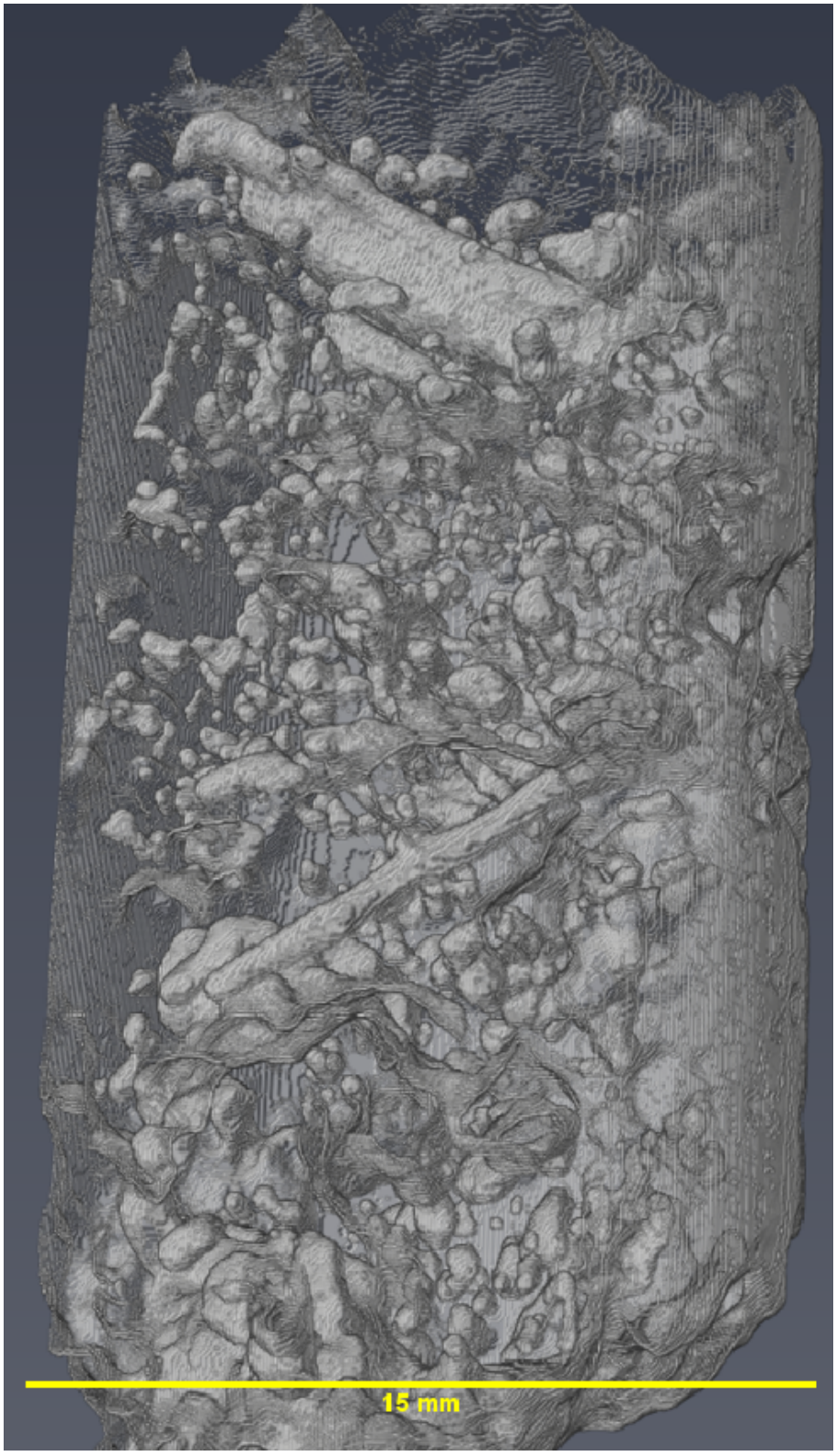


**Figure 52:** *Rendered 3D volume of DoB filtered neutron CT images*

# B Analyzing second peat sample using X-ray phase CT in Ghent and X-ray micro CT in Delft

The obtained images by the X-ray (phase) CT were filtered and denoised first to get a smoother result of the images.

## B.1 Non-local means filter

The Non-local means filter is used for image denoising as shown in figure 53. The mean of all pixels in the image is taken. This is weighted by the similarity of these pixels compared to the target pixel. The Non-local means filter adds a so-called 'method noise' which looks like white noise, this results in a less disturbing denoised product (Buades et al. (2005)).

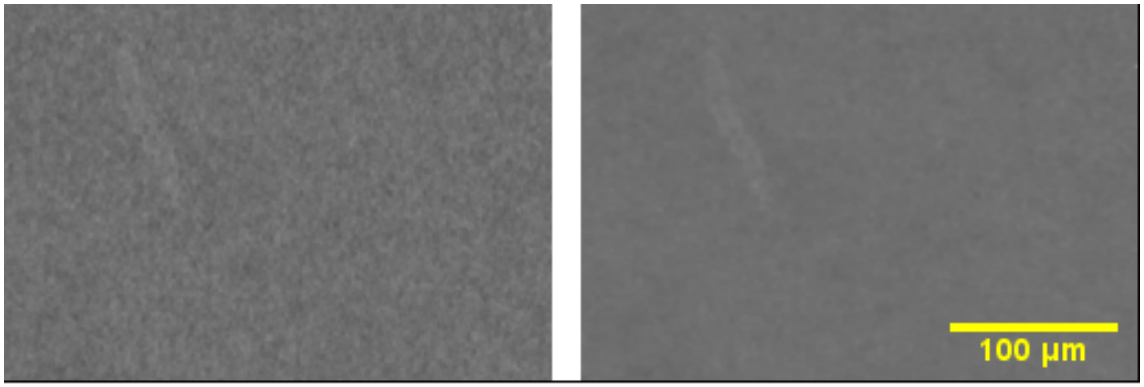


**Figure 53:**
*Effect of non-local means filter;*
*Left: non-filtered selection of a tomographic image of X-ray phase CT images;*
*Right: Filtered selection of the same tomographic image using non-local means filter*

As one can see the right tomographic image of the figure above is smoother than the left one. This is the result of the added 'method noise'.

## B.2 Interactive thresholding

To threshold the X-ray phase CT data one needs to distinguish two intensity regions. For X-ray phase CT images one region is the plastic sample holder and the second peak is the peat. The intensity is for techniques density driven. Therefore the intensity values are picked to highlight the fibres of the peat sample, as shown in figure 54.

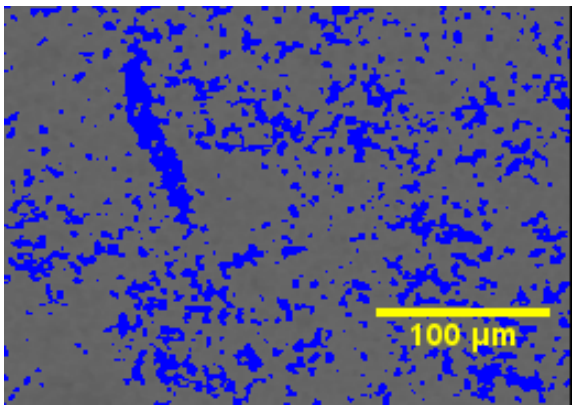


**Figure 54:** *Thresholding X-ray CT images;*
*Blue region represents the selected peat material to analyze further*

## B.3 Label analysis

The label analysis tool measures the amount objects in the sample observed by avizo.

| | index |
|---|---|
| Mean | 26539.5 |
| Min | 1 |
| Max | 53079 |
| Median | 26540 |
| Variance | 2.34791e+08 |
| Kurtosis | -1.19973 |
| Skewness | -0.00018864 |

**Figure 55:** *Label analysis output values with the amount of objects highlighted*

## B.4 Filtering by measure

The filtering by measure tool measures individual objects and ranks them according to the chosen measure. For this research the volume 3D measure is most suitable because the 3D representation of fibres is of interest. This measure calculates the spherical volume of the objects. It uses equation 29 to calculate the volume of a sphere.

$$\frac{4(\pi)r^3}{3} \tag{29}$$

Label analysis showed that for the selected region of the tomographic image 53079 objects were found for X-ray phase data. By using the filter by measure lowest values tool the biggest artifacts could be removed digitally in avizo. To remove the smaller artifacts the filter by measure highest values tool is used. In the case of X-ray phase CT images, the 10 biggest fibres were selected and shown on the right image of figure 56, using the volume rendering tool.

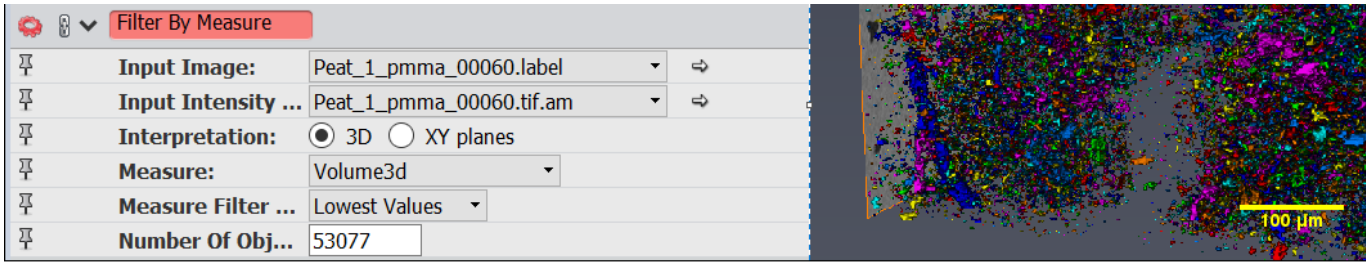


**Figure 56:** *Filtering by measure filtering the lowest artifacts digitally out*

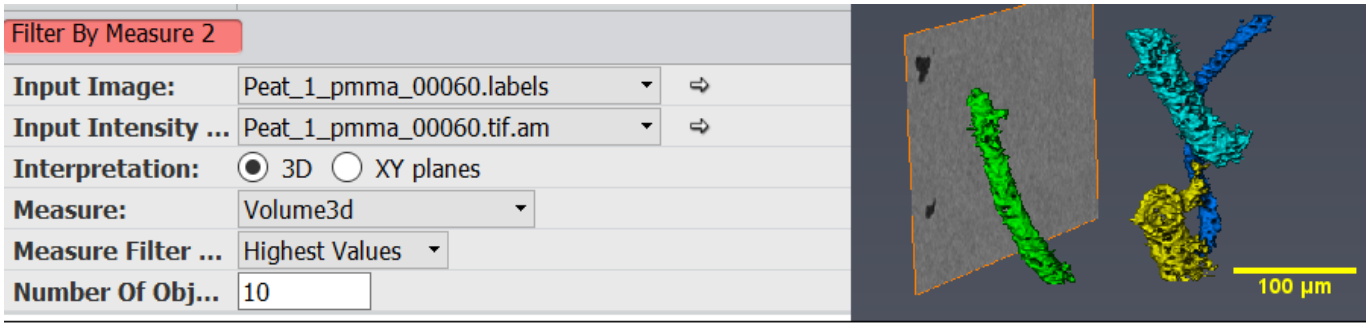


**Figure 57:** *Filtering by measure filtering the biggest artifacts digitally out*

## B.5 Morphological image processing dilation and closing

To get a smoother surface of the fibres two morphological image processing tools are used in avizo, i.e. dilation and closing. Dilation is performed because it better displays the edges of fibres, which is clearly shown on the yellow fibre if one compares the right undilated 3D volume with the middle dilated 3D volume of the selected region of X-ray phase tomographic data shown on figure 58. Closing is performed because it smoothens the surface of the fibres as clearly shown for the light blueish fibre if one compares the middle 3D volume with the left 3D volume of the fibres shown on figure 58.

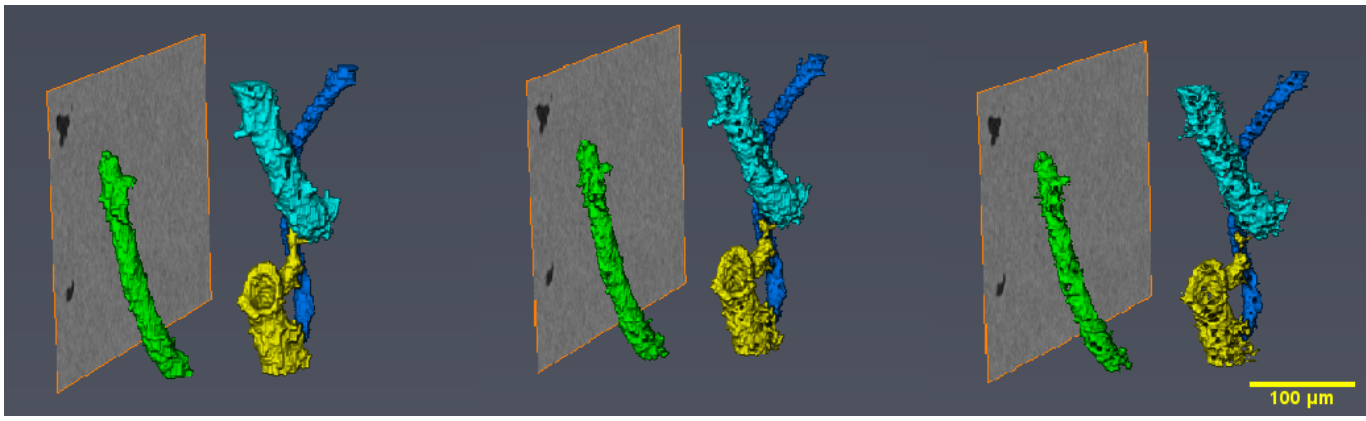


**Figure 58:**
*Smoothening fibres using dilation and closing in avizo;*
*Right: Fibres as shown in figure 57;*
*Middle: Dilation performed on the right picture resulting in a smoother surface of the fibres;*
*Left: Closing performed on middle volume image*

# C Data

The raw and filtered datasets can be found at the following link:
https://data.4tu.nl/repository/
By searching on the next titles, the datasets can be found found.

- Raw neutron data : Neutron tomographic data of peat sample
  This set of images contains the reconstructed images of a heavy water flushed peat sample from Uitdam scanned with neutron CT at the Reactor Institute Delft (RID).
  Keywords: Peat; heavy water; thermal neutrons; Computed Tomography (CT); Image reconstruction
- Filtered neutron data: Filtered tomographic data of peat sample
  This set of images contains the DOB-filtered images of the heavy water flushed peat sample from Uitdam scanned with neutron CT at the Reactor Institute Delft (RID).
  Keywords: Peat; heavy water; Neutron; Computed Tomography (CT); Image reconstruction; Difference of Boxes (DOB)
- X-ray micro CT projections of peat sample(neutron)
  This set of images contains the reconstructed images of the heavy water flushed peat sample from Uitdam scanned with X-ray micro CT at TU Delft.
  Keywords: Peat; micro CT; computed tomography (CT)
- X-ray micro CT projections of dry peat sample(neutron)
  This set of images contains the reconstructed images of the dry peat sample from Uitdam scanned with X-ray micro CT at TU Delft. This sample was also scanned in a wet state (flushed with heavy water) using both Neutron CT and micro X-ray CT.
  Keywords: Peat; micro CT; computed tomography (CT)
- X-ray phase CT projections of peat sample(plastic)
  This set of images contains the reconstructed images of a peat sample from Uitdam scanned with X-ray phase CT at UGCT - Centre for X-ray Tomography of the Ghent University, Belgium.
  Keywords: Peat; micro CT; computed tomography (CT)
- Filtered X-ray phase CT projections of peat sample(plastic)
  This set of images contains the filtered images of a peat sample from Uitdam scanned with X-ray phase CT at the Centre for X-ray Tomography in Ghent.
  Keywords: Peat; X-ray phase micro CT; computed tomography (CT)
- Filtered micro X-ray CT projections of dry peat (plastic)
  This set of images contains the filtered images of the dry peat sample from Uitdam scanned with X-ray micro CT at TU Delft which was scanned in a wet state using X-ray phase CT in Ghent.
  Keywords: Peat; micro CT; computed tomography (CT)